

ORGANIC/INORGANIC FILMS FOR BIOSENSOR APPLICATION

by

Netzahualcóyotl Palomera-Arias

A thesis submitted in partial fulfillment of the requirements for the degree of

MASTER OF SCIENCE
In
MECHANICAL ENGINEERING

UNIVERSITY OF PUERTO RICO
MAYAGÜEZ CAMPUS
2011

Approved by:

Surinder P. Singh, PhD
President, Graduate Committee

Date

Jay E. Banerjee, PhD
Member, Graduate Committee

Date

Jaime E. Ramírez-Vick, PhD
Member, Graduate Committee

Date

Ricky Valentín, PhD
Member, Graduate Committee

Date

Martha López-Moreno, PhD
Representative of Graduate Studies

Date

Gustavo Gutiérrez, PhD
Chairperson of the Department

Date

ABSTRACT

Biosensors are becoming increasingly important as practical tools in pathogen detection and molecular diagnostics. Electrochemical biosensors are of particular interest due to several advantages including low-cost, easy operation, and small size. During the development of efficient biosensors, a crucial part is the choice of material onto which a biomolecule has to be immobilized while providing good electron transfer rate at the electrode as a result of a biochemical reaction.

Present work deals with the development of novel nanostructured metal oxides and conducting polymer nanocomposites as promising material matrix for biomolecule immobilization, because of their high surface to volume ratio and efficient electron transport properties.

We have synthesized ferrocene-polypyrrole based nanocomposites with excellent mechanical and electronic properties. The optimized nanocomposite films have been used for glucose biosensor. Results indicate the good performance of the electropolymerized copolymer of pyrrole and ferrocenecarboxylate modified pyrrole P(Py-FcPy) on indium-tin-oxide (ITO) coated glass for glucose biosensor.

On the other hand an inorganic material structure, ZnO nanorods (ZnONR), has been grown on indium tin oxide (ITO) films on glass. This could easily be upgraded with existing MEMS technology to fabricate miniaturized biosensors. Urease (Urs) enzyme was physically immobilized on nanorods exploiting high isoelectric point of ZnO to fabricate Urs/ZnONR/ITO bioelectrode. Urs/ZnONR/ITO bioelectrode revealed a very high sensitivity of 10 $\mu\text{A}/\text{dL}/\text{mg}$ (1.66 $\mu\text{A}/\text{mM}$) in a urea concentration range of 10-25 mg/dl with enhanced linearity.

RESUMEN

La tecnología de los biosensores ha adquirido gran importancia como herramienta en detección de patógenos y diagnosis molecular. Los biosensores electroquímicos son de particular interés debido a ventajas que incluyen fácil y bajo costo de operación. En el desarrollo de biosensores eficientes, es crucial la selección de un material en donde una biomolécula pueda ser inmovilizada a la vez que provea una buena transferencia de electrones a un electrodo como resultado de una reacción bioquímica.

El trabajo presente cubre el desarrollo de óxidos metálicos nano-estructurados y nanocompuestos con polímeros conductivos, ya que estos materiales presentan potencial como plataforma para inmovilizar biomoléculas, debido a que presentan una razón superficie-volumen grande, así como propiedades eficientes en transferencia de electrones.

Hemos sintetizado un nanocompuesto de polipirrol con ferroceno, con excelentes propiedades mecánicas y electrónicas. La película optimizada del nanocompuesto ha sido utilizada para un biosensor de glucosa. Los resultados indican una excelente operación como biosensor de glucosa del co-polímero electropolimerizado de pirrol y pirrol modificado con ferrocenocarboxilato P(Py-FcPy) en piezas de cristal cubiertos con óxido de estaño-indio (ITO).

Por otra parte, un material inorganico, nano-barillas de óxido de zinc (ZnONR) ha sido crecido en ITO. La enzima ureasa (Urs) fué inmovilizada físicamente sobre las nano-barillas, sacando ventaja del elevado punto isoelectrico del óxido de zinc, para fabricar un bio-electrodo denominado Urs/ZnONR/ITO. Este bio-electrodo mostró una gran sensibilidad de 0.4 $\mu\text{A}/\text{mM}$ hacia la urea, con una vasta linearidad de 1 a 20 mM.

To my family . . .

ACKNOWLEDGEMENTS

I would like to recognize the support received by the persons and institutions that collaborated directly and indirectly during the development of this work.

I express an acknowledgement to my advisor, Dr. Surinder P. Singh for the opportunity to do research under his guidance, support and patience. I also would like to thank my graduate committee for their guidance and support. Dr. Banerjee for his full and unconditional support in the Mechanical Engineering department. Dr. Jaime E. Ramírez-Vick for sharing his knowledge and resources. Dr. Ricky E. Valentín for his support. Dr. Enrique E. Meléndez and graduate student José L. Vera from the Chemistry department for the training, resources and direct collaboration with a part of this work. Dr. Maharaj Tomar from the Physics department for providing resources.

The IFN-NSF-EPSCoRE start up grant OIA-0701525 is gratefully acknowledged. I am very thankful to Dean College of Engineering and IFN for financial assistantship. I also want to thank my family, for their unconditional support and love.

Table of Contents

ABSTRACT	II
RESUMEN	III
ACKNOWLEDGEMENTS	V
TABLE OF CONTENTS	VI
TABLE LIST	II
FIGURE LIST	IX
1 INTRODUCTION	1
1.1 Motivation	2
1.2 Types of biosensors.....	4
1.2.1 Electrochemical biosensors.....	4
1.2.2 Amperometric electrochemical biosensors.....	5
1.3 Analyte detection through the use of enzymes.....	7
1.3.1 Glucose biosensors.....	8
1.3.2 Urea biosensors.....	10
1.3.3 Enzyme immobilization.....	11
1.4 Matrices.....	15
1.4.1 Nanostructured zinc oxide.....	15
1.4.2 Polypyrrole and ferrocene.....	17
1.4.2.1 Conductive polymers.....	17
1.4.2.2 Polypyrrole.....	20
1.4.2.3 Ferrocene.....	23
1.4.2.4 Ferrocene modified pyrrole.....	24
1.5 Literature Review.....	27
1.5.1 Amperometric urea biosensors.....	27
1.5.2 Polypyrrole/mediator matrices for amperometric glucose biosensors.....	31
2 THEORETICAL BACKGROUND	36
2.1 Electrode material characterization.....	36
2.1.1 X-Ray diffraction (XRD).....	36
2.1.2 Scanning electron microscopy (SEM) and field emission scanning electron microscopy (FE-SEM).....	38
2.1.3 Fourier transform infrared (FT-IR) spectroscopic measurements.....	41

2.1.4 Nuclear magnetic resonance (NMR) spectroscopy.....	42
2.2 Electrochemical measurements.....	43
2.2.1 Mass-transport limited reactions.....	45
2.2.2 Electron-transfer limited reactions.....	46
2.2.3 Electric double layer.....	46
2.3 Amperometric measurements.....	48
2.3.1 Cyclic voltammetry.....	48
2.3.2. Nernstian redox processes on deposited films.....	52
2.4 Parameters related to the performance of biosensors.....	55
2.4.1 Linear range, sensitivity and Michaelis-Menten constant (K_m).....	56
2.4.2 Detection limit.....	57
2.4.3 Effect of pH.....	57
2.4.4 Amount of immobilized enzyme.....	58
3 POLY(PYRROLE-N-FERROCENE-PYRROLE) COPOLYMER FILM FOR GLUCOSE BIOSENSING	59
3.1 Materials and methods.....	59
3.1.1 Materials used.....	59
3.1.2 Synthesis of 4-(1H-Pyrrol-1-yl)phenyl ferrocenecarboxylate (“FcPy”).....	60
3.1.3 P(Py-FcPy)/ITO electrode and Gox-P(Py-FcPy)/ITO bioelectrode preparation.....	61
3.2 Results and discussion.....	62
3.2.1 4-(1H-Pyrrol-1-yl)phenyl ferrocenecarboxylate (“FcPy”).....	62
3.2.2 Gox-P(Py-FcPy) bioelectrode.....	67
4 ZINC OXIDE NANORODS AS FILMS FOR AMPEROMETRIC UREA BIOSENSOR 72	
4.1 Materials and Methods.....	72
4.1.1 Materials used.....	72
4.1.2 Preparation of ZnO nanorods films.....	73
4.1.3 Urease immobilization.....	74
4.2 Results and discussion.....	74
4.2.1 Structure analysis and electrochemical study of zinc oxide nanorods film.....	74
4.2.2 Urs/ZnONR/ITO bioelectrode for detection of urea.....	77
5 CONCLUSIONS	84
REFERENCES.....	86
APPENDIX A: ELEMENTAL ANALYSIS OF 4-(1H-PYRROL-1-YL) PHENYL FERROCENECARBOXYLATE.....	95

Table List

Table	Page
Table 1 Comparison of Gox-P(Py-FcPy)/ITO bioelectrode with other Gox- based amperometric glucose biosensors reported in literature [68,69,73,94-98].....	71
Table 2 Data from ZnO nanorods XRD in figure 42(a).....	75
Table 3 Comparison of Urs/ZnONR/ITO bioelectrode with others Urs- based amperometric urea biosensors reported in literature [13,60,62-65].....	83

Figure List

Figure	Page
Figure 1 Schematic of a biosensing system.	2
Figure 2 a) Amperometric electrochemical biosensor, b) electrical schematic of a potentiostat/galvanostat.....	5
Figure 3 Mechanism of second generation glucose biosensors through the use of electron mediators.....	9
Figure 4 Ion-sensing mechanism of amperometric urea biosensor.	11
Figure 5 Immobilization methods: a) physisorption, b) entrapment, c) entrapment with redox mediators, d) cross-linking, e) cross-linked to entrapment matrix, f) covalent binding.	13
Figure 6 a) Binding in a 2 dimensional matrix, b) spatial distribution of enzyme in a tridimensional entrapment matrix.	13
Figure 7 Zinc oxide: a) hexagonal Wurtzite structure, b) crystal unit cell, c) ionic tetrahedral arrangement.....	16
Figure 8 Carbon atom: a) regular tetrahedral configuration, b) σ binding configuration, c) π orbital configuration orthogonal to the σ bonds, d) π binding in a double bond.	18
Figure 9 Conductive polymer's backbone: a) neutral chain and subsequent electron removal, b) polaron state and subsequent electron removal, c) bipolaron state.	19
Figure 10 a) Pyrrole (Py) monomer, b) resonance configurations of Py.....	20
Figure 11 Electropolymerization of Py between 0.6 – 0.8 V versus Ag/AgCl.....	22
Figure 12 a) Cyclopentadienyl ion with a distance between the carbon atoms of 1.40 Å.....	23
Figure 13 Ferrocene derivatives, where R = SO ₃ H, (CH ₂) _n SO ₃ H, COOH, COCl, (CH ₂) ₆ Br, etc.....	25
Figure 14 a) Pre-functionalization of Py through acylation, b) post-functionalization of PPy through acylation.	25
Figure 15 4-(1H-Pyrrol-1-yl)phenol.....	26
Figure 16 X-Ray diffraction process scheme.....	37

Figure 17 Configuration scheme of a scanning electron microscope.	39
Figure 18 JEOL - JSM-5410 LV Scanning electron microscope.	39
Figure 19 SEM image of nickel oxide nanoparticles (from reference 77).	40
Figure 20 FE-SEM images of a) ferrocene chloride magnetic hollow spheres, b) aluminum oxide nano brushes (from references 78 and 79).	41
Figure 21 FT-IR spectra of polystyrene film.	42
Figure 22 ¹ H NMR spectrum of ethanol (from reference 83).	43
Figure 23 Electrical double-layer: a) metal- electrolyte interface, b) semiconductor-electrolyte interface.	47
Figure 24 Cyclic voltammogram of 5 mM potassium ferro-ferricyanide redox couple on ITO working electrode in PBS (pH 7.0, 50 mM, 0.9% NaCl).	49
Figure 25 Cyclic voltammograms of nickel oxide film on ITO coated electrode at different scan rates.	50
Figure 26 a) Cyclic voltammograms of 5 mM potassium ferro-ferricyanide redox couple on ITO working electrode at different scan rates; b) Peak current vs. scan rate; c) Peak current vs. square root of scan rate; d) Peak Potential vs. log of scan rate.	51
Figure 27 Cyclic voltammograms of deposited polypyrrole film on platinum coated electrode at different scan rates in PBS. Inset a) Peak current vs. scan rate. b) Peak current vs. square root of scan rate.	53
Figure 28 a) Voltage step from 0 V to 0.6 V and b) amperometric response at constant potential.	55
Figure 29 Amperometric response linearization of Gox/PPy bioelectrode to different concentrations.	57
Figure 30 Synthesis route of 4-(1H-Pyrrol-1-yl) phenyl ferrocenecarboxylate.	61
Figure 31 Fabrication route of Gox-P(Py-Fc-Py)/ITO bioelectrode and glucose detection mechanism.	62
Figure 32 ¹ H NMR spectra of (a) 4-(1H-Pyrrol-1-yl) phenol and (b) 4-(1H-Pyrrol-1-yl) phenyl ferrocenecarboxylate.	63
Figure 33 ¹³ C NMR spectra of 4-(1H-Pyrrol-1-yl) phenyl ferrocenecarboxylate.	64

Figure 34 FTIR: 4(1H-pyrrol-yl)phenyl ferrocenecarboxylate.....	64
Figure 35 a) Cyclic voltammogram of P(Py-FcPy) electrodes at 75 mV/s in PBS (50mM, 0.9% NaCl), b) Cyclic voltammogram spectra in the same buffer at different scan rates.	65
Figure 36 Cyclic voltammograms of P(Py-FcPy)/ITO electrode at different scan rates in a solution containing 5 mM ferro-ferricyanide redox couple in PBS (pH 7.0, 50 mM, 0.9% NaCl). Inset a) Peak current vs. scan rate; b) Peak Voltage vs. Log(Scan Rate).	66
Figure 37 SEM micrographs of glucose oxidase entrapped in a) PPy film, b) P(Py-FcPy) film.	67
Figure 38 Response of Gox- P(Py-FcPy) bioelectrode at different pH in PBS (50 mM, 0.9%NaCl).	68
Figure 39 CV spectra of Gox-P(Py-FcPy) bioelectrode in PBS (50 mM, pH 7.0) at 100mV/sec for glucose concentrations: (- - -) buffer, (i) 1.4 mM, (ii) 2.8 mM, (iii) 5.6 mM, (vi) 8.4 mM and (v) 11.2 mM.	69
Figure 40 Amperometric response of Gox-P(Py-FcPy)/ITO bioelectrode to the successive addition of 2.8 mM glucose in 50 mM PBS (pH 7.0) at +175 mV. Inset: a) Linear current response with glucose concentration, b) Lineweaver-Burk Plot.	70
Figure 41 a) Sputtering process to deposit ZnO seed on top of ITO substrate, b) thermal formation of ZnO nanorods on ZnO seeded ITO substrate.	74
Figure 42 a) XRD spectra of ZnONR/ITO electrode, b) XRD of ITO coated glass surface.....	75
Figure 43 a) FE-SEM image of ZnONR/ITO electrode, b) FE-SEM image of ZnO seeded surface of the substrate.	76
Figure 44 Cyclic voltammograms of the ZnONR/ITO electrode in PBS containing $\text{Fe}(\text{CN})_6^{3-/4-}$ at different scan rates. Inset: (a) Peak Current vs. square root of scan rate. (b) Peak Voltage vs. log of scan rate.	77
Figure 45 Cyclic voltammograms at 50 mV/s of Urs/ZnONR/ITO bioelectrode response to 2 mM urea as a function of pH in PBS with $\text{Fe}(\text{CN})_6^{3-/4-}$ at 50 mV/s.	78
Figure 46 Cyclic voltammograms at 50 mV/s of Urs/ZnONR/ITO bioelectrode response to 2 mM urea as a function of temperature in PBS containing $\text{Fe}(\text{CN})_6^{3-/4-}$ at 50 mV/s. Inset: Current response vs. temperature.	79
Figure 47 Cyclic voltammograms at 50 mV/s of ZnONR/ITO electrode (----) and Urs/ZnONR/ITO bioelectrode (—) in PBS containing $\text{Fe}(\text{CN})_6^{3-/4-}$ at 50 mV/s.	79

Figure 48 Cyclic voltammograms of Urs/ZnONR/ITO bioelectrode in the absence(----) and presence(—) of different urea concentrations in PBS containing $\text{Fe}(\text{CN})_6^{3-/4-}$ at 50 mV/s. 80

Figure 49 Schematic for urea detection mechanism of Urs/ZnONR/ITO bioelectrode. 80

Figure 50 Current response of Urs/ZnONR/ITO bioelectrode to urea concentration in PBS. Inset a) Amperometric response to successive additions of 1mM urea, b) Lineweaver-Burk plot..... 81

Figure 51 Amperometric response of Urs/ZnONR/ITO bioelectrode for 1 mM urea, 1mM urea + 0.1 mM ascorbic acid, and 1 mM urea + 5 mM glucose solutions in PBS. Inset: Current response to interferants 82

1 INTRODUCTION

Modern technological development has permeated almost all fields of human activity. To mention a few of them, healthcare, chemical and biological analysis, environmental monitoring and food processing have been greatly benefited. Focusing on health care, a considerable increase of research areas has emerged with the aim to improve proper diagnosis and prevention of diseases, since the undesired development of these ones represents expensive treatments and life risk situations, with economical and social interaction consequences. Treatment of serious diseases usually implies expensive drugs and diagnostics. Besides the economical drawback, these treatments offer the risk of destabilizing physical and psychological side effects which seriously affect a reintegration into the previous lifestyle of the patient. These are just some examples to evidence the advantage of a preventive approach.

Prevention requires a diagnosis based on monitoring of activity in the human body to detect abnormal or dangerous conditions. With this in mind, medical scientists have developed techniques which include physical observation, as well as physical and chemical analysis of samples of blood, cell tissue, urine and so on. Applications of technologies in medicine have facilitated faster and accurate identification of pathological substances present in the body that act as important indicators of disease development. These technologies rely on the use of appropriate sensors and complicated electronics.

This work focuses towards the development of innovative biosensor technologies capitalizing on material science and nanotechnology. We have synthesized two different materials, organic

polypyrrole-ferrocene composite and inorganic ZnO nanorods, and evaluated their performance to develop electrochemical biosensors.

A biosensor is a device consisting of a biological element such as DNA, cell tissue, antibody, microorganism, or enzyme attached to a material substrate, which allows a biochemical reaction to proceed and manifest into a method of transduction. The biochemical reaction should correspond to a unique interaction of the biological element with the target molecule being monitored. Figure 1 presents the schematic of a biosensor based system.

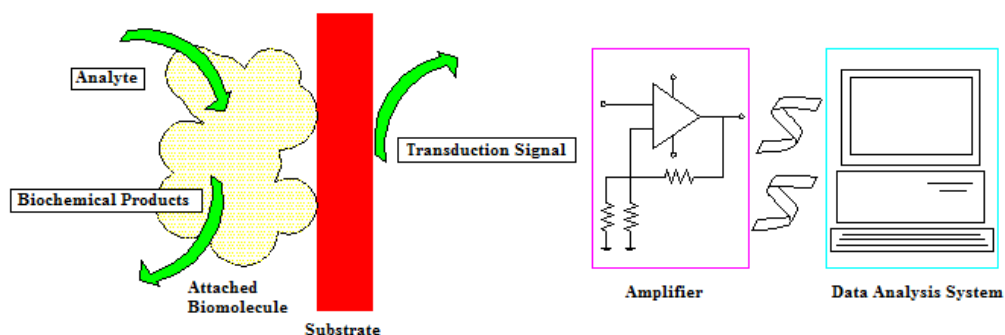


Figure 1 Schematic of a biosensing system.

1.1 Motivation

Urea is known to be an important marker for evaluating uremic toxin levels and indicates the kidney functionality and staging of kidney diseases. The normal level of urea in blood is from 15 to 40 mg/dl (2.5–7.5 mM). In patients suffering from renal insufficiency, urea concentrations in serum vary from 180 to 480 mg/dl [1,2]. Aronson et al. [3] have shown that blood urea nitrogen is a simple clinical variable that provides useful prognostic information in patients admitted for decompensated heart failure. Elevated blood urea nitrogen levels can result in renal

failure whereas a decrease in urea concentration causes hepatic failure, nephritic syndrome, and cachexia. Therefore, there is an urgent need to develop a device that rapidly monitors urea concentrations in the body. One of the objectives of this thesis work focuses on this goal.

Another important, and much more studied marker in the body is glucose. Concentrations of glucose outside the normal blood level range of 80-120 mg/dL (4.4 – 6.6 mM) represent a deficiency associated with diabetes mellitus. This disease can be the cause of long term complications such as loss of vision, failure of heart, kidney, and blood vessels. It is calculated to affect almost 10 percent of the world population [4,5]. Jansson et al. [6] conducted a survey where they found that diabetic subjects have higher mortality rates associated with coronary heart diseases and cardiovascular diseases. Furthermore, their finding showed that these rates did not diminished significantly when compared to non diabetic subjects in a 33 year follow up between 1972 and 2004. Blood glucose measurement is one of the most useful tools for patient monitoring and management of diabetes [7]. Glucose biosensors represent nearly 85% of the biosensor market share, yet its field research is not considered fully accomplished. Wireless and micro-electromechanical systems (MEMS) configurations for continuous and subcutaneous monitoring are still in an early development stage. Feasible materials for both glucose biosensor fabrication and MEMS configurations are in mind for the research work of this thesis.

1.2 Types of biosensors.

Biosensors eliminate the need for sample gathering and pre-treatment, since they are used for direct measurement of the target analytes [8]. For this measurement, the transduction method used for biosensors can be optical, electrochemical, magnetic, thermoelectric or piezoelectric [9]. In this work, only electrochemical biosensors are covered in detail.

1.2.1 Electrochemical biosensors.

Electrochemical sensors are devices that use an electrode as the transduction element in a system that provides a relationship between an electrical circuit and a chemical reaction. A major amount of current biosensors are of the electrochemical type because of their better sensitivity, reproducibility, easy maintenance and low cost. For this reason, they have been adopted for many applications in the clinical field, since they have shown great promise for fast and accurate measurement in healthcare monitoring.

These biosensors are highly selective due to the immobilized biological recognition element on the substrate, providing a specific binding affinity to the desired molecule [10]. The electrical signal derived from the biochemical reaction relates to the concentration of the desired analyte. This electrical response subdivides electrochemical biosensors into potentiometric (potential monitoring at constant current) and amperometric (current monitoring at constant potential) [11].

1.2.2 Amperometric electrochemical biosensors.

Amperometric electrochemical biosensors monitor currents generated when electrons are exchanged either directly or indirectly between a biological system and a working electrode [12]. The amperometric techniques offer fast, simple and low cost detection, with the advantages of sensitivity, linear response and low detection limits [13]. These characteristics have made them potential candidates for commercial fabrication. They can work on a two or three electrode system. However, nowadays, the latter has been more commonly adopted because of its improved electrical performance. Figure 2a shows the schematic of a three electrode cell configuration (working electrode, reference electrode and counter electrode for electrochemical biosensing.

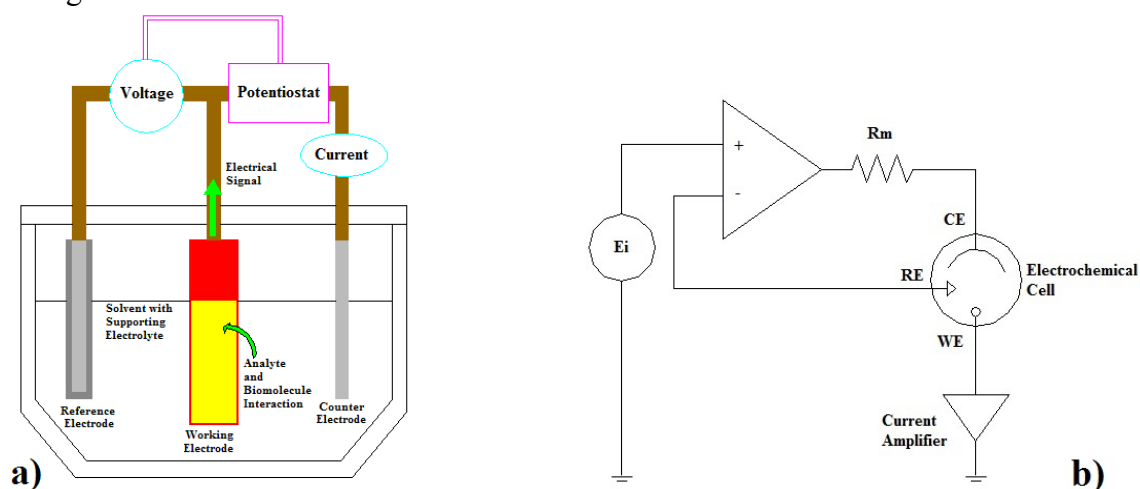


Figure 2 a) Amperometric electrochemical biosensor, b) electrical schematic of a potentiostat/galvanostat.

The amperometric methodology consists in a voltage modulation applied between the working and reference electrode. Electroactive species, generated at the surface of the working electrode by the chemical interaction between the biomolecule and the analyte, react within the potential window and generate a current response. The electrodes are immersed in a solvent medium

containing a supporting electrolyte. The solvent most commonly used is water, with buffer and inorganic salts as electrolytes. These electrolytes, such as potassium and sodium chloride, are required to decrease the resistance of the solution and maintain a stable ionic strength [14]. Buffer salts (i.e. monobasic and dibasic sodium phosphate) consist of a conjugate acid and base pair and are used to maintain a pH control of the medium.

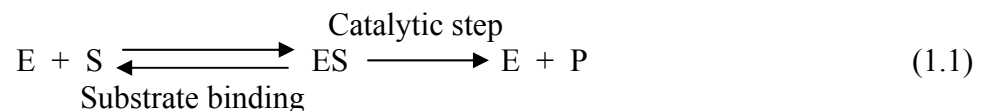
While limited amount of voltage could be obtained in the presence of current, implementation of a third auxiliary electrode, the counter electrode, facilitates a path for the current, eliminating it from the voltage measurement between the working and reference electrode. The counter electrode is made of a non-reactive conductive material such as platinum, while the reference electrode is a standard Ag/AgCl electrode. Anodic response is achieved by using a noble metal or modified surface substrate as the working electrode.

The system that operates and monitors the electrochemical cell consists of a potentiostat that controls the potential between the working and reference electrodes by adjusting the current at the counter electrode, and a galvanostat that monitors the cell current. To achieve this with currents in the micro to nanoampere range in presence of the cell electrical resistance, a circuit design of operational amplifiers and feedback loops is used (fig. 2b). The current in the reference electrode is eliminated by connecting it through a high resistant circuit, and the flowing current in the working electrode can be measured without disturbing the specified voltage by the use of current-to-voltage converter operational amplifier [14].

Typical recognition elements used in biosensors are: enzymes for metabolites, nucleic acids for other nucleic acids, antibodies, whole cells, and receptors for ligands. From all of these, enzymes are among the most common [10], with the glucose oxidase (Gox) being the most widely used. Other examples of enzymes include glucose dehydrogenase for glucose assays, cholesterol oxidase and cholesterol esterase for cholesterol, urease for urea and alcohol oxidase for ethanol. Two important components in the human system, urea and glucose, are going to be utilized as analytes for level determination in the data gathered for this work.

1.3 Analyte detection through the use of enzymes.

Enzymes are globular proteins that serve as selective catalysts in organic systems. Being speedy, precise and inexpensive, they are the preferred molecular recognition elements in biosensor fabrication. Their operation consists in generating detectable species through the following catalysis process:



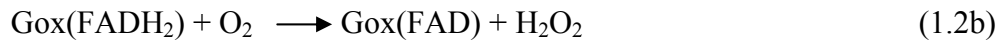
In this expression, the substrate S is the specific molecule that interacts with the enzyme E and gets converted into another molecule called the product P. The catalytic step occurs during a process in which the substrate gets bound with the enzyme (ES) in a specific region called the active site of the enzyme. After the catalysis, the product molecules get detached from the enzyme. Attachment of the enzyme to a surface alters significantly its behavior, as opposed to the case as in an homogeneous solution. Access to the specific location of the active site, amongst other parameters, plays an important role in biosensor design.

1.3.1 Glucose biosensors.

Glucose Oxidase (Gox) is the first and most widely used enzyme, due to its relatively broad pH and temperature range of operation, as well as its high catalytic activity. It belongs to the enzyme family of the oxidoreductases, which catalyzes the transfer of electrons between molecules. In the case of glucose oxidase, this electron transfer occurs within its active site at the coenzyme flavin adenine dinucleotide (FAD), which behaves as an electron acceptor in the presence of glucose, becoming 1,5-dihydro-FAD (FADH₂). This reaction is represented as



While gluconolactone hydrolyses in water and becomes gluconic acid, FADH₂ gets regenerated into FAD by reacting with oxygen, leading to the formation of hydrogen peroxide, as expressed by the following expression.



Location of the coenzyme it's called the redox center, and finds itself deep within the protein's structure. Electroactive reaction of the hydrogen peroxide liberation occurs at an anodic potential of 0.6 V, making it possible to be amperometrically monitored at the electrode surface [15]:



This measurement method, which established the first generation of glucose biosensors, offered a simple detection way, but also identified two main setbacks to overcome: a) interference of electroactive species at the relatively high voltage applied, such as ascorbic acid, uric acid and

drugs like acetaminophen, and b) reading errors caused by either deficit or undesired fluctuations of oxygen. Biosensor development aimed at tuning the operating potential to an optimal region between -0.20 V and 0.00 V by using materials for the electrodes that presented electro active behavior towards the presence of hydrogen peroxide [16,17].

The replacement of oxygen as the electron acceptor in the redox center with synthetic particles defined the second-generation glucose biosensor (Fig 3). Surface of the electrode cannot be used to transport electrons directly from the redox center of the enzyme due to distance imposed by the protein layer that covers the co-enzyme. As an approach to solve this problem, implementation of nanoparticles and nanocomposite materials to the substrate have been used to position electrical conductivity closer to the center of the enzyme. Presence of synthetic mediators in the substrate's configuration will be addressed further ahead while explaining one of the electrode's material modifications investigated in this thesis.

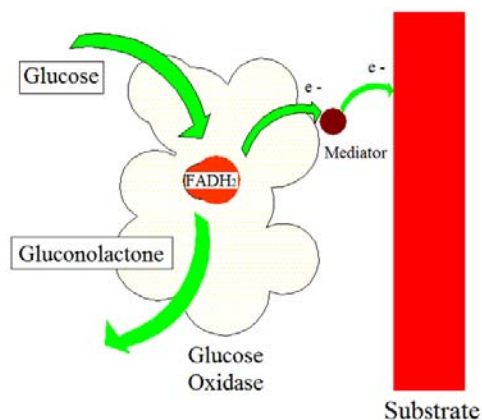


Figure 3 Mechanism of second generation glucose biosensors through the use of electron mediators.

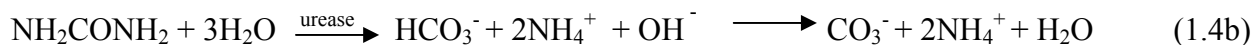
1.3.2 Urea biosensors.

In the estimation of biologically important analytes, urea estimation has recently gained much attention. The use of urease as a biocatalyst for the development of biosensors has attracted continuous interest and various kind of urea biosensors have thus been reported [18].

Urease belongs to the hydrolase enzyme family, which catalyzes the hydrolysis of a chemical bond. The following equations show the reaction of urea with urease.



This reaction subsequently derives ion production:



As it can be seen, urease reacts with urea catalytically converting it into ammonium and bicarbonate ions. The efficiency of any urea biosensor depends on the effective detection of these ions, and various materials and transducers have been used for their estimation in fabrication of urea biosensor [19]. Guilbaut and Montalvo [20] developed the first urease enzyme electrode by using a cation-selective glass electrode and measured the potential difference with the catalyzed ammonium ion.

Although potentiometric detection is used more often for urea detection, it lacks the sensitivity, time response and low detection limit offered by the amperometric method. Researchers on the amperometric electrochemical detection have worked on this catalysis through different mechanisms such as the use of pH sensitive redox mediators [21], the use of glutamate

dehydrogenase as ammonium-ion reactive redox mediator [22], ammonium-ion selective membranes [23], hydroxide-ion sensitive membrane [24] and ammonium-ion reactive conductive polymers [25]. Figure 4 presents the scheme for an amperometric urea biosensor.

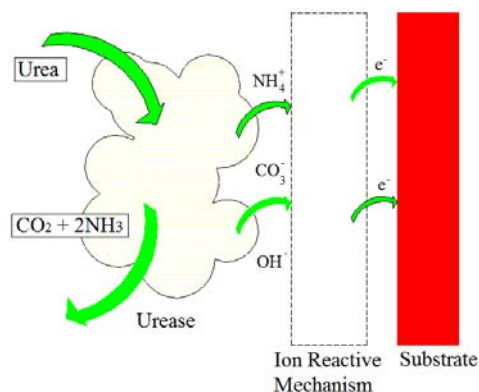


Figure 4 Ion-sensing mechanism of amperometric urea biosensor.

1.3.3 Enzyme immobilization.

A critical aspect in electrochemical biosensor design and development is the selection of the material onto which the biorecognition element will be immobilized, since it will affect its sensitivity and stability. To this end, the electrochemical biosensors field has developed numerous techniques in the search for biocompatibility, robust enzyme immobilization on the substrate and electron transfer providing mechanisms. A variety of intelligent materials such as sol-gels, metal oxides, self-assembled monolayers, conducting polymers and nanocomposites [26-29] have been used to enhance electron transfer rate and to provide biomolecule stabilization.

The solid support holding the enzyme is known as matrix, and it can be of organic or inorganic nature. Selection of matrices for proper binding of biomolecules and improvement in performance is still a major concern. Suitable matrix films should possess reproducibility and be adaptable to a wide range of physiological, pH, temperature, ionic strength and chemical environments.

Immobilization methods can be classified as physical or chemical. Physical methods are divided in physisorption and entrapment. Physisorption refers to adhesion by electrostatic interaction (Van der Waals forces) (fig. 5a). This interaction is governed by the electrical charges of the molecules, which can be expressed in terms of isoelectric points. Isoelectric points (IEP) are defined as the pH values at which a surface or molecule has no charge. Values below the IEP tend to accumulate the predominant presence of positively charged species on the molecule, while values above the IEP present negatively charged ones. Although other methods present stronger binding capacities, physisorption maintains a maximal bioactivity of the enzyme. Improvement of the binding can be obtained by choosing a substrate material that offers a strong electrostatic interaction with the desired biomolecule.

Entrapment methods include retention of the biomolecule by means of membranes, gel matrices or incorporation into pastes, liquid plastifiers, polymers and composites electrodes (fig 5b). These methods offer a tridimensional matrix providing spatial distribution of the enzyme, thus facilitating access to different oriented active sites of the enzyme (Fig 6a and 6b). One attractive method is a one step entrapment by electropolymerization within a polymer matrix. The enzyme is added in a monomer containing solution that gets solidified on top of the electrode at an

applied potential [30,31]. Gradual loss of the enzyme and a diffusion barrier to the substrate/products transport by the bulk material of the solid matrix are some of the disadvantages of entrapment. Improvement on this method includes the use of redox mediators such as metal nanoparticles for electron transport efficiency (fig 5c) [32], and the use of conductive polymers. A more robust attachment of the enzyme can be attained by synthetically attaching it to the entrapment material.

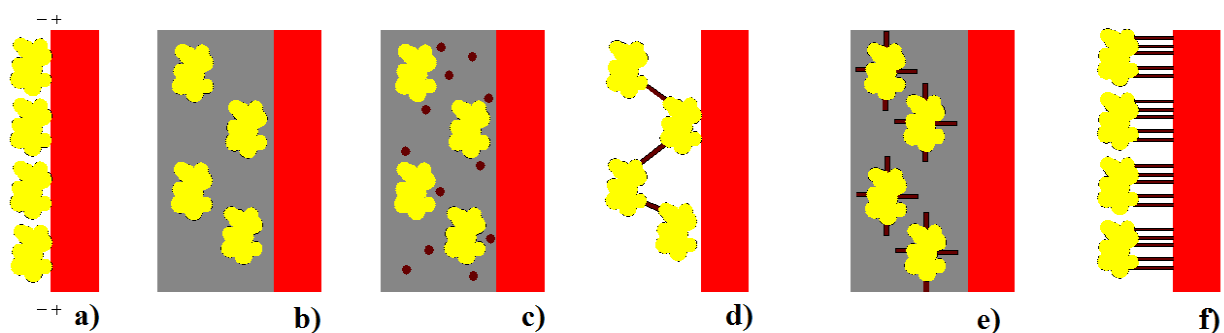


Figure 5 Immobilization methods: a) physisorption, b) entrapment, c) entrapment with redox mediators, d) cross-linking, e) cross-linked to entrapment matrix, f) covalent binding.

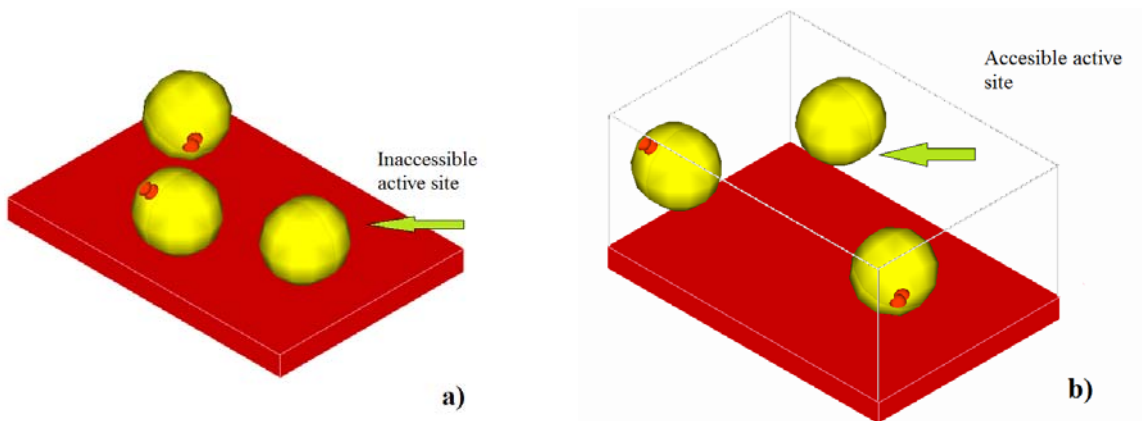


Figure 6 a) Binding in a 2 dimensional matrix, b) spatial distribution of enzyme in a tridimensional entrapment matrix.

Chemical immobilization can be classified as covalent binding and cross-linking. They consist on chemical surface alteration of either the biomolecule, substrate surface or entrapment matrix. Cross-linking methodology produces covalent attachment between biomolecules, biomolecules and entrapment matrices, or biomolecules and electron mediators [61]. Common methods for cross-linking are the use of glutaraldehyde and the mediated reaction of N, N'-dicyclohexylcarbodiimide and N-hydroxysuccinimide (NHS and DCC) [33,34]. Glutaraldehyde is a molecule with multiple reactive ends capable of attaching to the functional groups of the enzymes (fig 5d). A brief example of NHS/ DCC chemistry consists in functional group activation on a conductive polymer chain by the use of NHS and enzyme cross-linking with the use of DCC (fig 5e). Cross-linking does not activate conjugation with the electrode's surface, but it offers the advantage of biomolecule bulk retention, multiple enzyme co-immobilization and enhanced substrate receptor complex.

Covalent binding relies on functionalization of the electrode surface and cross-linking of the enzyme (fig 5f). A common example for surface functionalization includes the adsorption of thiol compounds on gold surfaces [35]. A second functionalization of the enzyme by a coupling agent allows the conjugation and subsequent binding. Covalent binding method offers a considerable strong attachment between the enzyme and the surface of the electrode and stability against adverse conditions such as pH changes or ionic strength of the solution. Disadvantages of the chemical approaches are toxicity of the chemicals used, physical irreversible alteration of the matrix surface and diminution of bioactivity in the enzyme.

The attachment methods utilized in this work will be from the physical variety. The contributions in this thesis include experiments done with urease physisorbed on a zinc oxide nanorods surface and entrapment of glucose in a new mediator functionalized conductive polymer matrix.

1.4 Matrices

1.4.1 Nanostructured zinc oxide.

Recently, nanostructured metal oxides have gained much attention as promising material to provide biomolecule friendly environment for their binding in proper orientation with retained activity. Nanostructured metal oxides exhibit unique optical, electrical, molecular and surface charge properties for biosensor applications [36]. Nanostructured based sensors have shown faster response and higher sensitivity than the planar sensor configurations, due to their smaller dimensions combined with dramatically increased sensing surface and strong binding properties. Therefore, they greatly increase sensitivity to the point where single-molecule detection becomes possible.

Zinc oxide (ZnO) nanostructures have recently become the choice for application as suitable matrix in biosensors [37]. This oxide is abundant and a low cost non-silica biocompatible n-type semiconducting material from group II-VI with a wide band gap (3.37eV). It possesses chemical stability, electrochemical activity and high surface to volume ratio. This latter property is one important characteristic of nanoparticles and nanostructured surfaces, because it considerably enhances the amount of enzyme loading and provides a tridimensional arrangement to the structure of the matrix.

Another important feature that makes ZnO nanostructures a prominent matrix for biosensor application is a high electron communication and high isoelectric point (~ 9.0). This property can be used to immobilize biomolecules with low isoelectric point (IEP), carrying an opposite charge in biological pH, by electrostatic interaction [38].

Under regular pressure conditions ZnO crystallizes in the hexagonal Wurtzite structure (figure 7a). The unit cell (fig 7b) has lattice parameters of $a = b = 3.25 \text{ \AA}$, $c = 5.2 \text{ \AA}$, and has no inversion symmetry. These characteristics give ZnO special properties like piezoelectricity and piroelectricity. Ionic binding predominates in the structure with tetrahedrally coordinated O^{2-} and Zn^{+2} ions along the c-axis (fig 7c). The c-axis is the preferred growth direction for the crystal structure, making it energetically favorable due to the higher energy polar of the $\{0,0,0,1\}$ plane [39].

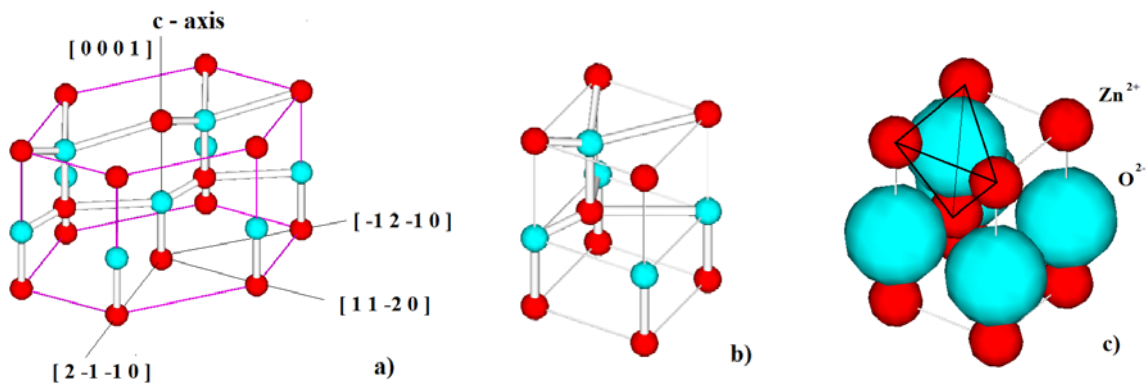


Figure 7 Zinc oxide: a) hexagonal Wurtzite structure, b) crystal unit cell, c) ionic tetrahedral arrangement.

Synthesis methods to grow ZnO nanostructured surfaces on substrates have proven to be low-cost and relatively simple in different techniques such as sputtering, electrochemical deposition and hydrothermal route synthesis [28, 40, 41].

The growth mechanism of ZnO nanorods through heating zinc nitrate hexahydrate with hexamethylenetetramine has recently been described by Zhao et al. [42]. They suggest that during the heating process, hexamethylenetetramine hydrolyzes and releases OH⁻ ions into solution, which then reacts with Zn²⁺ to form ZnO₂²⁻. ZnO crystallization then occurs from homogeneous precipitation under these mild conditions. Kim and coworkers [43] pointed out the optimal achievement of this hydrothermal method by the use of previously patterned substrates with ZnO seeds. They studied the effect of the seed layer thickness on the growth of the nanorods. This work studies the physisorption of urease on ZnO nanorods grown on ZnO seeded ITO substrates.

1.4.2 Polypyrrole and ferrocene.

1.4.2.1 Conductive polymers.

Conductive polymers have been the subject of interest for many years as suitable matrices for the immobilization of biomolecules as well as advantageous material in the fabrication of various kinds of transducers. Polymers were thought to be exclusively insulators, until the discovery of polysulphur nitride (inorganic), which exhibited conducting properties at low temperatures, and polyacetylene (organic), which became conductive when n-doped or p-doped. Organic

conjugated polymers (conductive polymers) are mostly based on rings (monomers) of carbon – carbon double and single bonds that form chain structures when polymerized.

These single and double bonds may have the ability to alternate their position along the chain when induced with electron movement via resonance in the presence of doping or current. Electronic configurations in these polymers are in the sp^2p_z arrangement with an extended π orbital system (fig 8c and 8d.). This structure differs from the regular covalent attachment model (fig 8a) that consist in a σ bonding configuration (fig 8b), offering a more stable structure, which lacks the conductivity offered by π bonding configuration.

The accumulation of the carbon bonds in the structure of the polymer provides an overlapping of the π orbitals delocating unpaired electrons caused by doping and promoting charge mobility through a conductive “backbone” (chain structure of the polymer) (fig 9a). When exposed to electrical induction, the polymer chain develops charge defects known as polarons, bipolarons, and in some cases, solitons [44].

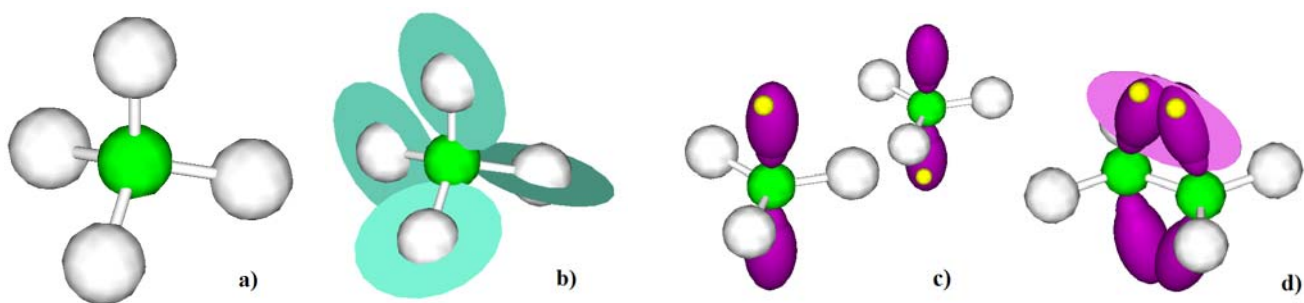


Figure 8 Carbon atom: a) regular tetrahedral configuration, b) σ bonding configuration, c) π orbital configuration orthogonal to the σ bonds, d) π bonding in a double bond.

When a neutral chain with a high energy binding configuration is oxidized, a delocalized π electron is removed producing a free radical and a positive charge (cation), bound together by resonance in the chain structure (fig 9b). This structural defect is known as polaron. Further oxidation of the polaron state removes the remaining π electron producing a second cation in the chain (fig 9c). These configurations are called bipolarons and are believed to occur in clusters of four monomers. The electron “hopping” in the polymer structure is thought to happen between bipolarons that create conduction bands in the material’s band gap [45]. These arrangements make conductive polymers potential electroactive species themselves for electrochemical experiments.

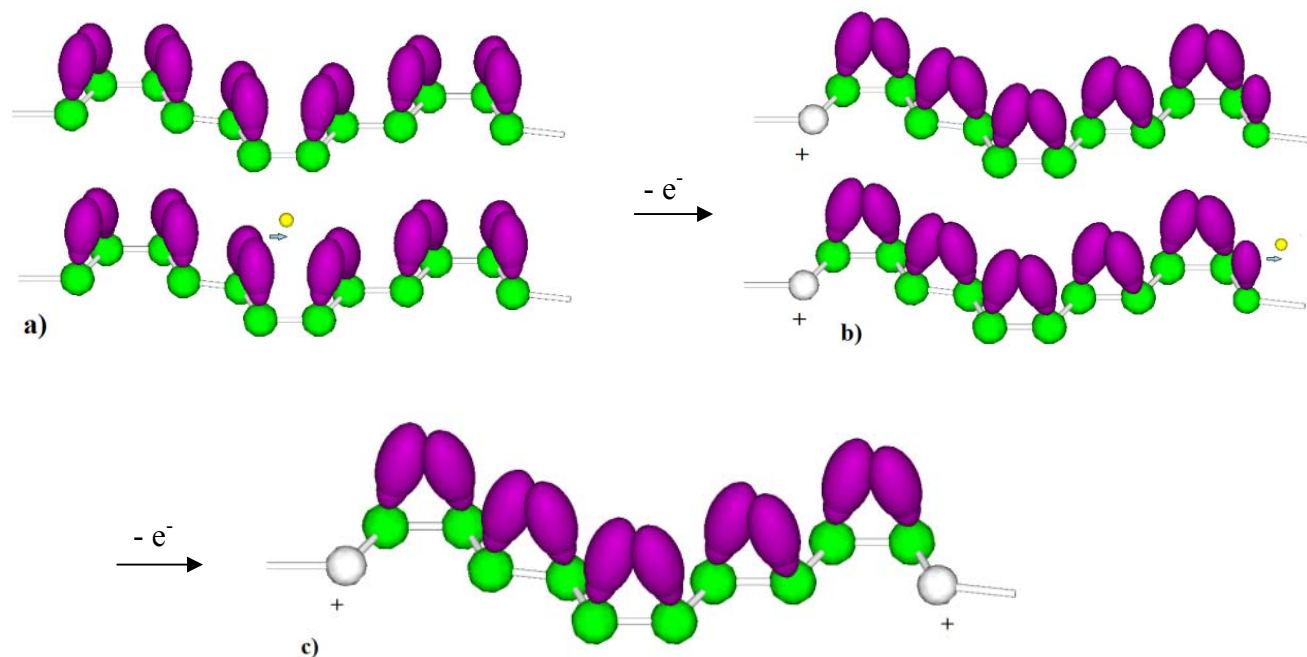


Figure 9 Conductive polymer’s backbone: a) neutral chain and subsequent electron removal, b) polaron state and subsequent electron removal, c) bipolaron state.

The chain structures of conductive polymers can be formed through electrochemical synthesis. This is an attractive feature for biosensing matrices, since a one step film deposition can be

achieved through this method, with either subsequent or instantaneous entrapment of the enzyme. Doping of the polymer, time and voltage of deposition provide easy control of film's characteristics like conductivity, thickness, morphology, spatial distribution of the enzyme and modulation of its activity.

Examples of the conductive polymer families include polyacetylene, polyaniline, polypyrrole, polyfluorine, poly (p-phenylene) etc. Polymers like polyaniline and polythiophene have good conductivity, but they polymerize at an acidic pH which is harsh for biomolecules. Polypyrrole can be polymerized at neutral pH making itself a suitable candidate for biomolecule immobilization.

1.4.2.2 Polypyrrole

Pyrrole (Py) is an aromatic five member ring (monomer) of chemical formula C_4H_4NH (fig 10a) containing two delocalized lone pair of electrons in the nitrogen atom. When electron removal (oxidation) is induced in the monomer, the pyrrole molecule acquires a structure with an NH^+ proton. This structure contains a resonance feature that can relocate the remaining unpaired electron along different positions within the ring providing two different resonance categories, the α - α' and β - β' positions (fig 10b). In a neutral chain structure configuration, dimension of each side of the pentagon is near 1.44 Å.

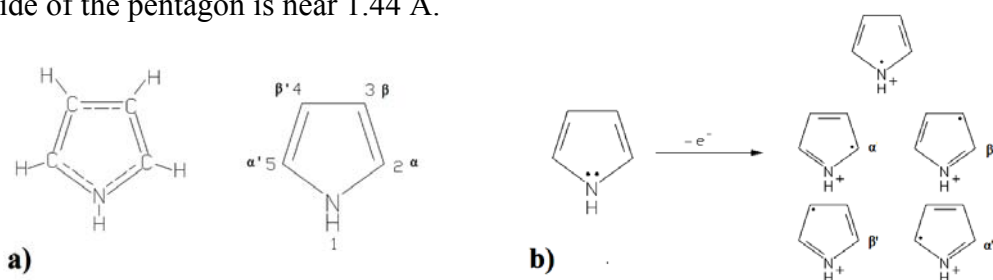
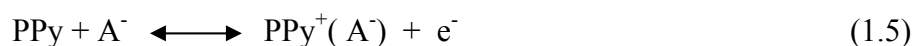


Figure 10 a) Pyrrole (Py) monomer, b) resonance configurations of Py.

Synthesis of polypyrrole (PPy) consists in oxidation of the monomers which causes their consecutive chemical binding until a polymerized chain is formed. Chain formation can be induced by chemical initiation with the use of oxidative agents, photo induced synthesis and electropolymerization [46]. Of all these, electrochemical deposition of PPy films over substrate surfaces has demonstrated better adhesion as well as a complete and uniform coverage of the desired surface. This method provides films with good electrical conductivity, and their fabrication in aqueous media can be exploited in environments that contain biomolecule activity.

Through electropolymerization, the monomer gets oxidized on the surface of the electrode by an applied anodic voltage. Prior to synthesis, it gets dissolved in an appropriate solvent containing a desired doping salt with a small mobile anion. After the voltage or current is applied, the insoluble polypyrrole precipitates onto the electrode. Insertion of the anion and associated solvent molecules (e.g. Cl⁻ anion from a KCl solution) increases its volume and represents 30 % of the polymer weight [47]. The reaction can be expressed as follows:



The polymerization mechanism theories of polypyrrole have been reviewed by Said et al. [48] and they depict oxidation of the monomer with a π orbital in the α position binding with a similar monomer, causing two hydrogen protons to be expelled from the structure, stabilizing the molecule into a dimer (fig 11). Subsequent oxidation of the dimer by the applied current repeats the process to form a trimer (three monomers) and so on until the polymerization is eventually quenched in the solvent. These polymer chains can be synthesized at neutral aqueous conditions,

and maintain their conductive properties. These features are ideal for biomolecular environments.

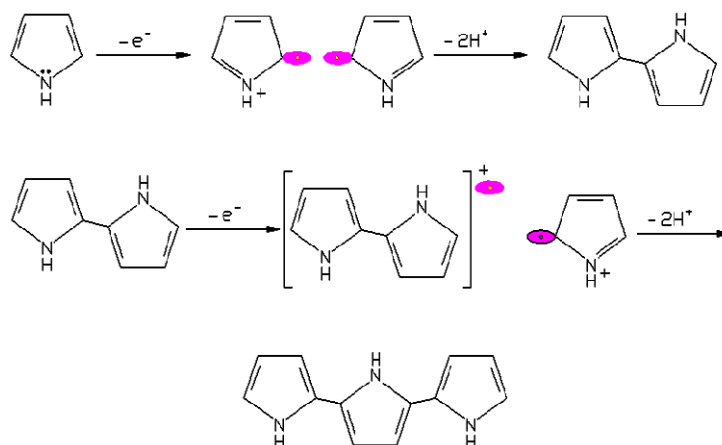


Figure 11 Electropolymerization of Py between 0.6 – 0.8 V versus Ag/AgCl.

Polypyrrole is a biocompatible material, meaning that it can interact with the biomolecule's activity without causing damage or adverse conditions. Biomolecules can easily be attached to polypyrrole by adsorption or entrapment during the electropolymerization step. Proper doping of polypyrrole produces permeability and permselectivity, making PPy a membrane capable of discriminating anions and cations [49]. This membrane also serves as a protective coating for the electrode against fouling and interfering species, which are mainly anions [50]. It might also be exploited as a redox mediator when an oxidoreductase enzyme gets entrapped between its conductive backbones net.

In addition, redox active groups such as porphyrins and ferrocene molecules have been used to enhance the electron transfer characteristics, important for the sensitivity of bioelectrodes, of the electroactive conducting polymers [51]. These nanoparticles can be incorporated into the polypyrrole matrix either by entrapment in the electropolymerization step, or by grafting of the

pyrrole molecule. Cross-linking of the nanoparticles with the monomer allows the fabrication of an enhanced nanocomposite material.

1.4.2.3 Ferrocene

Ferrocene (Fc) is an organometallic sandwich compound of chemical formula $\text{Fe}(\text{C}_5\text{H}_5)_2$. This special kind of compound consists of two cyclopentadienyl (Cp^-) ligand rings, C_5H_5^- (fig 12a), that bind at orthogonal opposite sites an iron atom of positive charge +2 (fig 12b). The binding nature of the structure resides between ionic and covalent binding between the d orbitals of the iron atom with the π electrons of the carbons. Resonance of Cp^- and lack of individual σ bonds make the rings freely rotate around their center in the ends of the orthogonal axis [52].

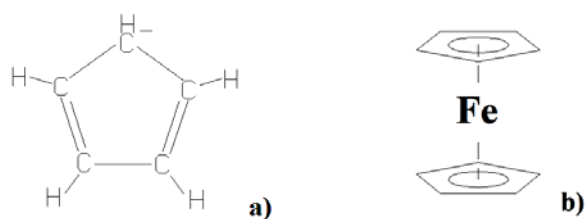


Figure 12 a) Cyclopentadienyl ion with a distance between the carbon atoms of 1.40 Å.

Ferrocene belongs to the chemical species known as metallocenes, and presents several features such as versatile synthetic chemistry and modification, accessible ferrocene/ferrocenium redox (oxidation/reduction) states, biocompatibility, high room temperature conductivity and strong adsorption of biomolecules. One of the important contributions of ferrocene to the field of material science has been its use as mediator for electrochemical sensors in a wide variety of biochemical applications.

Dramatic signal amplification can be achieved by linking a redox tracer such as ferrocene to the biorecognition element, as pendant group to the backbone of a conducting polymer, or just directly entrapped in the polymer matrix. Ferrocene and its derivatives have been a popular choice of mediators, since they fulfill most of the requirements as an ideal mediator in anaerobic redox-enzyme catalysis. Many challenges still need to be overcome to obtain a highly stable and reliable bioanalytical monitoring. The development of novel alternatives based on nanomaterials and nanostructured surfaces offer many possibilities for overcoming these challenges. One such example, is the improvement of electrical contact between the active center of enzymes and the electrode support.

A simple method to immobilize the enzyme along with the mediator is by electrodeposition of conducting polymers from solutions containing monomer (pyrrole), enzyme and mediator. In such configuration, the mediator has access to the redox site. However, there are a few problems in such mediated electrodes, the most serious of which is mediator leaching from the electrode surface, affecting both sensitivity and linearity [53]. One of the possible solutions to this is to functionalize the monomer with the redox mediator by covalently binding them. This alternative yields a high mediator concentration within the film, thereby obtaining an effective electron transfer.

1.4.2.4 Ferrocene modified pyrrole.

Incorporation of ferrocene into conductive polymer matrix by covalent binding (and in most of the entrapment cases) is done with the utilization of ferrocene derivatives [51] (fig 13). The functionalization can be performed on the monomer (pre-functionalization) or the PPy chain

(post-functionalization). Post-functionalization usually provides a polymeric chain with the metallocene bound on the outer surface layer. Pre-functionalization got the advantage of providing a greater and expanded concentration of Fc centers in the matrix, although electropolymerization of the monomer is not always achieved. Improvement on this matter has been seen when using longer reactive chains between ferrocene and the monomer.

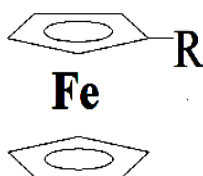


Figure 13 Ferrocene derivatives, where R = SO₃H, (CH₂)_n SO₃H, COOH, COCl, (CH₂)₆ Br, etc.

Simpler attachment of ferrocene can be processed in position 1 of pyrrole, since the hydrogen atom at nitrogen is the most reactive and can be easily substituted. One of the earliest methods of Fc-Py binding to this site was through the use of a CO-N bond, which can be achieved through the acylation synthetic methodology with the use of ferrocene carbonyl chloride in an organic solvent like acetonitrile (Fig 14 a). Post-functionalization through acylation was utilized for the first Fc conjugated polymer ever achieved [54] (Fig 14 b).

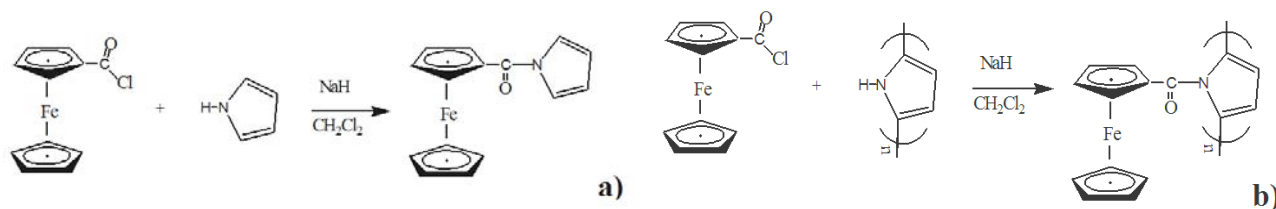


Figure 14 a) Pre-functionalization of Py through acylation, b) post-functionalization of PPy through acylation.

Binding methodology usually includes previous functionalization of either pure ferrocene or a derivative, as well as the use of a pyrrole derivative [55-57]. Although these processes secure the mediator, the film formed through the use of N-modified monomers may suffer from low conductivity and relatively thin formation. These flaws have been overcome by a subsequent copolymerization with the parent monomer.

We base our work in the methodologies presented above by modifying a derived pyrrole, 4-(1*H*-Pyrrol-1-yl)phenol (fig 15), with ferrocene. Then, we implement electrochemical copolymerization with the unmodified monomer, overcoming leaching problem of mediator and polymerization problems of the modified pyrrole. Glucose oxidase has also been included in polymerization entrapment to study the application of the film for glucose biosensing.

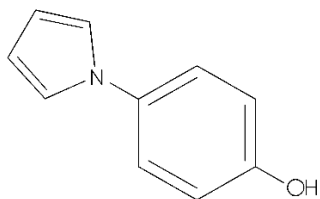


Figure 15 4-(1*H*-Pyrrol-1-yl)phenol

1.5 Literature Review.

1.5.1 Amperometric urea biosensors.

Although electrochemical potentiometric detection is used more often for urea biosensors [58], for it offers a simple measurement of the potential change in the electrode surface caused by the ion production during hydrolysis of urea, the literature review is based on the amperometric method utilized in this work, since it presents improvement in sensitivity, detection limit, response time, ease of fabrication and availability of instrumentation [59, 60, 62-66]. These types of sensor require an intermediate ion-sensitive mechanism to provide the electric signal.

Osakai, Katutani and Senda [59] worked a couple of sensor configurations based on a PVC nitrobenzene-dibenzo-18-crown-6 (DB18C6) gel electrode with specificity for ammonia ion. Electroreactivity of DB18C6 at an applied potential of 0.37 V depended on the amount of NH_4^+ attached to its functional groups. In one of the sensor designs, the electrode was covered with additional layers. Urease was cross-linked with glutaraldehyde to a gas-permeable Teflon membrane that allowed ammonia into an intermediate basic solution layer. There, the ammonia was partially changed to ammonia ion, and subsequent binding with the DB18C6 occurred. The response time of the sensor was 1 minute, and it maintained linearity in urea concentrations from $1\ \mu\text{M}$ to $2\ \text{mM}$.

Cho and Huang [60] used a Nafion covered glassy carbon electrode to electropolymerize a polyaniline film. Nafion is a ionic synthetic polymer with permeability towards cations. Also, sulfonate groups in Nafion serve as charge compensator and promote cation doping in the

electropolymerization process, as opposed to the usual anion doping of conductive polymers. A coenzyme solution of urease and bovine serum albumin (BSA) was cross-linked to the polymeric matrix via glutaraldehyde. BSA is an inert protein with functional groups that facilitate cross-linking, enhances robustness of the enzyme complex, and possess electron mediator properties [61]. The mechanism of the sensor consisted in the permeability of NH_4^+ through the membrane and doping of the backbone promoting electron expulsion. The biosensor presented a linear dynamic range of 0.5 μM to 1 mM for urea detection, with a response time between 40 and 120 seconds.

Massafera and Córdoba de Torresi [62] compared urease immobilization methods based on a bi-polymeric film composed of polypyrrole and poly(5-amino-1-naphtol). Both polymers were electrodeposited in the respective sequence over a platinum electrode. The first one was used as conductive mediator and the second one as permselective coatings against interferant anions. The methods compared were physical adsorption, entrapment under a cellulose layer, cross-linking with glutaraldehyde/ BSA, and covalently bound to the poly(5-NH₂-1-NAP) film. For covalent binding, chemical alteration of the polymer was performed by submerging the bi-polymeric electrode in a cyanuric chloride ethanolic solution. Optimal sensitivity was achieved through covalent binding with 3.44 $\mu\text{A}\text{mM}^{-1}$, and enhanced linearity of 0.34 – 100 mM occurred with the cross-linking method.

Pizzariello et al. [63] used the electrochemical properties of hematein, a natural dye added in the electrolyte solution of the cell that reacts with the change in pH caused by the hydrolysis of urea. Urease solution was mixed in a graphite composite paste and placed between a platinum

electrode and a membrane. Measurements at 45 mV (vs. AgCl) revealed a linear range of 10 μ M to 250 μ M, sensitivity of 1.95 μ AmM⁻¹ and a detection limit of 3 μ M.

Tiwari et al. [13] also used hematein as the signal inducer. Their method of urease immobilization was covalent utilizing a repetitive step of DDC/NHS chemistry. Functionalized gold nanoparticles with carboxyl groups were cross linked with amine functionalized H40polyester (H40-Au) via DDC/NHS. A solution containing the nanocomposite was drop coated on an indium tin oxide (ITO) glass coated substrate, covalently binding it on top of its surface by the amine branches of H40. Subsequent cross-linking of urease with the nanocomposite layer was performed utilizing once again the DDC/NHS method, thus covalently binding the urease with the substrate. A linear range of 10 μ M to 35mM was obtained with a sensitivity of 7.48 nAmM⁻¹, response time of 3 seconds and detection limit of 10 μ M.

Kaushik and Solanky [64] co-immobilized urease and glutamate dehydrogenase (GLDH) by physical interaction on a iron oxide-chitosan film deposited on an indium tin oxide coated glass substrate. The bi-enzyme solution was used to capitalize the redox center of GLDH that activates in the presence of the NH₄⁺ ion. Iron oxide (Fe₃O₄) nanoparticles were used as electron mediators while entrapped in a chitosan matrix. Chitosan solution dries into a copolymer with good adhesion and film forming characteristics. Presence of the nanoparticles in the composite material also enhanced the enzymes loading capacity of the matrix. As an additive electron mediator, the use of potassium ferrocyanide/ potassium ferrocyanate salts ([Fe(CN)₆]^{-3/-4}) are added in the solvent for electrochemical signal amplification. The biosensor exhibited urea

estimation between 1 to 17 mM with a detection limit of 0.3 mM, sensitivity of $12.5 \mu\text{A}\text{mM}^{-1}$ and response time of 10 seconds.

Solanki [23] utilized an approach with the same methodology to investigate the effect of ZnO nanoparticles. A chitosan solution containing ZnO nanoparticles was spin-coated on top on an indium tin oxide film to obtain a CH-ZnO nanocomposite film. Physisorption of urease and glutamate dehydrogenase was then performed along with urea measurements in $[\text{Fe}(\text{CN})_6]^{-3/4}$ solution. The sensor had linearity from 1 to 17 mM, a response time of 10 seconds, sensitivity of $0.13 \mu\text{A}\text{mM}^{-1}$ and detection limit of 0.5 mM.

Ansari et al. [65] studied the direct response of physisorbed urease on a nanostructured ZnO surface. Synthesis of ZnO powder was obtained for different concentrations of zinc acetate dehydrate with sodium hydroxide. Different crystalline nanostructures such as nanobelts and flower-like structures were obtained depending on the concentration of $\text{Zn}(\text{CH}_3\text{COO})_2 \cdot 2\text{H}_2\text{O}$ used. A thick film was prepared by mixing the ZnO powder with organic additives and deposited over an aluminum substrate. The substrate was immersed for 3 hours at 25°C in an urease containing solution for enzyme physisorption. Urea measurements with a detection time of 6 seconds were carried between concentrations of 1mM to 100 mM , with a decreased sensibility after 10 mM. A decrease in sensitivity was also observed with increase of the ZnO crystal structures. No other significant parameters were measured, and an explanation of the ionic interaction of the products with the ZnO electronic band-gap was provided. Further details about this mechanism will be discussed in chapter 4.

Performance characteristics of amperometric urea biosensor design aimed in this work are:

- a) Bioactivity preservation by the use of the physisorption method while maintaining robust stabilization.
- b) Faster response time under 6 seconds.
- c) Linearity inside the blood level range of 15 to 40 mg/dL.

Using these criteria, the papers revised do not completely fulfill our goals.

1.5.2 Polypyrrole/mediator matrices for amperometric glucose biosensors.

Use of polypyrrole has been a very convenient and elegant technique for glucose oxidase entrapment since early first generation glucose biosensors. This is due to the one-step incorporation of the enzyme into the matrix. Nonetheless, polypyrrole may go through over oxidation and suffer from conductivity loss on its properties and material degradation.

Fortier, Brassard and Bélanger [66] conducted an optimization experiment on the bio-film based on electrical conductivity and substrate/product kinetics, quantified with the Michaelis-Menten constant, K_m . The optimization parameters investigated were concentration of Py monomer and enzyme amount in the solution used for electropolymerization. With 0.01M KCl as the supporting electrolyte and a platinum electrode as the substrate, optimal conditions were found for a concentration of 0.3 M of pyrrole, 65 U/mL of glucose oxidase and film thickness of 0.17 μm . Glucose concentrations based on hydrogen peroxide detection were performed at an applied voltage of 0.65 mV. The biosensor performed measurements from 1 mM to 100 mM with linearity from 1 mM to 7.5 mM, response time of 30 seconds and K_m of 33.4 mM. Observations

about diffusional problems of hydrogen peroxide through the bulk of the polymeric film were remarked.

Kim and Gu [67] used similar settings for polypyrrole /Gox membrane on indium tin oxide substrate. For glucose measurements, their electrolyte solution contained p-quinone, an electron acceptor that acts as mediator, allowing an operational voltage of 0.350 V, thus a better study of the redox center and polypyrrole's π system dynamics. Their study included impedance measurements, showing a reduced conductivity of the film with increasing glucose oxidase concentrations due to the insulating nature of the enzyme's structure. It also observed pH changes during glucose measurements due to the expulsion of the H^+ proton by the oxidized Gox, affecting the isoelectric interaction between the film and the enzyme, thus its electrical communication. The K_m for the electrode obtained was 30.7 mM, suggesting no decrease of bioactivity by electrochemical coupling.

Berkkan et al. [68] investigated the biosensing properties of composite poly(pyrrole-2-aminobenzoic acid) by electropolymerizing a solution containing both pyrrole and 2-aminobenzoic acid, with subsequent covalent attachment of glucose oxidase to the film. Glucose estimation was performed at 0.7 V yielding a response time of 5 seconds, linear range of 3 to 40 mM and sensitivity of 58 nAmM^{-1} .

Tsai and coworkers [69] fabricated a polypyrrole-multi-walled carbon nanotubes composite via electropolymerization. This was achieved by previous functionalization of the carbon nanotubes in a sulfuric and nitric acid solution to form carboxyl groups on the tubes' surface. This provided

anionic charge to the MWCNT, to serve as dopants in the polymer formation, and gave them solubility in aqueous medium. MWCNT possesses mechanical strength and electric properties, thus an upgraded film was expected. Polymerization was performed on a glassy carbon electrode, using distilled water with the pyrrole monomer and a defined concentration of MWCNT's, with no supporting electrolyte. Glucose oxidase entrapment was performed by adding the enzyme to the solution prior to the electrochemical synthesis. Optimization of the amount of glucose oxidase in the solution was performed as well as response studies of PPy/MWCNT's films towards hydrogen peroxide. Glucose measurements were performed with the Gox/PPy/MWCNT's biosensor at 0.7 V yielding a response time of 8 seconds, sensitivity of 95 nAmM⁻¹ and linear range up to 4 mM.

Mala Ekanayake et al. [70] addressed hydrogen peroxide diffusional problems and amount of enzyme utilized by designing a polypyrrole nanotubes array deposited on a nonporous platinum substrate. The enzyme loading gets enhanced on nanostructured surfaces, and the bulk of the matrix gets diminished improving its diffusional properties. This structure was accomplished by controlling the electrodeposition time in a sodium tetrafluorophosphate electrolyte solution. Glucose oxidase was attached by the physisorption method. The sensor was able to operate at a lower voltage of 0.4 V with a sensitivity of 7.4 μAmM⁻¹, linear range of 0.5 mM to 10 mM, response time of 3 seconds and K_m of 7.01.

Ferrocene carboxylic acid (FCA) has been used as redox mediator by Tian and Zhu [71] in a bi-enzymatic amperometric glucose biosensor. For electrochemical synthesis of a glucose oxidase polypyrrole film, a substrate was fabricated with a conductive ceramic composite consisting of

graphite powder, horseradish peroxidase (HRP) and FCA. Hydrogen peroxide produced by Gox gets selectively reduced by peroxidase and subsequent reduction of the oxidized peroxidase is mediated through FCA. The sensor maintained enzyme loading, and operational voltage for glucose readings was achieved at 0.2 V. The response time of the biosensor was of 25 seconds, with linearity between 0.08 mM 1.3 mM.

One of the most cited and known work of glucose oxidase immobilized on a ferrocene modified polypyrrole belongs to Foulds and Lowe [55]. Two kinds of Fc-Py were synthesized from the use of N-(2-Cyanoethyl)pyrrole and ferrocenecarboxylic acid, and added to the working solutions in small volumes of acetonitrile (organic solvent). Films of both modified polypyrrole were achieved in platinum substrates, but exhibited thin films with low conductivity. For glucose oxidase entrapment during electropolymerization, 1mM of pyrrole monomer was included for robust conductive film formation. Glucose readings were performed at 0.3 V between 1 and 100 mM in the presence and absence of oxygen with defined linearity between 20 mM and 100 mM, and sensitivity of $0.625 \mu\text{A}\text{mM}^{-1}$. Oxygen dependence was found to be necessary for measurements after two days of fabrication.

Dicks et al. [72] conducted experiments on polypyrrole films-deposited gold microelectrodes. Dimethyl ferrocene was immobilized by adsorption on the polypyrrole film and tested for glucose biosensing with adsorbed glucose oxidase. Good responses were achieved, although eventual loss of the mediator occurred. Better stability was obtained by covalent binding of the film with ferrocene-carbonyl chloride.

Fiorito and Córdoba de Torresi [73] studied the direct use of ferrocene as electron mediator. Ferrocene presents insolubility in aqueous medium, covalent binding diminishes bioactivity and ferrocene-derivatives non-covalently attached to the substrate suffer from leaching of the electrode. Their approach consisted in using an ethanol ferrocene suspension mixed with an aqueous solution containing the enzyme and pyrrole monomer. The three components were successfully entrapped in an electropolymerization step, using a platinum substrate and potassium chloride as supporting electrolyte. Polymerization kinetics were slowed down by the presence of ethanol, but the enzyme electrode exposed a considerable increase in current response and lowering of operational voltage when compared to a plain Gox/polypyrrole electrode. Linearity from 1 mM to 10 mM was obtained at 0.4 V with a sensitivity of $0.23 \mu\text{AmM}^{-1}$.

Performance characteristics of ferrocene-modified polypyrrole glucose biosensor design aimed in this work are:

- a) Enzyme kinetics performance evidenced by a low Michaelis-Menten value under 2 mM.
- b) Preservation of redox mediator in matrix.
- c) Lowering of detection voltage under 250 mV.
- e) Faster response time under 10 seconds.
- e) Linearity inside the blood level range of 80 to 120 mg/dL.

Using this criteria, the papers revised do not completely fulfill our goals.

2 THEORETICAL BACKGROUND

This chapter presents the materials and methods along with theoretical background especially for electrochemical methods pertinent to characterization of synthesized bioelectrodes (specifically the matrix material) for biosensing applications presented in subsequent chapters 3 and 4.

2.1 Electrode material characterization.

The matrix material synthesized for bioelectrode preparation has been characterized for their structural, morphological and functional properties using X-Ray diffraction, FE-SEM, FTIR, and NMR. The following text discusses these techniques in brief.

2.1.1 X-Ray diffraction (XRD).

X-ray diffraction (XRD) is a technique which gives structural information of the desired materials. In this technique a directed X-ray beam hits the sample at a certain plane of a crystalline structure and the diffracted beam at a specific angle is used to identify the corresponding plane present in the structure using a detector. XRD is a powerful tool which along with structural parameters also gives strain state in crystal, strains at interface of thin films, crystallite size, phase composition amongst other analysis included with the advancement of technology [74]. Figure 16 shows the schematics of X-rays diffraction from crystalline planes in a diffraction experiment according to Bragg's law.

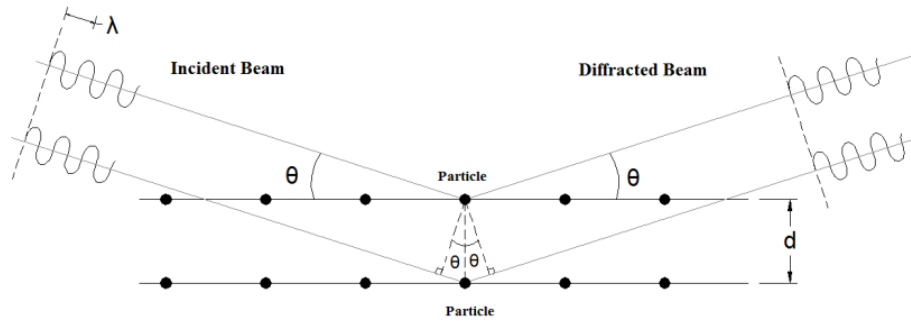


Figure 16 X-Ray diffraction process scheme.

Bragg's equation is

$$(2.1)$$

Where, λ is the wavelength of the X-ray, θ is angle of reflection also known as Bragg's angle, and d is interplanar distance. By varying the angle of angle of incident equipment can scan the different crystal planes which results in different reflection angles and thus identifying the specific crystal structure among 14- Bravias lattices.

The crystallite or grain size t of the particle can be estimated using the Scherrer's equation

$$\text{—————} (2.2)$$

Where, λ is the wavelength of x-rays used and β is full-width at half maximum (FWHM) and is calculated from the following relationship:

$$\text{—————} (2.3)$$

The overall effective size ε of the crystallite or grain under lattice strain τ could be calculated using following equation [75]:

$$\frac{\beta \cos \theta}{\lambda} = \frac{1}{\varepsilon} + \frac{\tau \sin \theta}{\lambda} \quad (2.4)$$

The overall particle size can be estimated from the linear extrapolation of a plot of $\beta \cos \theta / \lambda$ vs. $\sin \theta / \lambda$ to find the inverse of the intercept of $1 / \lambda$.

2.1.2 Scanning electron microscopy (SEM) and field emission scanning electron microscopy (FE-SEM).

The scanning electron microscopy (SEM) reveals external morphology (texture), chemical composition, and crystalline structure including orientation of materials in a specimen sample. An electron microscope utilizes a beam of energetic electrons to examine microstructures which are inaccessible due to limitation of light microscopy [76]. The essential components of an electron microscope is a tower with a high vacuum chamber containing an electron beam gun, magnetic coils, a sample holder, and electron sensors, as shown in schematics 17.

The energetic electron source gun is composed of a thermionic emitter that provides high energy electrons which are further accelerated using an external electric field. The electrons generated by the gun, called primary electrons, interact with the surface of the specimen through an impact that provokes a series of signals coming from backscattered electrons and secondary electrons forced out of the material's surface and used to recollect information about the sample. A special detector for the secondary electron signal is used to build a surface image. A column containing magnets between the gun and the sample is used to manipulate the direction of the electron beams, allowing the sample surface to be scanned point by point to create the image of the investigated portion of sample surface. The sample requires an electrically conductive surface.

When the material of interest is not of conductive nature, a gold coating is previously deposited on top of the surface, or else a conductive carbon tab is placed between the sample and the sample holder. Figure 18 shows a JEOL - JSM-5410 LV Scanning Electron Microscope.

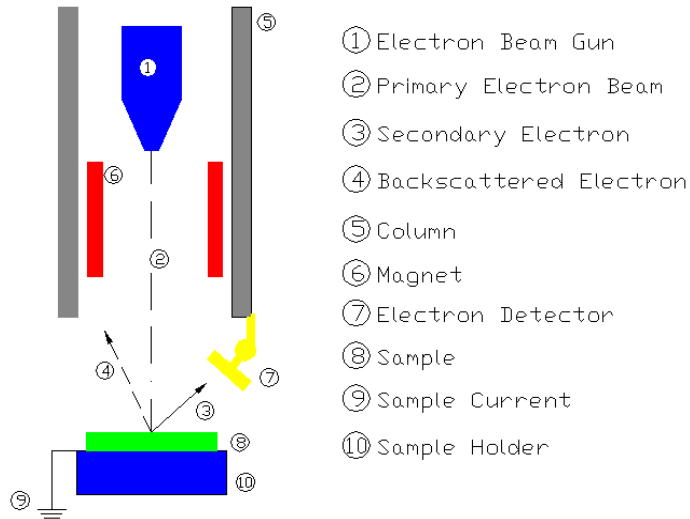


Figure 17 Configuration scheme of a scanning electron microscope.



Figure 18 JEOL - JSM-5410 LV Scanning electron microscope.

The image generated by SEM is used to obtain information concerning morphology, composition, particle size, surface topography and electrical conductivity. Figure 19 shows a scanning electron micrograph of nickel oxide nanoparticles [77].

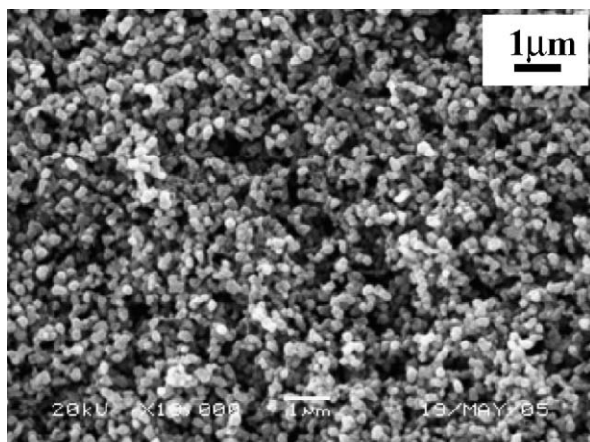


Figure 19 SEM image of nickel oxide nanoparticles (from reference 77).

In a traditional SEM, a high energy beam is used to achieve good resolution and small probe diameters with coated non-conductive materials, to avoid charging problems. Development of new materials such as polymers, carbon-hydrogen compounds and nano materials leads to the invention of field emission scanning electron microscopy (FESEM) because it was not possible to have true surface information by normal SEM as it uses high energy electron beam. In FESEM, on the other hand, cold electron source is employed as it is able to reveal the surface information from non-conducting nanostructures and soft materials without any conductive coatings. Figures 20(a) and 20(b) show the FE-SEM micrographs of ferrocene chloride magnetic hollow spheres and aluminum oxide nanorods, respectively [78,79].

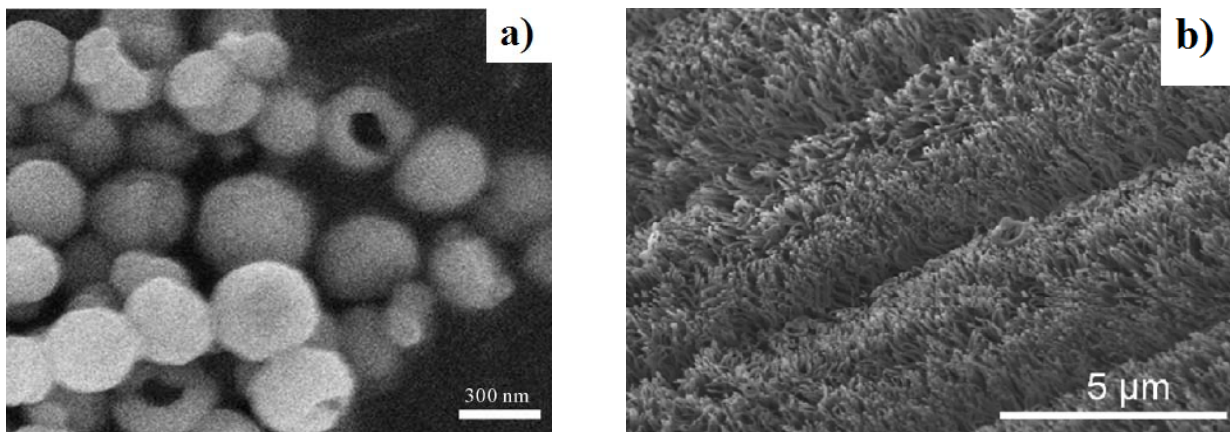


Figure 20 FE-SEM images of a) ferrocene chloride magnetic hollow spheres, b) aluminum oxide nano brushes (from references 78 and 79).

2.1.3 Fourier transform infrared (FT-IR) spectroscopic measurements.

Fourier transform infrared (FT-IR) spectroscopy is an analytical technique used to identify organic (and in some cases inorganic) materials [80]. It measures the absorption of various infrared frequencies by the specimen from material of interest. These infrared absorption bands identify specific molecular components and structural aspect of the specimen. In order for a vibration mode in a molecule to be IR active, it must be associated with changes in the permanent dipole [81].

To characterize the desired electrodes, FT-IR spectra (Chapter III) of Polypyrrole –Ferrocene has been recorded with a Bruker instrument, model IFS 66v/S. For each sample, the FT-IR spectrum has been recorded over 10 scans with wave number resolution of 2 cm^{-1} . To avoid the interference from the CO_2 and water, IR chamber is flushed with nitrogen and fresh background has been recorded and utilized prior to recording spectra of sample. Also the sample is dried carefully to minimize the water interference. Figure 21 shows a typical FT-IR spectrum of

polystyrene recorded for calibration testing wherein the characteristic peaks at 3080, 3059, 1600, 1582 and 1028 cm^{-1} , respectively, confirm the material as polystyrene.

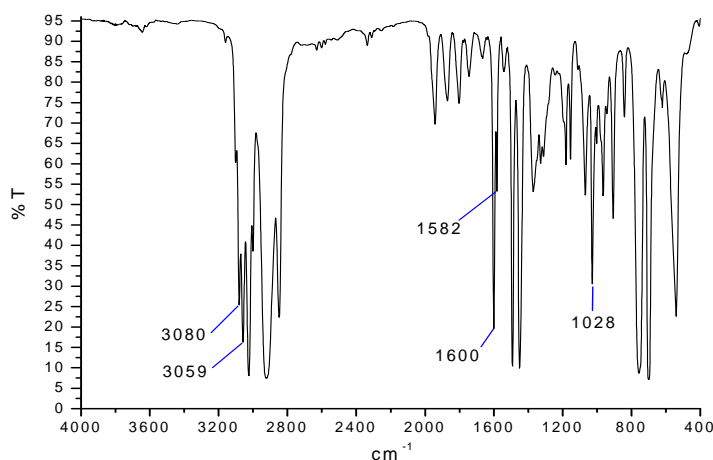


Figure 21 FT-IR spectra of polystyrene film.

2.1.4 Nuclear magnetic resonance (NMR) spectroscopy.

Nuclear magnetic resonance (NMR) spectroscopy, exploits the magnetic properties of certain atomic nuclei to determine physical and chemical properties of atoms or the molecules and provides information about the structure, dynamics, reaction state, and chemical environment of molecules. The principle on which this method is based consists in the application of a magnetic field to the atom. Relaxation energy generated by the NMR active nuclei of ^1H and ^{13}C in a magnetic field absorbs electromagnetic radiation and generates a coupling frequency between protons cluster which gets registered in an output spectra. In order to obtain information about the chemical environment interference of the magnetic field to the nucleus is calculated from the surrounding electron density [82].

Figure 22 shows a typical ^1H NMR spectrum of ethanol with the peaks derived from the coupling between its methyl (CH_3) and methylene (CH_2) groups [83]. The spacing between the peaks of

the methyl triplet are equal to the spacing between the peaks of the methylene quartet. This spacing is measured in Hertz and is called the coupling constant, J.

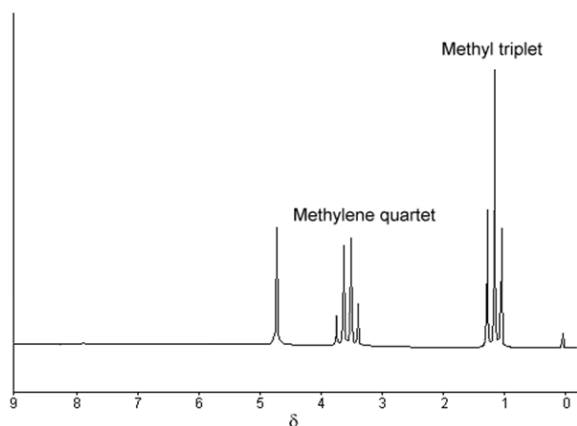


Figure 22 ¹H NMR spectrum of ethanol (from reference 83).

2.2 Electrochemical measurements.

Electrochemical methods are based on interaction between chemical and electrical processes that occur at a boundary between electrolyte and electrode surface [9]. Potentiodynamic and potentiostatic are the two major measurements involved in electrochemical methods. Electrochemical detection is based on monitoring changes of an electrical signal due to an electrochemical reaction at an electrode surface, usually as a result of an applied potential or current. In a solution, the equilibrium concentrations of the reduced and oxidized forms of a redox couple are linked to the potential (E) via the Nernst's Equation.

$$E = E_o + \frac{RT}{nF} \ln \frac{C_{ox}}{C_{red}} \quad (2.5)$$

where F is Faraday's constant (96487), R the gas constant (8.314 JK⁻¹mol⁻¹), T is absolute temperature, C_{ox} and C_{red} are concentrations of oxidation and reduction centers. For each redox

couple, there exists a potential, known as the standard potential E_0 at which the reduced and oxidized forms are present at equal concentrations. If the potential E with respect to the reference electrode is applied to the working electrode, e.g. by the use of a potentiostat, the redox couples present at the electrode respond to this change and adjust their concentration ratios according to equation 2.5 [8].

For reference electrodes, a characteristic constant potential is maintained independent of the potential derived from the reactions in the solution. This is achieved by a constant composition of a redox couple, as in the silver-silver chloride electrode, whose reaction can be expressed as follows:



The electrode is isolated from the solution and the potential derived from the interaction between the Ag/AgCl couple is used as the point of reference for the voltage produced in the working electrode during the electrochemical reactions.

Reactions at the surface of the working electrode include mass transport of the electroactive species to the electrode surface, transfer of electrons at the interface and transport of the products back to the bulk solution. The first two interactions play a more significant role in the rate of the reactions and in providing current relationships to the analyte concentrations. The rate of the reaction can be governed either by the rate of mass transport or by the rate of the electron transfer, depending mainly on the time limiting one.

2.2.1 Mass-transport limited reactions.

Limitation by mass transport implies an easy electron transfer process and the rate of the reaction can be measured in terms of mass flux to the electrode [8], J (mol cm⁻² s⁻¹), in a thermodynamic relation using the Nernst-Planck equation:

$$J(x, t) = -D \frac{dC(x,t)}{dx} - \frac{zFDC}{RT} \frac{d\phi(x,t)}{dx} + C(x, t)V(x, t) \quad (2.7)$$

(a) (b) (c)

where D is the diffusion coefficient (cm² s⁻¹), C is the concentration of the electroactive species (mol cm⁻²), z is the ion charge and $d\phi(x,t)/dx$ the potential gradient. This equation quantifies the three kind of categories found for mass transport in an electrochemical cell:

a) Diffusion: spontaneous movement from regions of high concentrations to regions of lower ones; b) Migration: movement of charged particles (ions) along an electrical field; c) Convection: flowing or stirring of the solution produces an induced physical movement of substances.

The current derived from the concentration ratio C_{ox}/C_{red} is known as the Faradic current, and it is associated with rate of the redox reaction. When generated by mass transport, Faradic current in an electrode of area A (cm²) can be correlated by the following equation:

$$i = - nFAJ \quad (2.8)$$

Use of excess of inert salts as electrolyte in the solution can suppress the electromigration in the flux (part b), while no induced convection and the use of a no reactive solution suppress the third part of the flux equation (part c) . Thus the current can be expressed as

$$i = nFAD \frac{\partial C(x,t)}{\partial x} \quad (2.9)$$

The solution of this partial differential equation provides a proportional relationship between the current and the square root of time, known as Nernstian behavior [8].

2.2.2 Electron-transfer limited reactions.

When the mass transport occurs at a sufficiently fast rate or the electron transfer possesses kinetic limitations, the faradic current is measured in terms of the rate of electron transfer with the Butler-Volmer equation:

$$i = nFk_s \left\{ C_{\text{ox}}(0, t) \exp \left[\frac{-\alpha nF(E-E^0)}{RT} \right] - C_{\text{red}}(0, t) \exp \left[\frac{(1-\alpha)nF(E-E^0)}{RT} \right] \right\} \quad (2.10)$$

k_s is the standard heterogeneous rate constant between the reactant and the electrode material, and α is the transfer coefficient. The transfer coefficient is the difference between the potential energy (E) and the vibrational kinetic energy generated by the electrons at the moment of the redox process [84]. These parameters can be estimated through amperometric experiments as explained further below in section 2.3.1.

2.2.3 Electric double layer.

Besides electron transfer across the interface, electrodes in contact with an electrolyte solution also possess a charge q spread over its surface, directly proportional to the potential difference E across the cell:

$$q = CE \quad (2.11)$$

where C is the capacitance (in Farads). This charge attracts ions of opposite signs from the solution that form a layer which acts as a condenser, called the electrical double-layer.

The electrical double layer consists of two layers known as the compact and diffusive layers. The first one consists of adsorbed ions to the surface of the electrode, while the second one is conformed of scattered ions attracted to the surface by long range Coulombic forces. Figure 23(a) depicts a double layer arrangement for the interface between a metal electrode and an electrolyte solution. This arrangement of ions prevails as long as a concentrated electrolyte solution is maintained, preventing the ions in the diffusive layers to completely escape the double layer as a cause of thermal motion. Double layer arrangements for semiconductors contain lesser amounts of permittivity and charge-carrier concentrations, with a diffusive double layer on the inside of the material known as the space-charge region (fig 24 b).

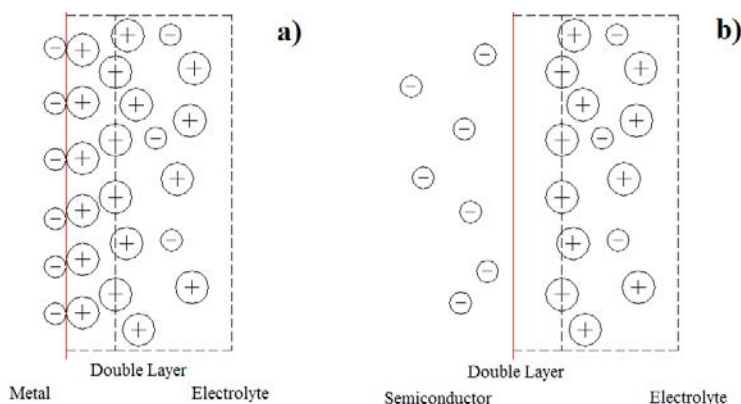


Figure 23 Electrical double-layer: a) metal- electrolyte interface, b) semiconductor-electrolyte interface.

When the electrode is initially submerged in the electrolyte solution, no charge is present in the double layer, and the voltage present in the interface is known as the zero charge potential, E_{pzc} .

When exposed to a potential change, the acquired charge will be expressed as:

$$q = C_{dl}A(E - E_{pzc}) \quad (2.12)$$

where C_{dl} is the capacitance per unit area and usually is in the range of 10-40 $\mu\text{F}/\text{cm}^2$. Change in voltage across the capacitor (or possible change in capacitance) produces a current increase since:

$$i = \frac{dq}{dt} = C_{dl}A \frac{dE}{dt} + A(E - E_{pzc}) \frac{dC_{dl}}{dt} \quad (2.13)$$

where dE/dt is the potential scan rate and dC_{dl}/dt occurs when ion adsorption changes the double layer capacitance [84]. This increase is followed by a rapid drop characteristic of a charging current (non faradic), until its merging with the Faradic current corresponding to the redox reaction.

2.3 Amperometric measurements.

2.3.1 Cyclic voltammetry.

Cyclic voltammetry is an electrochemical measurement technique in the potentiodynamic category. It consists of a bi-directional potential sweep over the working electrode, while measuring the change in current derived with respect to the change in voltage. The current-voltage plot is called a voltammogram, and it provides a rapid location of the redox potentials of the electroactive species, and can be used to evaluate the redox process. Figure 24 shows the cyclic voltammogram of 5 mM potassium ferro-ferricyanide redox couple in phosphate buffer saline (PBS) (pH 7.0, 50 mM, 0.9% NaCl) using an Autolab (EcoChemie, Netherlands)

Potentiostat/Galvanostat with indium tin oxide (ITO) coated glass as working electrode, silver/silver-chloride as reference electrode and platinum wire as counter electrode.

For a voltammogram, a current response is measured in a potential window, starting at an initial value and varying the potential in a linear manner with respect to time up to a limiting value. As the potential approaches the characteristic E° of the redox process, the current starts to increase significantly until the potential reaches the oxidation potential of the analyte. After this point, it falls off as the concentration of the analyte is depleted close to the electrode surface. At this potential, which should be at least $90/n$ mV beyond the peak, the direction of the potential scan is reversed, and the same potential window is scanned in the opposite direction. As the applied potential is reversed, it will reach a potential where the reduction of product formed during forward scan starts producing a current of reverse polarity from the forward scan. These potentials are called the peak potentials, and they are the potentials needed to overcome the barrier activation energy G_a of the material's electrons.

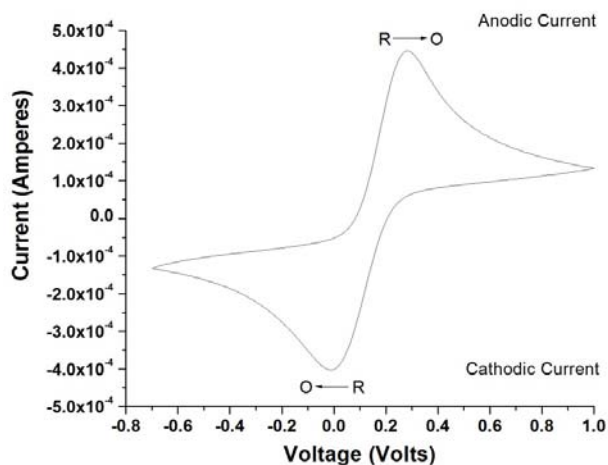


Figure 24 Cyclic voltammogram of 5 mM potassium ferro-ferricyanide redox couple on ITO working electrode in PBS (pH 7.0, 50 mM, 0.9% NaCl).

Redox processes are divided into reversible or mass transport limited, quasi reversible, and irreversible, which are those with sluggish electron exchange. For a process to be reversible, the oxidation and reduction peaks in the voltammogram have to present a separation ΔE_p of $\frac{59}{n} mV$ and $i_a = i_c$. Peak potentials are independent of the scan rate and the voltammograms can also possess several distinct peaks for multielectron-transfer processes, occurring at different potentials. Figure 25 shows cyclic voltammograms at different scan rates of a nickel oxide film deposited on an ITO coated glass working electrode. Diffusion-less reversible processes can be obtained in surface confined species, evidenced by a linear dependence between the peak currents and the scan rates, as shown in inset a of figure 25.

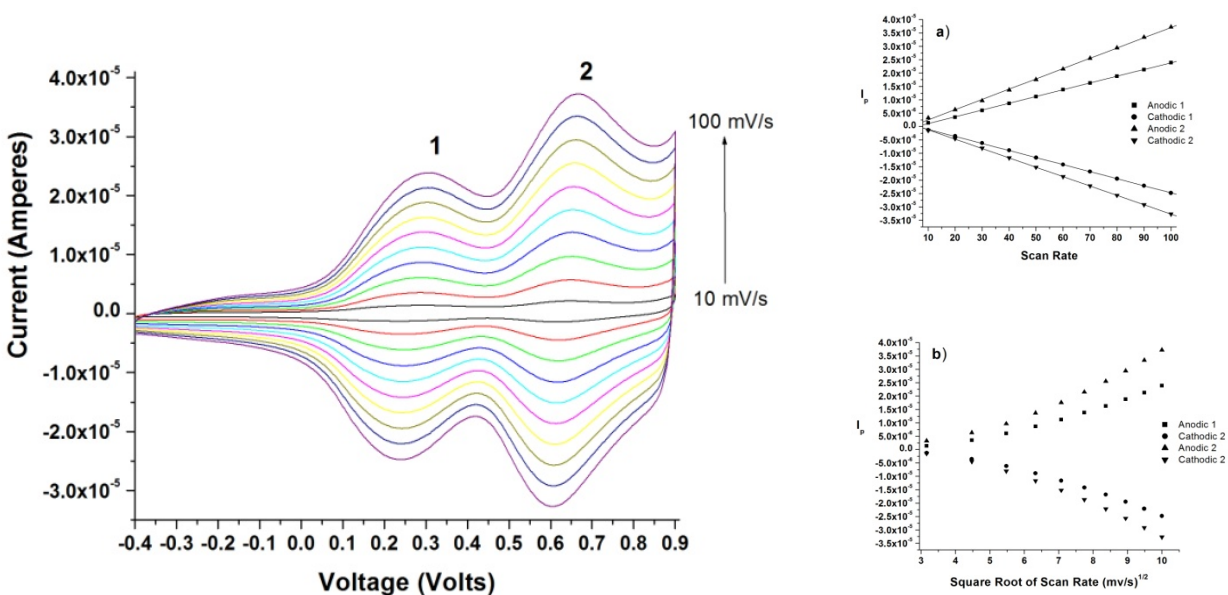


Figure 25 Cyclic voltammograms of nickel oxide film on ITO coated electrode at different scan

Electrochemical processes that possess a linear dependence of the peak currents towards variation of the square root of the scan rates (Nernstian behavior), can be treated under the

assumption of a reversible system as well, where the standard potential is the average of the peak potentials.

$$E_o = \frac{E_a + E_p}{2} \quad (2.14)$$

Characteristic of quasi-reversible systems is the divergence of the oxidation and reduction peaks towards higher and lower voltage values, respectively, with increase in potential scan rate. This behavior indicates a limitation in charge transfer kinetics, and in these cases, electron transfer rate also plays a role as the limiting factor in the reaction. Figure 26 shows cyclic voltammograms of 5 mM potassium ferro-ferricyanide redox couple in phosphate buffer saline on an indium tin oxide (ITO) coated glass as working electrode.

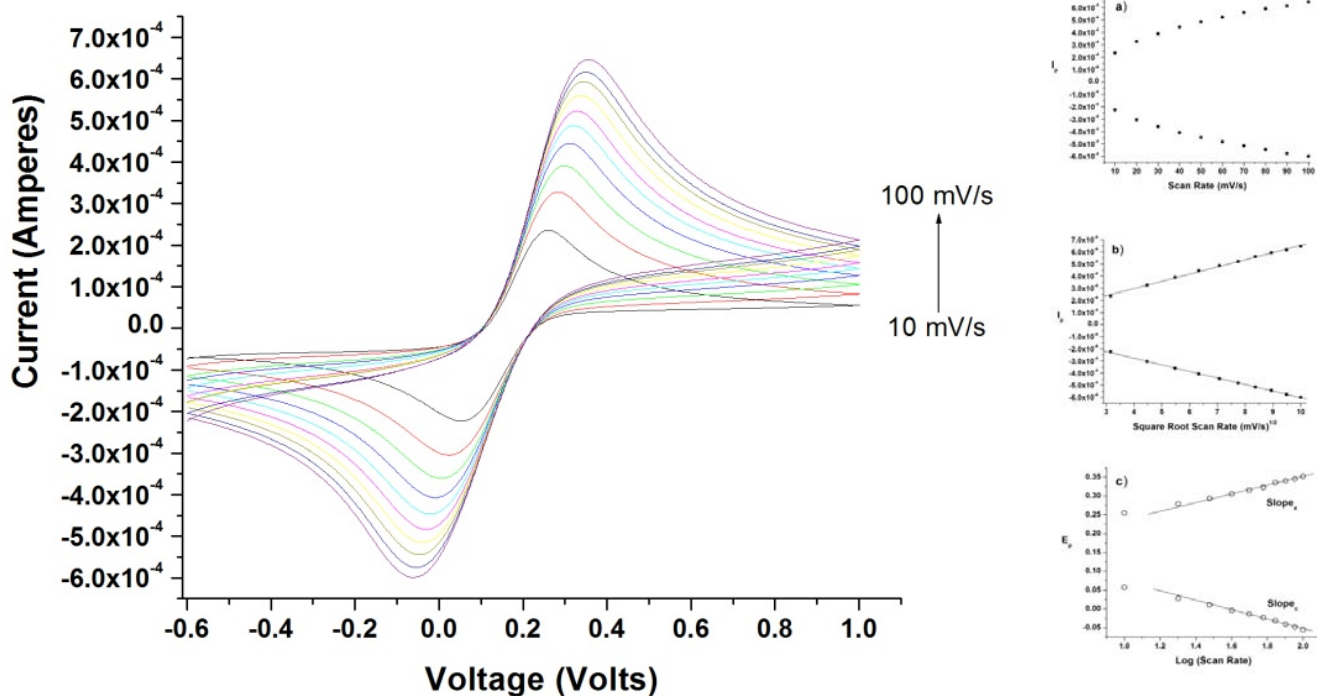


Figure 26 a) Cyclic voltammograms of 5 mM potassium ferro-ferricyanide redox couple on ITO working electrode at different scan rates; b) Peak current vs. scan rate; c) Peak current vs. square root of scan rate; d) Peak Potential vs. log of scan rate.

Inset b presents the Nernstian behavior of the system evidenced in the linear dependence with the square root of the scan rate. Still, quantification of the electron transfer reaction is necessary since the system is quasi-reversible, as evidenced by the diverging peaks.

Rate transfer constants and transfer coefficients can be obtained for the electrochemical reaction of a system with any degree of reversibility when voltammograms obtained with a ΔE_p greater than $200/n$ mV are available [85]. These relationships are directly derived from the Butler-Volmer equation (2.10). Inset c on figure 26 shows the peak potentials as a function of the logarithm of the scan rates. The slopes of the straight lines, formed with the data under the above criteria, are used to find the transfer coefficients α_a and α_c using the following relationships:

$$\text{Slope}_a = 2.3RT/(1 - \alpha_a)nF \quad (2.15a)$$

$$\text{Slope}_c = -2.3RT/\alpha_cnF \quad (2.15b)$$

The heterogeneous rate transfer constant is obtained through the following equation:

$$k_s = \alpha_cnFv_c/RT = (1-\alpha_a)nFv_a/RT \quad (2.16)$$

This identity is derived at the moment the reaction is at the standard potential, thus $k_s = k_a = k_c$.

For quasi-reversible systems, k_s is in the range of 10^{-1} to 10^{-5} .

2.3.2. Nernstian redox processes on deposited films.

The variation in the potential of scan rate can be used to provide data regarding surface concentration of material confined in the surface of the working electrode and evaluation of the mass diffusion processes, as long as the Nernstian behavior is maintained. Figure 27 shows

cyclic voltammograms at relatively low scan rates of polypyrrole film deposited on a platinum working electrode. Insets a and b show the peak currents dependence to the scan rate (\square) and the square root of the scan rate ($\square^{1/2}$), respectively.

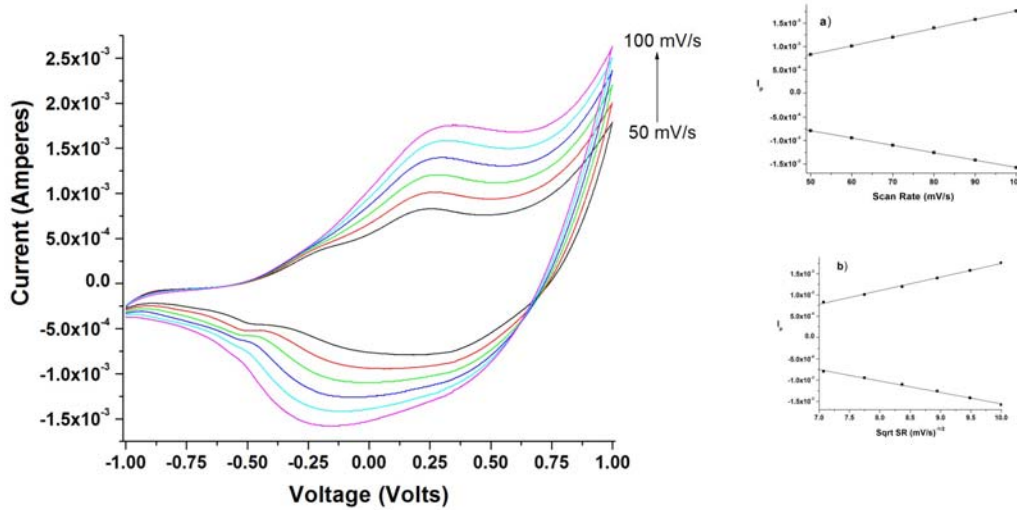


Figure 27 Cyclic voltammograms of deposited polypyrrole film on platinum coated electrode at different scan rates in PBS. Inset a) Peak current vs. scan rate. b) Peak current vs. square root of scan rate.

Linear dependence to scan rate variation of anodic and cathodic peaks is typical for adsorbed species. This behavior illustrates that the materials are well cramped on the working electrode [86]. The surface coverage of a monolayer can be calculated for low scan rates as long as a $\square^{1/2}$ dependence is provided. The relationship for the peak current is given by the Brown-Anson model [65]:

$$i_p = \frac{n^2 F^2 C A v}{4RT} \quad (2.17)$$

where i_p is the peak current at the given scan rate, in Amperes, \square is the scan rate in Volts/second, A is the area of the electrode in cm^2 , and C is the surface concentration of the monolayer, in

mol/ cm². The diffusion coefficient of the electroactive species in the electrode can be found from the Randles-Svick equation:

$$i_p = (2.69 \times 10^5)n^{3/2}ACD^{1/2}v^{1/2} \quad (2.18)$$

where D is the diffusion coefficient in cm²/s.

2.3.3 Constant-potential amperometry.

Constant potential amperometry is the simplest of the electrochemical potentiostatic measurements. For this experiment, a potential is selected where consumption of an analyte occurs during electrolysis. This potential can be investigated by a previous cyclic voltammetry scan, and is chosen close to one of the potential peaks of the process, where electron transfer is facilitated, thus providing a mass transfer limitation [87]. Figure 28 shows a potential step applied at the surface of an ITO electrode in PBS solution from 0.0 volts to 0.6 volts. Such a potential step, E, across the double layer of the electrode produces a charging current, i_{cc} known as the background current, calculated with the following relationship:

$$i_{cc} = \frac{E}{R_{soln}} e^{-t/R_{ct}Cdl} \quad (2.19)$$

where R_{soln} is the solution resistance and R_{ct} is the charge-transfer resistance. This charging current is negligible after the first 50 milliseconds of the potential step. Current associated with diffusion in the electrode surface due to the potential step is expected to decay with time as given by the Cottrell equation:

$$i = \frac{nFACD^{1/2}}{\pi^{1/2}t^{1/2}} \quad (2.20)$$

After the capacitance gets stabilized at the surface and currents associated with the electrode's material are dissipated, the current signal of the analyte oxidation or reduction can be obtained, because only a single potential is maintained. Figure 28 b shows the current response to the potential step applied to the ITO electrode surface, with subsequent additions of 1 mM hydrogen peroxide to the PBS solution. The chosen potential step of 0.6 volts corresponds to the electrolysis potential of H_2O_2 , which provides a current associated with its concentration gradient in the electrode's surface. The current is proportional to the concentration of the analyte and can be continuously measured at the electrode. This characteristic of constant potential amperometry offers an improved temporal resolution of an electrochemical event over other techniques, useful to determine the response time of the biosensor.

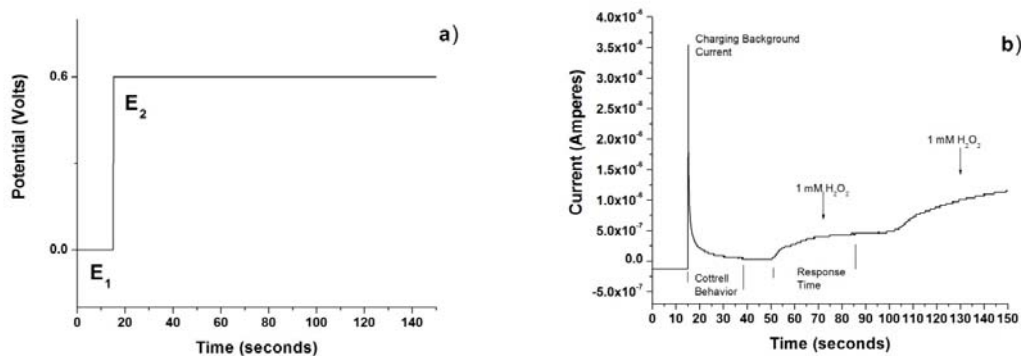


Figure 28 a) Voltage step from 0 V to 0.6 V and b) amperometric response at constant potential.

2.4 Parameters related to the performance of biosensors.

2.4.1 Linear range, sensitivity and Michaelis-Menten constant (K_m).

The linear range shows a linear response of bioelectrode with variation of biomolecule concentration. The linear range in this work is determined by the bioelectrode response using amperometric measurements. The sensitivity is estimated from the slope of the linearity curve.

The value of K_m , which gives indication of the enzyme-substrate kinetics, is determined by the analysis of the enzymatic reaction. The constant K_m for the bound enzyme can be lower or higher than that for purified enzyme depending on the changes occurring in the conformation of enzyme after its binding on the solid support. This constant determines the affinity of the enzyme for its substrate. A smaller value of K_m indicates an increased affinity of the enzyme for its substrate.

This parameter can be estimated by using a Lineweaver-Burke plot.

The Lineweaver-Burke plot is a graph of the inverse of the peak current response versus the inverse of the analyte concentration. In the Lineweaver-Burke plot, inverse of X-axis intercept gives the value of K_m . Figure 29 presents a linearization curve of glucose measurements performed with a biosensor fabricated with entrapment of glucose oxidase in a polypyrrole matrix deposited on a platinum working electrode. The amperometric response was recorded in phosphate buffer solution at 0.6 Volts and the measurements in the plot include the standard deviation error bars. Inset is the Lineweaver-Burk of the recorded data.

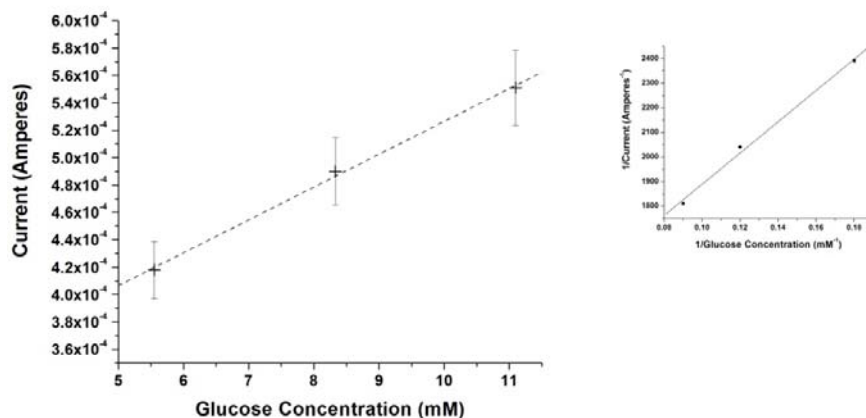


Figure 29 Amperometric response linearization of Gox/PPy bioelectrode to different concentrations.

2.4.2 Detection limit.

The detection limit of the bioelectrode is calculated using the 3σ criteria in the linearity plot of current vs. analyte concentration, using the following equation [88]:

$$\text{Detection limit} = 3\sigma/m \quad (2.21)$$

where σ is the standard deviation of the blank signal and m is the sensitivity of the electrode.

2.4.3 Effect of pH.

Optimization of the working pH and temperature for the enzyme electrode are important. The ability of amino acids present at the active sites of the enzyme to interact with the substrate depends on their electrostatic state, which in turn depends on the pH of the solution. To find the optimum pH, activity of the bioelectrode is investigated within a pH range to obtain an improved current response.

2.4.4 Amount of immobilized enzyme.

The amount of immobilized enzyme can be derived from the response provided by the interaction at the enzyme-substrate complex. This amount is derived from the Langmuir isotherm and a quasi-steady-state approximation of the enzyme kinetics [89].

$$C_E = C_{ES} \frac{\left(\frac{1}{K_m} C_S\right)}{\left(1 + \left(\frac{1}{K_m} C_S\right)\right)} \quad (2.22a)$$

where C_E is the concentration amount of enzyme, C_{ES} is the concentration amount of the enzyme-substrate complex and C_S is that of the substrate, which is the analyte of interest for the biosensor. At sufficiently high amounts of analyte, the biosensor starts reaching a saturation point at the end of its linearity range. At this point, the amount of enzyme concentration equals the amount of enzyme-substrate complex.

$$C_E = C_{ES} \quad (2.22b)$$

This concentration can be estimated using a cyclic voltammogram response to a high analyte concentration, with the help of the Brown-Anson equation (2.17).

3 POLY(PYRROLE-N-FERROCENE-PYRROLE) COPOLYMER FILM FOR GLUCOSE BIOSENSING

This chapter presents the current work of the synthesis and characterization of ferrocene modified 4-(1H-Pyrrol-1-yl)phenol, Py-Fc, along its electrical co-polymerization with pyrrole, Py. Electropolymerized copolymer of pyrrole and ferrocenecarboxylate modified pyrrole P(Py-FcPy) on indium-tin-oxide (ITO) coated glass surface has been used to fabricate an electrochemical glucose biosensor. Glucose oxidase (Gox) was entrapped in P(Py-FcPy) through electro-deposition. The Gox-P(Py-FcPy)/ITO bio-electrodes were utilized for the estimation of glucose concentration in standard solutions using cyclic voltammetry and amperometric response.

3.1 Materials and methods.

3.1.1 Materials used.

Glucose oxidase {(E.C.1.3.4), type VII, from aspergillum niger, 162000 units/g solid}, Glucose, pyridine, 4-(1H-Pyrrol-1-yl)phenol, ferrocenecarboxylic acid, hexane, ethanol, sodium sulfate, potassium chloride, silica gel, and Indium-tin-oxide (ITO) coated glass (15-25 W/sq.) were obtained from Sigma-Aldrich and used as received. Pyrrole and dichloromethane (DCM) from Sigma-Aldrich were distilled before use. All solutions were prepared using deionized water of resistivity no less than 17 M Ω cm (Milli-Q, USA). The solution of Gox (1 mg/ml) was prepared freshly in phosphate buffer (50 mM, pH 7.0) prior to being used. Stock solution of glucose was prepared fresh in deionized water.

3.1.2 Synthesis of 4-(1H-Pyrrol-1-yl)phenyl ferrocenecarboxylate (“FcPy”).

All reactions were performed at room temperature under an atmosphere of dry nitrogen using schlenk glassware or a glove box, unless otherwise stated. Reaction vessels were flame dried under a stream of nitrogen, and anhydrous solvents were transferred by oven-dried syringes or cannula. DCM was dried and deoxygenated by distillation over calcium hydride under nitrogen. The synthesis of FcPy was carried out using modified method reported in literature [56, 57]. To obtain the acyl chloride, ferrocenecarboxylic acid (0.23g, 0.001 mol) was dissolved in 20 mL dry DCM and oxalyl chloride (130 mL, 0.0015 mol) was added drop wise. The reaction was carried out for six to eight hours to get dark red color product and monitored using NMR. The synthesis at NMR facility of ferrocene modified 4-(1H-Pyrrol-1-yl)phenol was characterized using ^1H NMR, ^{13}C NMR and FTIR in Chemistry Department at University of Puerto Rico Mayagüez Campus.

For the etherification, 4-(1H-Pyrrol-1-yl) phenol (0.1592 g, 0.001 mol) and pyridine (161.0 μL , 0.002 mol) were dissolved in 40 mL DCM. The ferrocenecarboxyl chloride was added drop wise and the reaction was carried out overnight. Three consecutive extractions with 0.01M HCl were carried out after completion. Organic phase was dried over sodium sulfate and celite was used to remove insoluble impurities. The ester was purified by column chromatography using silica gel and DCM. The product was re-crystallized with hexane to obtain golden flakes like crystals. Figure 30 shows the schematic for the 4-(1H-Pyrrol-1-yl) phenyl ferrocenecarboxylate synthesis.

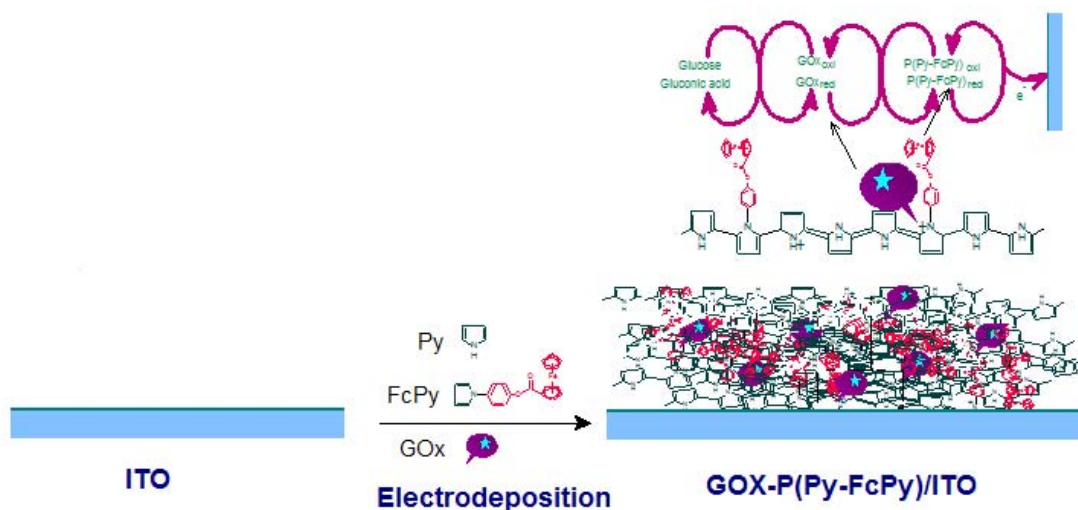


Figure 31 Fabrication route of Gox-P(Py-Fc-Py)/ITO bioelectrode and glucose detection mechanism.

3.2 Results and discussion.

3.2.1 4-(1H-Pyrrol-1-yl)phenyl ferrocenecarboxylate (“FcPy”).

Figure 32 shows the ¹H NMR spectra of (a) 4-(1H-Pyrrol-1-yl) phenol and (b) 4-(1H-Pyrrol-1-yl) phenyl ferrocenecarboxylate. NMR studies were carried out using 500 MHz Bruker spectrometer.

¹H NMR (500MHz, CDCl₃): d(ppm) 4.983[t, 2H, 3J(H, H) = 1.7 Hz, A2B2; Cp], 4.529[t, 2H, 3J(H, H) = 1.7 Hz; A2B2; Cp], 4.324[s, 5H, Cp], 6.367[d, 2H, 3J (H, H)=2.0], 7.085[d, 2H, 3J (H, H)=2.0], 7.446[d, 2H, 3J (H, H)=8.8], 7.455 [d, 2H, 3J (H, H)=8.8].

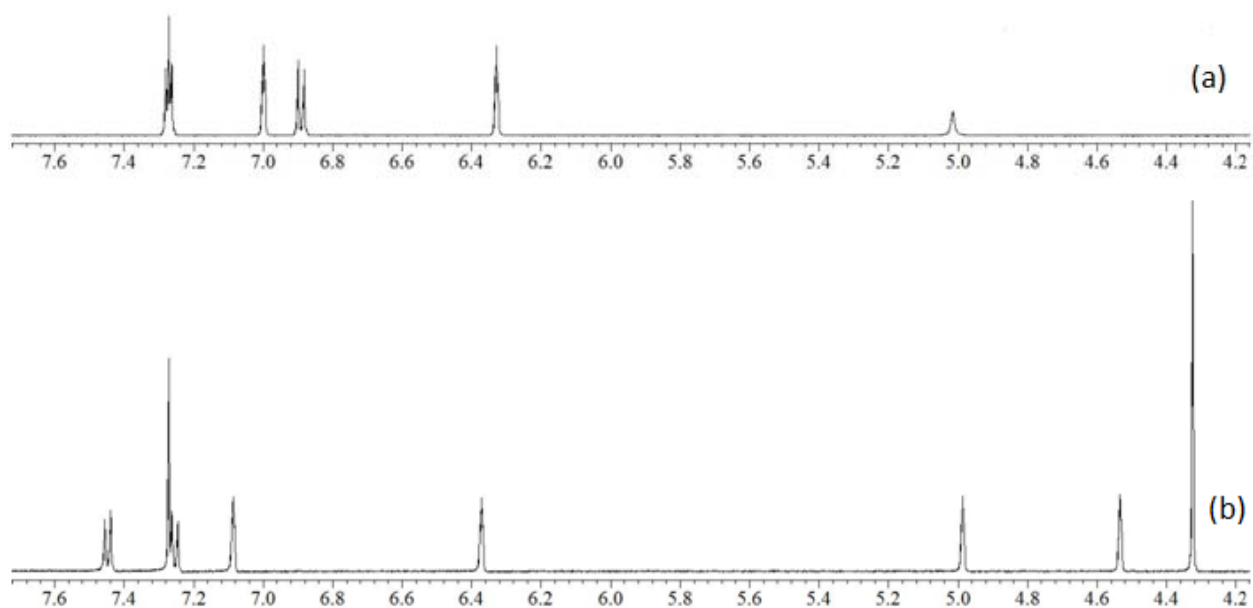


Figure 32 ^1H NMR spectra of (a) 4-(1H-Pyrrol-1-yl) phenol and (b) 4-(1H-Pyrrol-1-yl) phenyl ferrocenecarboxylate.

Disappearance of the HO- hydrogen signal (Fig 32 b) at ~ 5.0 ppm, the upfield change of the four peaks at the aromatic region, and the appearance of the ferrocene peaks at 4.983 ppm, 4.529 ppm and 4.324 ppm indicate the ester formation between the ferrocene carboxylic acid and the 4-(1H-Pyrrol-1-yl)phenol.

Figure 33 shows ^{13}C NMR spectra of 4-(1H-Pyrrol-1-yl) phenyl ferrocenecarboxylate.

^{13}C NMR(125MHz, CDCl_3): d(ppm) 170.59 (C=O), 151.06, 138.59, 123.00, 121.84, 119.79, 110.70, 72.28, 70.90, 70.21. The signal at 170.6 ppm in spectrum reveals the presence of the ester functional group.

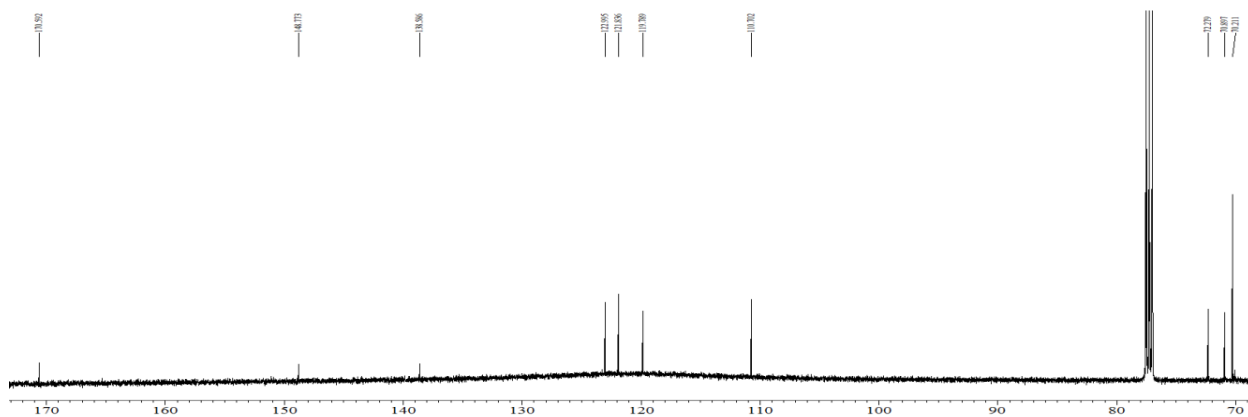


Figure 33 ^{13}C NMR spectra of 4-(1H-Pyrrol-1-yl) phenyl ferrocenecarboxylate.

Figure 34 shows FTIR spectra of 4-(1H-Pyrrol-1-yl) phenyl ferrocenecarboxylate.

FTIR (KBr, cm^{-1}): 3151, 3091, 1736, 1526, 1452, 1269, 1221, 1112, 726. An IR peak at 1736 cm^{-1} corresponds to the ester functional group of the compound [90].

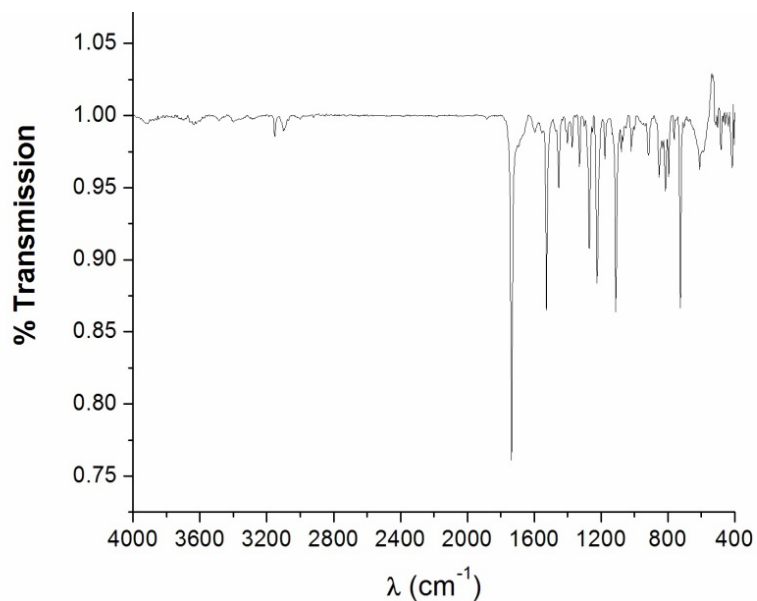


Figure 34 FTIR: 4(1H-pyrrol-yl)phenyl ferrocenecarboxylate.

Elemental formula for 4-(1H-Pyrrol-1-yl) phenyl ferrocenecarboxylate can be expressed as $\text{C}_{21}\text{H}_{17}\text{O}_2\text{NFe}$, where a mass of one mole is expected to be 371.21 g. This enhances considerably

the molecular weight of the ferrocene complex, thus eliminating any possible leaching problem when incorporated in a polymeric matrix. The composition of the compound is often expressed in terms of the weight percent of each element in the compound. The calculated composition of compound by percent of mass for carbon, hydrogen and nitrogen are 67.94, 4.67 and 3.77, respectively. Elemental analysis of the compound was experimentally confirmed by Atlantic Microlab Inc. with 67.67% for carbon, 4.43% for hydrogen and 3.68% for nitrogen. The provided sheet of the experimental results is included in appendix A.

Fig 35 a shows CV spectra of the P(Py-FcPy)/ITO film in PBS (50 mM, pH 7.0) at a scan rate of 75 mV/s. A well-defined anodic peak observed at 400 mV and cathodic peak at -100 mV are attributed to the oxidation and reduction of ferrocene moiety present in the modified pyrrole molecules, respectively. Presence of separation of these peaks confirms the incorporation of the FcPy molecule in the copolymer that makes the P(Py-FcPy) system quasi reversible.

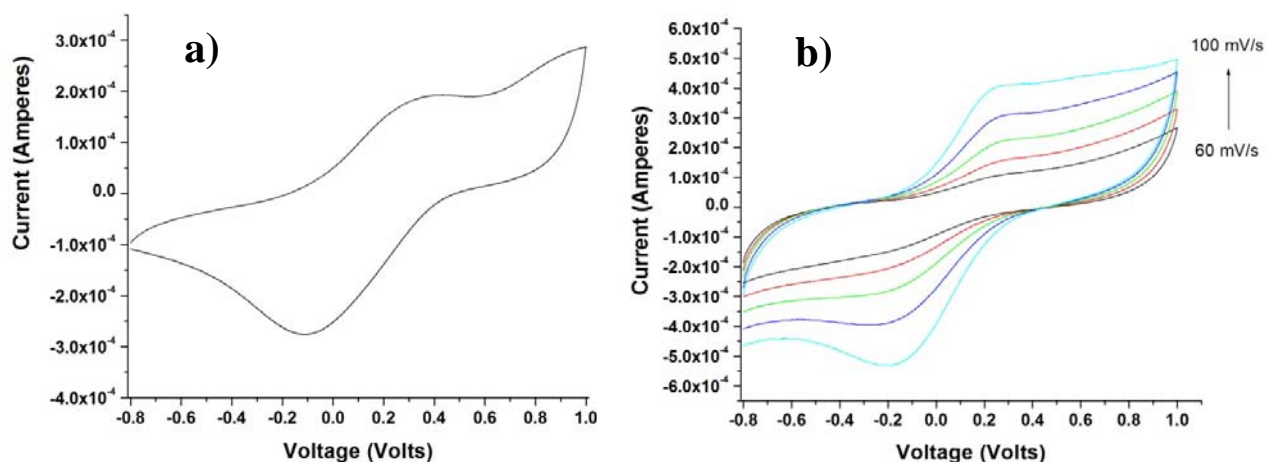


Figure 35 a) Cyclic voltammogram of P(Py-FcPy) electrodes at 75 mV/s in PBS (50mM, 0.9% NaCl), b) Cyclic voltammogram spectra in the same buffer at different scan rates.

The electrode's electrochemical properties has been tested on a solution containing 5mM potassium ferro-ferricyanide redox couple in phosphate buffer saline. Figure 36 presents the CV spectra at different scan rates in a $K^{3-/4}$ PBS solution.

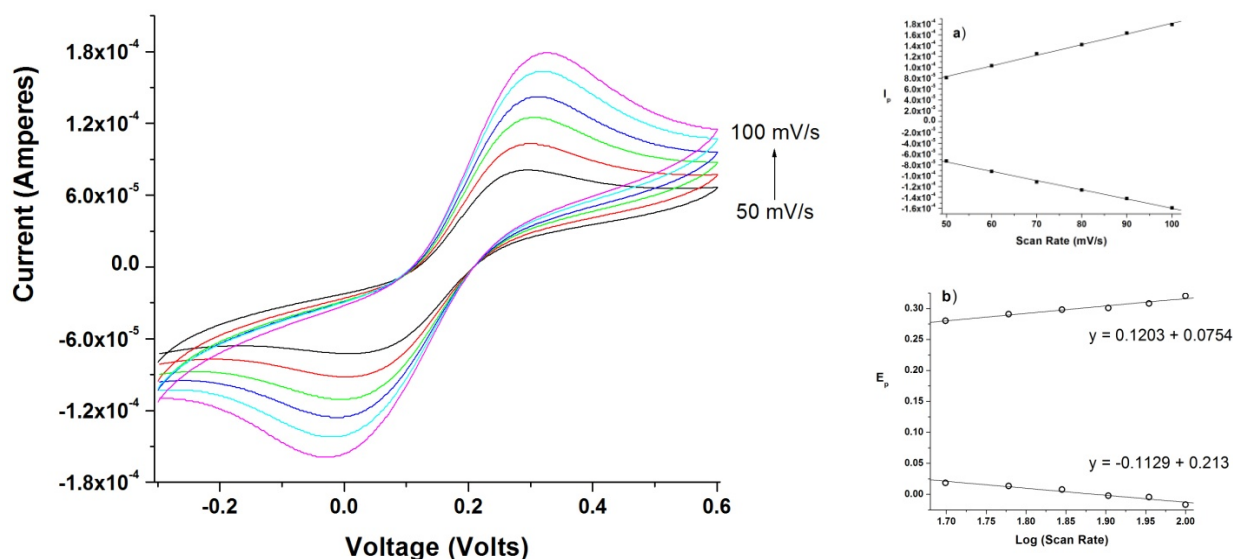


Figure 36 Cyclic voltammograms of P(Py-FcPy)/ITO electrode at different scan rates in a solution containing 5 mM ferro-ferricyanide redox couple in PBS (pH 7.0, 50 mM, 0.9% NaCl). Inset a) Peak current vs. scan rate; b) Peak Voltage vs. Log(Scan Rate).

It is clear from the figure that the magnitude of current response increases with increasing scan rate and exhibit a linear relationship with it (inset a). This suggests thin layer electrochemistry with surface controlled electrochemical process. These studies suggest that the P(Py-FcPy) based matrices can provide a useful matrix for mediator free electrochemical biosensors [91]. Inset b) shows the peak potentials vs. log (scan rate), used to calculate the film's transfer coefficient α , and the rate transfer constant k . They were found to be 0.51 and 1.96 cm/s respectively, for a scan rate of 100 mV/s.

3.2.2 Gox-P(Py-FcPy) bioelectrode.

Figure 37 presents SEM micrographs of glucose oxidase entrapped through electropolymerization in a) polypyrrole film and b) P(Py-FcPy) copolymer film.

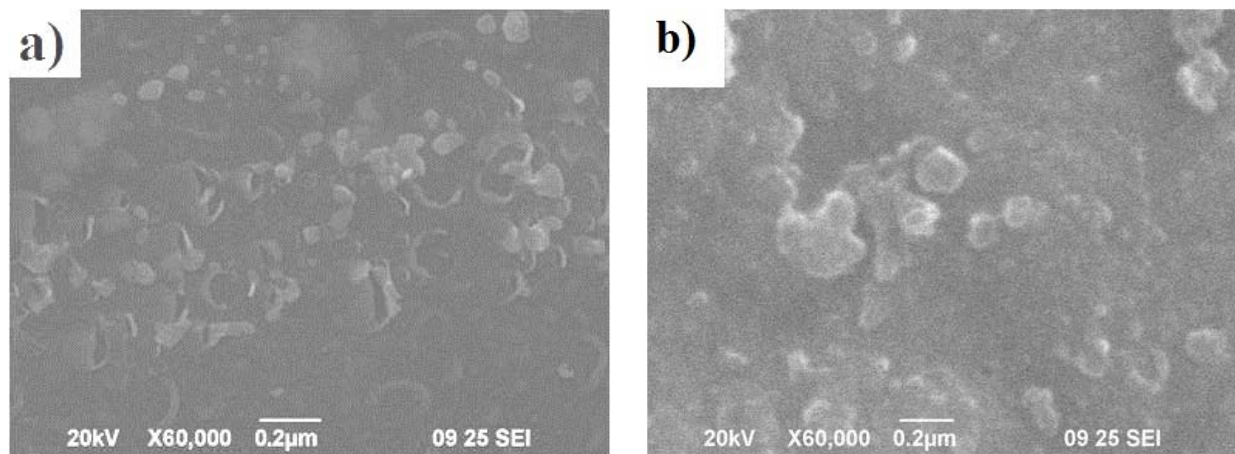


Figure 37 SEM micrographs of glucose oxidase entrapped in a) PPy film, b) P(Py-FcPy) film.

Although the insulating nature of Gox causes a low brightening intensity of the image, some conductivity provided by the polypyrrole films allows the appreciation of the enzyme entrapped in the film, as well as morphology exposition, with a rough surface typical of polypyrrole. Micrograph in figure 37 b suggests incorporation of the ferrocene moiety in the polymeric film as bigger clusters of entrapped enzyme can be appreciated by possible enhancement of the structure's loading capability.

The pH value of measuring solution results in great influence on biosensor as the acidity or basicity of solution affect the active site of bound enzyme. CV studies at 100 mV/s in PBS were carried out to check the pH effect in the range of 4.0 to 9.0 on the Gox-P(Py-FcPy) film. Figure 38 shows the oxidation current response at different pH. These values suggest that the

bioelectrodes exhibit maximum activity at around pH 7.0, providing optimal performance in a biocompatible environment. This can be attributed to the presence of polypyrrole as conducting material, whose optimal performance occurs at neutral pH. All experiments were thus carried out at pH 7.0.

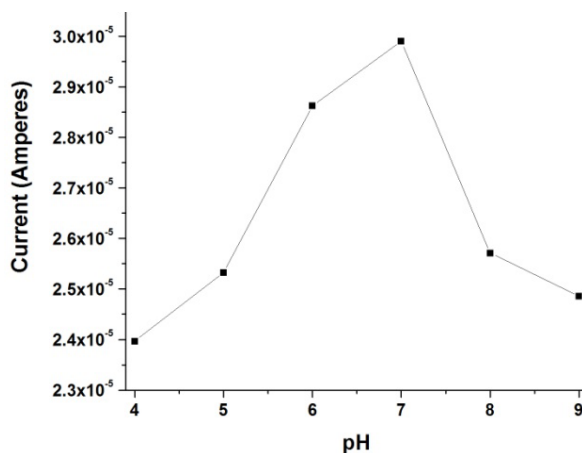


Figure 38 Response of Gox- P(Py-FcPy) bioelectrode at different pH in PBS (50 mM, 0.9%NaCl).

For glucose estimation, CV experiments have been conducted in the range of -0.6 to 1.1 V at 100 mV/s after the incubation of the bio-electrode for 10 s in 10 mL PBS buffer solution containing 100 μ L desired glucose concentration. Figure 39 shows cyclic voltammetry spectra for different concentration of glucose on the Gox-P(Py-FcPy)/ITO bioelectrode. It is clear from the figure that oxidation current increases with increasing concentration of glucose and can be attributed to the increasing enzymatic product formation and redox process of ferrocene molecule present in the matrix. Concentration of the amount of enzyme entrapped in the film was estimated using the peak current generated in the presence of 11.1 mM glucose using the Brown-Anson equation. The estimated amount of glucose oxidase (molecular weight; 1.6×10^5 g/mol) was estimated to be 4.62×10^{-9} mol/cm² on 0.77 cm² area films. It is important to remark the accentuation of the oxidation peaks and narrowing of the distance between the peak potentials, evidencing the

electrical coupling between the redox center of the enzyme and ferrocene moiety that facilitates electron transfer.

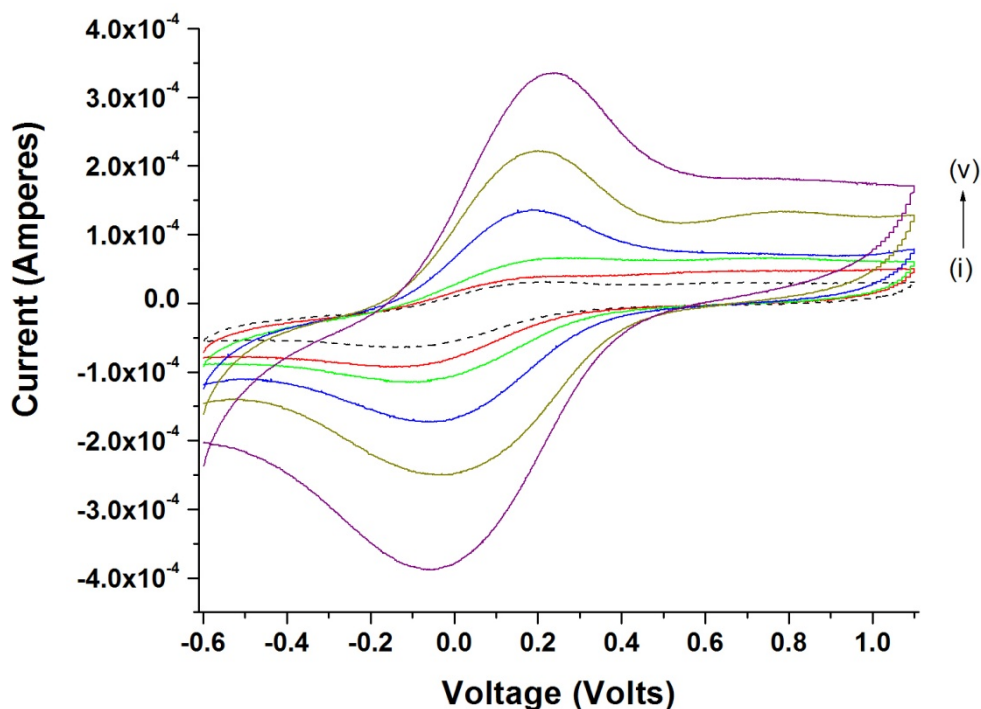


Figure 39 CV spectra of Gox-P(Py-FcPy) bioelectrode in PBS (50 mM, pH 7.0) at 100mV/sec for glucose concentrations: (- - -) buffer, (i) 1.4 mM, (ii) 2.8 mM, (iii) 5.6 mM, (vi) 8.4 mM and (v) 11.2 mM.

Amperometric studies were also carried out at operating potential of 175 mV for glucose estimation. This operating potential was chosen since it is close to the peak voltage of the reaction and it helps eliminate electrochemical interference of other analytes present in the solution. Figure 40 shows the amperometric response of Gox-P(Py-FcPy)/ITO bioelectrode for sequential addition of 2.8 mM glucose solution with stirring steps. It is clear from the figure that for every addition of glucose concentration, more than 90% of increase in current response is achieved in 2 to 5 sec thus indicating fast response of Gox-P(Py-FcPy)/ITO bioelectrode. Further with amperometric technique glucose can be estimated from 2.8 mM up to 16.8 mM. Linear current response with concentration (inset a) reveals that the bioelectrode can be used to estimate

glucose concentration in the range of 2.8 to 16.8 mM with a blank standard deviation of 0.345 μA . The sensitivity was found to be 2.28 $\mu\text{A}/\text{mM}$ with a lower detection limit of 0.45 mM.

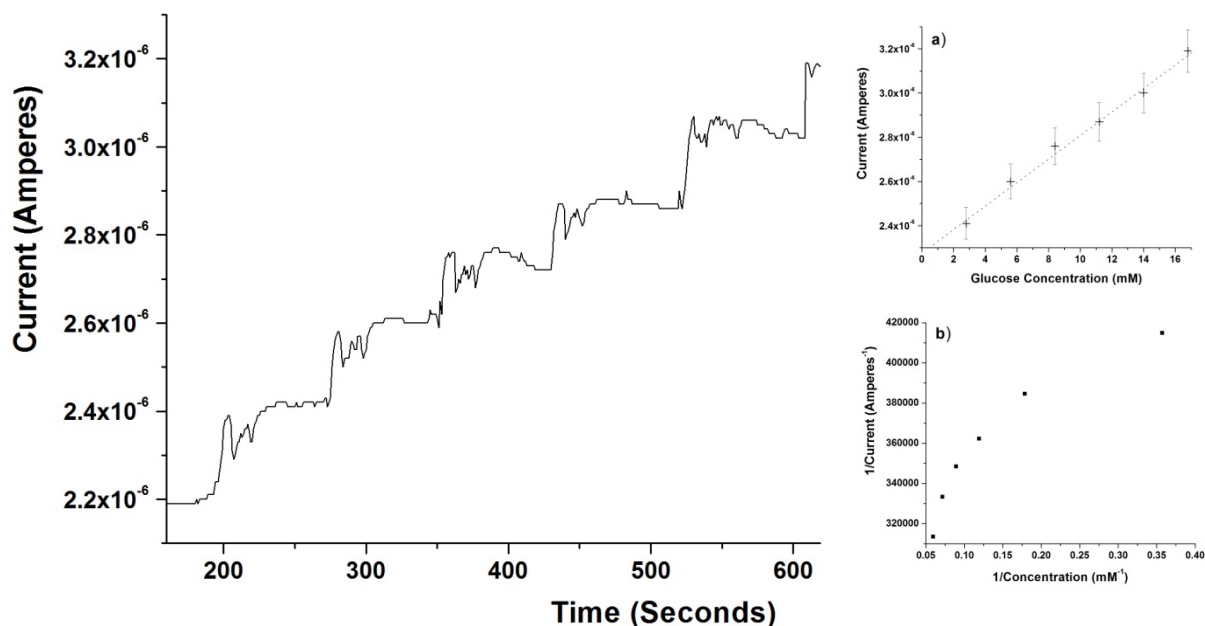


Figure 40 Amperometric response of Gox-P(Py-FcPy)/ITO bioelectrode to the successive addition of 2.8 mM glucose in 50 mM PBS (pH 7.0) at +175 mV. Inset: a) Linear current response with glucose concentration, b) Lineweaver-Burk Plot.

To study enzyme–substrate kinetics process, Michaelis-Menten constant, k_m , was estimated from the inverse of the x-axis intercept of Lineweaver-Burk plot, i.e., graph between inverse of glucose concentration and inverse of amperometric response current (inset b in figure 41). The value of 0.96 mM obtained for Gox-P(Py-FcPy)/ITO bio-electrode is found to be much smaller than reported value of 33.4 mM for plain PPy/Gox [66]. Further, the observed value is much smaller than 5.85 mM or 33 mM observed for free Gox in solution [34, 92]. Smaller values of K_m reveal higher affinity of enzyme for its substrate and can be attributed to the better conformation of immobilized enzyme for the enzymatic reaction [93]. The results suggest that the presence of pyrrole-ferrocene attached in the polypyrrole chain helps to retain a enzyme with a favorable orientation in the matrix for better shuttling of electron.

Table 1 summarizes the comparison of the characteristics of Gox-P(Py-FcPy)/ITO bioelectrode with others reported in literature. This analysis clearly indicates that the bioelectrode presented here reveals efficient activity and sensitivity compared to other polymer and polymeric nanocomposite based biosensors with the added advantage of being a mediator-less biosensor indicating improved properties of the synthesized material.

Matrix	Immobilization method	Linear range	K_M^{APP}	Sensitivity	Response time	Ref.
PP2ABA	Covalent	3-40 mM	1×10^{-2} mM	$0.0058 \mu\text{AmM}^{-1}$	5 s	[68]
PPy/MWCNT	Electrochemical	1-4 mM	-	95 nAmM^{-1}	8 s	[69]
PPy/Fc	Electrochemical	2-10 mM	-	$0.23 \mu\text{AmM}^{-1}$	2 s	[73]
PS/PANI/Au	Physical	0.04-2.04 mM	0.76 mM	-	10 s	[94]
Au-PPy	Physical	$2.5 \mu\text{M}$ – 5mM	43.45mM	$1.089 \mu\text{AmM}^{-1}$	10 s	[95]
PPy	Electrochemical	$5\mu\text{M}$ -20 mM	23.3 mM	-	-	[96]
PMMA-MWCNT(PDDA)	Covalent	$20 \mu\text{M}$ – 15mM	10.12 mM	$0.3137 \mu\text{AmM}^{-1}$	4 s	[97]
FMC-AMWNT's/CS	Covalent	0.01-4.2 mM	6.3 mM	-	7 s	[98]
P(Py-FcPy)	Electrochemical	2.8 to 16.8mM	0.96 mM	$2.28 \mu\text{AmM}^{-1}$	3 s	This work

•PS/PANI/Au = Polystyrene/Polyaniline/Gold

•Au-PPy = Gold Polypyrrole

•PPy/Fc = Polypyrrole entrapped with Ferrocene

•PPy = Polypyrrole

•PMMA-MWCNT(PDDA) = Polymethacrylate-MWCNT(poly(diallyldimethylammonium chloride))

•PP2ABA = poly(pyrrole-2-aminobenzoic acid)

•PPy/MWCNT = Polypyrrole/Multi-walled Carbon Nanotubes

•FMC-AMWNT's/CS = ferrocene monocarboxylic acid-modified 3-(aminopropyl) triethoxysilane – amino-functionalized Multi-walled Carbon Nanotubes/Chitosan

•P(Py-FcPy) = Poly(Pyrrole-N-Ferrocene-Pyrrole)

Table 1 Comparison of Gox-P(Py-FcPy)/ITO bioelectrode with others Gox- based amperometric glucose biosensors reported in literature [68,69,73,94-98].

4 ZINC OXIDE NANORODS AS FILMS FOR AMPEROMETRIC UREA BIOSENSOR

This chapter deals with the synthesis of ZnO nanorods (ZnONR) onto indium tin oxide (ITO) coated glass surface using zinc nitrate hexahydrate and hexamethylenetetramine (HMT) in aqueous phase and their use for urea biosensor.

4.1 Materials and Methods.

4.1.1 Materials used.

ITO coated glass ($15\text{-}25\ \Omega\text{cm}^{-2}$), zinc nitrate hexahydrate, hexamethylenetetramine (HMT), urease ($400\text{-}800\ \text{U mg}^{-1}$), urea, sodium chloride, and potassium ferrocyanate (Sigma-Aldrich). Sodium phosphate monobasic and sodium phosphate dibasic were obtained from Sargent-Welch (VWR Scientific). Deionized water ($18.2\ \text{M}\Omega\ \text{cm}^{-1}$) was used to prepare the solutions. ZnO sputtering substrate (99.99% purity, 0.15” thickness, 2” diameter) was acquired from Superconductor Materials Inc.

Radio frequency (RF) magnetron sputtering system was used for deposition of ZnO seeds on ITO surface. XRD measurements were carried out with Siemens D5000 x-ray diffractometer (XRD) using the Cu-K α radiation (1.5405\AA). Field emission scanning electron microscopy (FESEM) measurements were conducted on a Hitachi S4700 scanning electron microscope.

Phosphate buffer saline (PBS) 50 mM, (0.9% NaCl) solution was prepared by adjusting the proportion of monobasic sodium phosphate solution with dibasic sodium phosphate solution and then adding 0.9% NaCl to the solution. Urease (2 mg mL^{-1}) solution was prepared in PBS of pH 7.0. A concentrated urea solution was prepared in PBS containing 5mM ferro-ferricyanide ($\text{Fe}(\text{CN})_6^{3-/4-}$) redox couple and further diluted to different concentrations.

4.1.2 Preparation of ZnO nanorods films.

The ITO substrates were cleaned by sonication in acetone, 2-propanol and deionized water prior to deposition of ZnO seeds. Before sputtering and after cleaning, some surface of the substrates was covered with aluminum foil to obtain a half-covered substrate with a ZnO seeded film.

The ZnO seed deposition on ITO was carried out using radiofrequency sputtering with a power of 120 W under an argon atmosphere of 1×10^{-2} Torr at 120 °C. The seeded ITO substrate was hung vertical in a glass beaker containing zinc nitrate and HMT aqueous solution and refluxed at 120°C for 2 hours to grow ZnO nanorods. The concentration of both reactants in aqueous solutions was 0.1 M. After the thermal growth of nanorods, the films were thoroughly washed with deionized water to remove any residual amino complex and allowed to dry at room temperature. Figures 41 a) and b) show the sputtering and thermal step configurations, respectively.

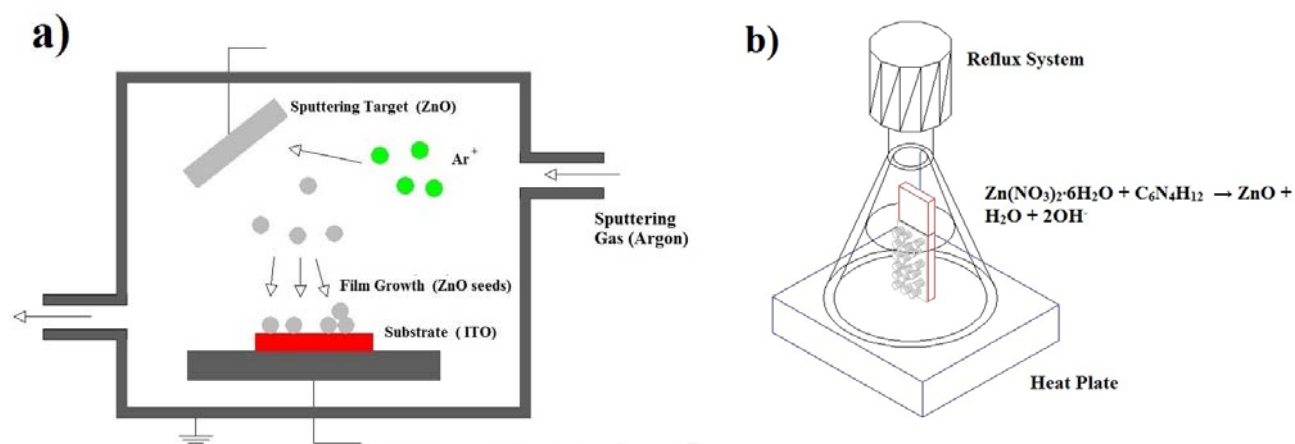


Figure 41 a) Sputtering process to deposit ZnO seed on top of ITO substrate, b) thermal formation of ZnO nanorods on ZnO seeded ITO substrate.

4.1.3 Urease immobilization.

For immobilization of the enzyme, 70 μl of the urease solution was dropped on the ZnONR/ITO surface of area 7 mm x 11 mm and kept overnight at 4 $^{\circ}\text{C}$. The electrode was then washed with PBS pH 7.0 to remove any unbound enzyme.

4.2 Results and discussion.

4.2.1 Structure analysis and electrochemical study of zinc oxide nanorods film.

Figure 42 (a) shows the XRD pattern for ZnONR/ITO surface in the range of $30^{\circ} < 2\theta < 60^{\circ}$. The well-defined diffraction peaks from planes (100), (002), (101), (102) and (110) at angles 32.10° , 34.86° , 36.58° , 47.99° , and 56.95° , respectively, indicates the formation of polycrystalline ZnO in Wurtzite crystalline structure [99]. Peaks corresponding to the ITO coated surface are marked as * in the figure. Spectra of the blank ITO signal are shown in figure 42 (b).

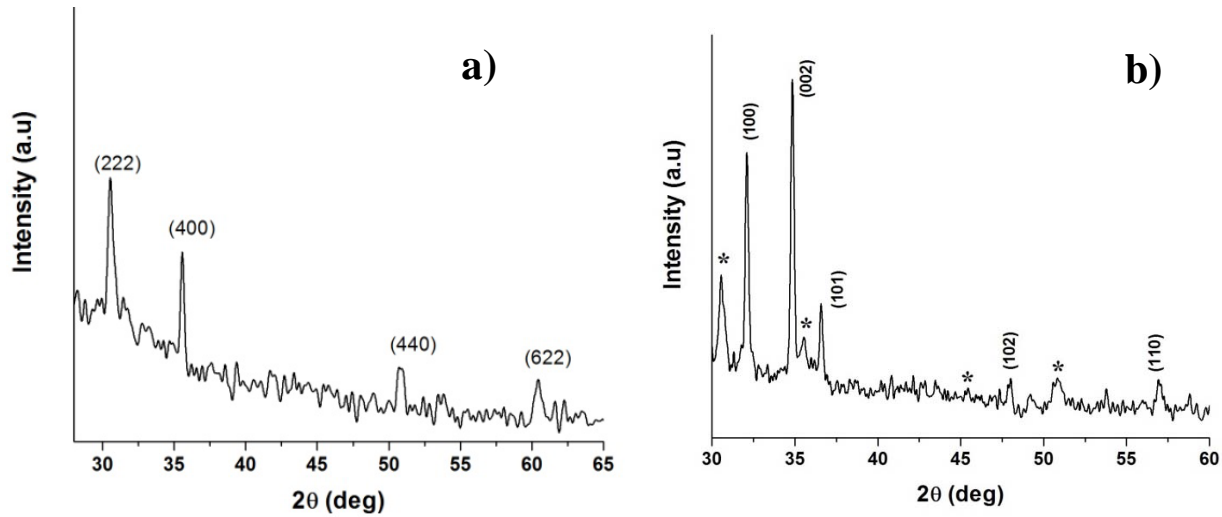


Figure 42 a) XRD spectra of ZnONR/ITO electrode, b) XRD of ITO coated glass surface.

As can be seen, greatest intensity of the (002) plane demonstrates predominant structural arrangement of the crystal in the c-axis direction. Data obtained from the XRD graph in figure 42a is shown in table 2. Grain sizes corresponding to each crystal plane of the Wurtzite structure are calculated using Scherrer's equation. The estimated average particle size of the crystal was at around 50 nm.

Plane	θ (deg)	θ_{max}	θ_{min}	β (deg)	$Landa\lambda$	θ (rad)	β (rad)	t
(100)	32.1	32.2	32	0.2	1.54E-10	0.560252	0.003491	4.94916E-08
(002)	34.86	34.99	34.73	0.26	1.54E-10	0.608423	0.004538	3.93032E-08
(101)	36.58	36.68	36.49	0.19	1.54E-10	0.638443	0.003316	5.49572E-08
(102)	47.99	48.12	47.79	0.33	1.54E-10	0.837585	0.00576	3.79664E-08
(110)	56.95	57.15	56.82	0.33	1.54E-10	0.993967	0.00576	4.65911E-08

Table 2 Data from ZnO nanorods XRD in figure 42(a). t is the grain size on each plane calculated using Scherrer's equation.

Figure 43 (a) shows the FESEM images of the fabricated film, clearly showing the formation of nanorods with tendency to align vertically in the c-direction (as confirmed with XRD). A constant dimension of approximately 300 nm length and 50 nm of diameter is appreciated in the

crystals. The value of the nanorods diameter obtained from FE-SEM is closer to the calculated particle size value of 50 nm from XRD. FESEM image of the previously ZnO seeded surface on the substrate is shown in figure 43 b.

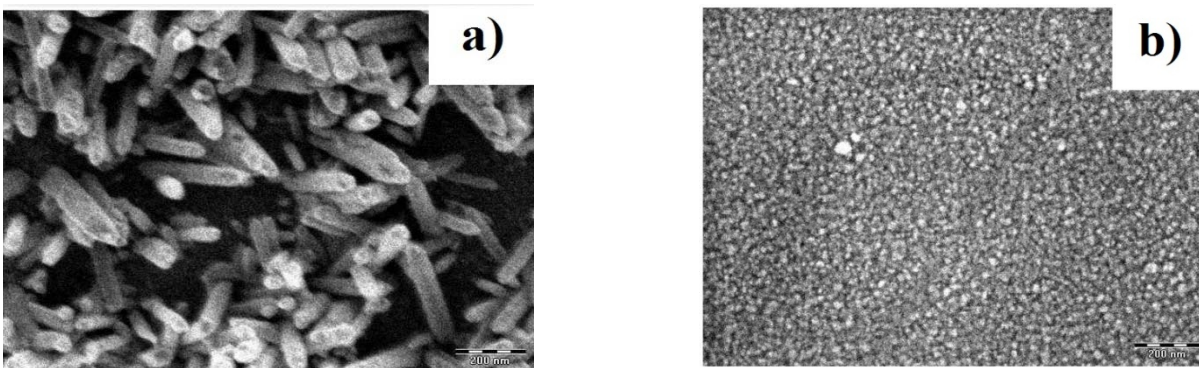


Figure 43 a) FE-SEM image of ZnONR/ITO electrode, b) FE-SEM image of ZnO seeded surface of the substrate.

Figure 44 shows cyclic voltammograms at different scan rates for the ZnONR/ITO electrode in PBS (50mM, pH 7.0, 0.9% NaCl) containing $\text{Fe}(\text{CN})_6^{3-/4-}$. The linearity in the plot (inset a) of anodic and cathodic peak currents versus the square root of scan rate reveals a diffusion-controlled process, indicating a thermodynamically favorable electron transfer and an improved electrochemical signal. Surface concentration, C , and diffusion coefficient, D , were found to be $2.41 \times 10^{-10} \text{ mol/cm}^2$ and $0.61 \text{ cm}^2/\text{s}$, using the Brown–Anson model and Randles-Svick equation, respectively.

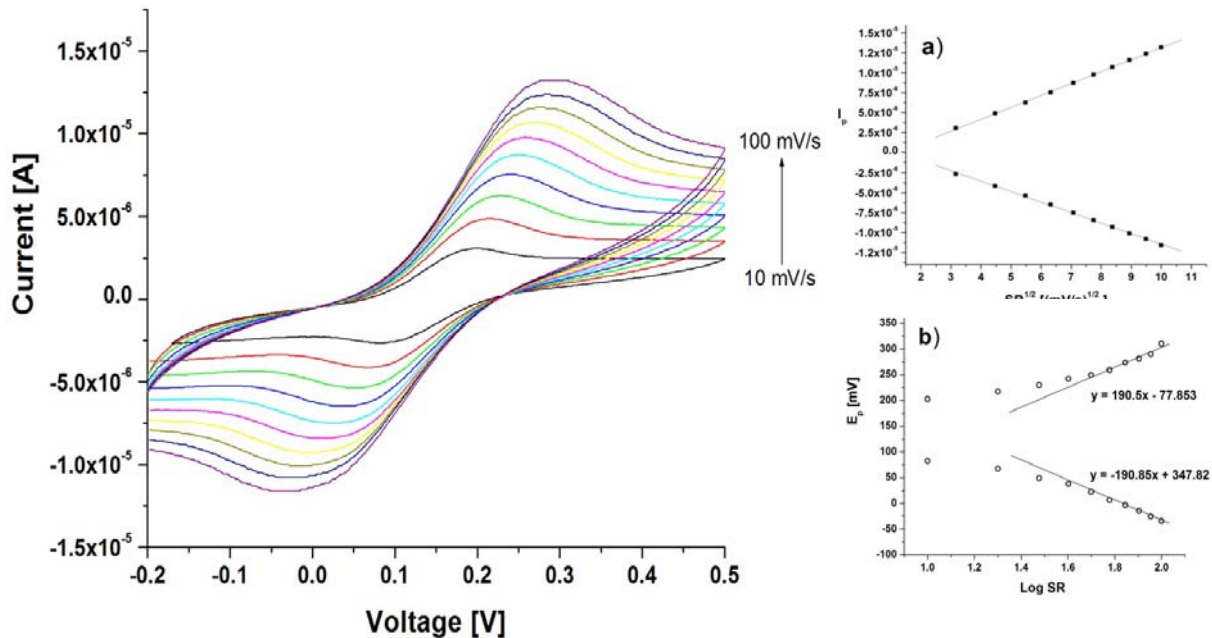


Figure 44 Cyclic voltammograms of the ZnONR/ITO electrode in PBS containing $\text{Fe}(\text{CN})_6^{3-/4-}$ at different scan rates. Inset: (a) Peak Current vs. square root of scan rate. (b) Peak Voltage vs. log of scan rate.

Divergence of the peaks with an increase in scan rate can be seen as the oxidation peak moves towards a higher voltage value while the reduction peak moves towards a lower one, indicating the quasi-reversibility of the system. Inset b on Figure 45 shows the peak potentials as a function of the logarithm of the scan rate. A transfer coefficient α of 0.69 was obtained from the linear fits of the graphs, and the heterogeneous rate transfer constant, k_s , was estimated as 0.6 cm/s for a 50 mV/s scan rate.

4.2.2 Urs/ZnONR/ITO bioelectrode for detection of urea.

Figure 45 shows the response of the bioelectrode at pH levels in the 6.0 to 8.0 range in presence of 2 mM urea, using cyclic voltammetry at 50 mV/s. pH behavior in presence of the analyte is to be considered since attachment of the enzyme to the electrode's surface is directly affected by

the electrostatic variation at the interface. Optimal pH activity for urease is known to be 7.4, and the highest current responses were obtained at pH 7.0, thus all the experiments were carried out at this pH level.

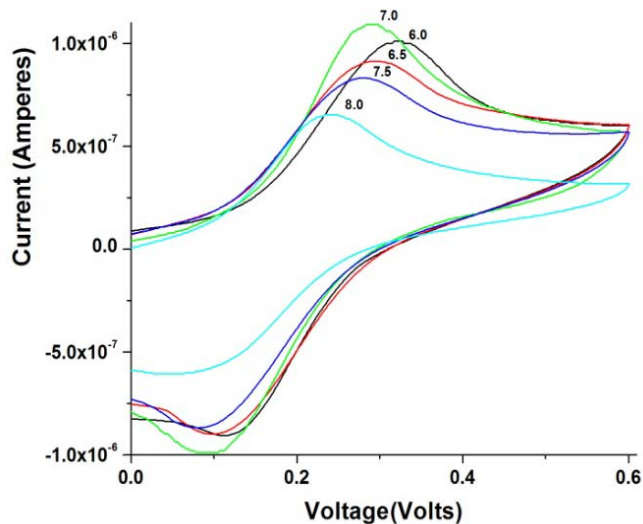


Figure 45 Cyclic voltammograms at 50 mV/s of Urs/ZnONR/ITO bioelectrode response to 2 mM urea as a function of pH in PBS with $\text{Fe}(\text{CN})_6^{3-/4-}$ at 50 mV/s.

Studies were performed on the Urs/ZnO/NR bioelectrode in 2 mM urea at different temperatures, using cyclic voltammetry at 40 mV/s. Figure 46 shows the response of the Urs/ZnO/NR at different temperatures in presence of 2 mM urea, using cyclic voltammetry at 50 mV/s. Increase in current was obtained with increasing temperature up to 40 °C, with a tendency to saturation after 30 °C. Therefore all experiments were carried out at room temperature.

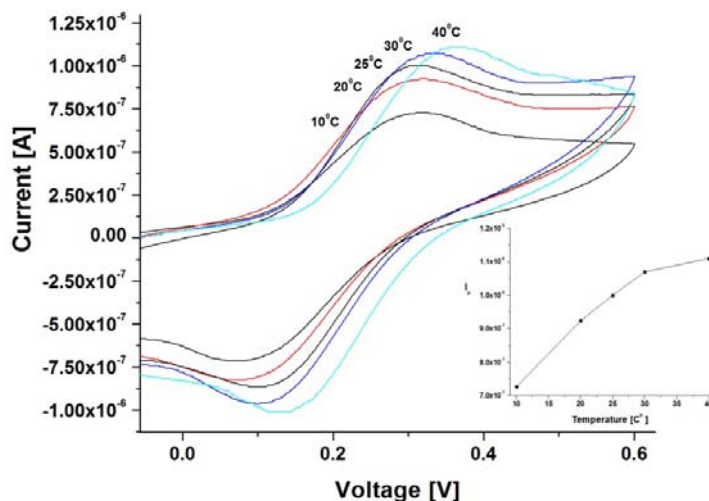


Figure 46 Cyclic voltammograms at 50 mV/s of Urs/ZnONR/ITO bioelectrode response to 2 mM urea as a function of temperature in PBS containing $\text{Fe}(\text{CN})_6^{3-/4-}$ at 50 mV/s. Inset: Current response vs. temperature.

Figure 47 shows the cyclic voltammogram of the ZnONR/ITO and Urs/ZnONR/ITO bioelectrodes. A decrease in the current signal after the Urs immobilization can be attributed to the insulating nature of the enzyme [100]. A reduction in the peak to peak voltage separation however may imply a faster electron transfer in the Urs/ZnONR composite as compared to electron transfer in ZnONR/ITO.

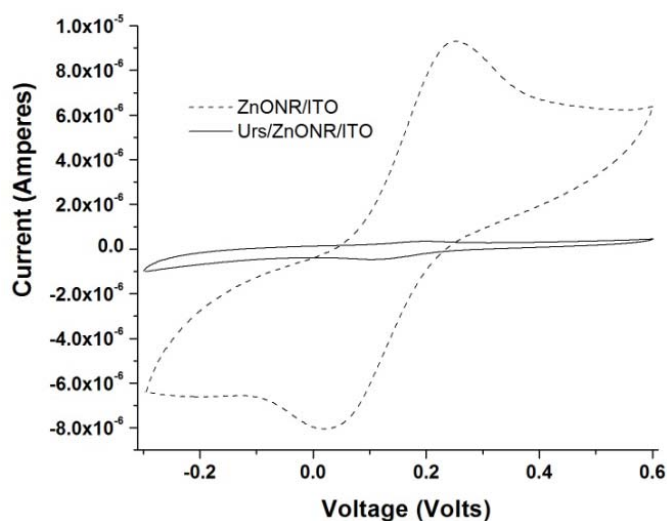


Figure 47 Cyclic voltammograms at 50 mV/s of ZnONR/ITO electrode (----) and Urs/ZnONR/ITO bioelectrode (—) in PBS containing $\text{Fe}(\text{CN})_6^{3-/4-}$ at 50 mV/s.

Figure 48 shows cyclic voltammograms at 50 mV/s of the response of the Urs/ZnONR/ITO bioelectrode to different urea concentrations. An increasing current with urea concentration indicates an increase in the amount of product formation, which includes the NH_4^+ and CO_3^{2-} charged species, thus increasing the conductivity at the electrode by providing more electrons to the conduction band of ZnO [65]. Figure 49 shows an schematic of the mentioned mechanism.

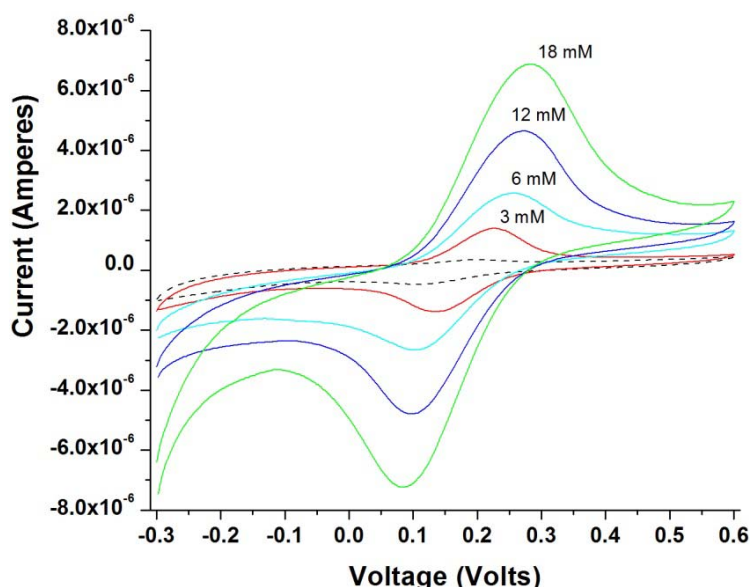


Figure 48 Cyclic voltammograms of Urs/ZnONR/ITO bioelectrode in the absence(----) and presence(—) of different urea concentrations in PBS containing $\text{Fe}(\text{CN})_6^{3-/4-}$ at 50 mV/s.

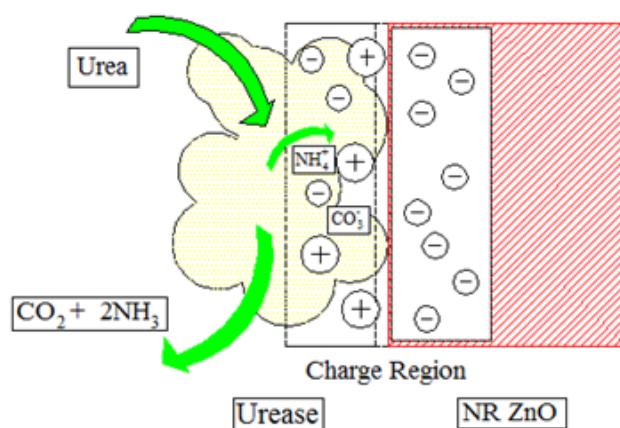


Figure 49 Schematic for urea detection mechanism of Urs/ZnONR/ITO bioelectrode.

Concentration of the amount of enzyme entrapped in the film was estimated using the peak current generated in the presence of 18 mM glucose using the Brown-Anson equation. The amount of glucose oxidase (molecular weight; 4.8×10^5 g/mol) was estimated to be 1.85×10^{-10} mol/cm² on 0.77 cm² area films. This corresponds to 68.5 μ g of surface confined enzyme out of approximately 140 μ g of urease in solution deposited over the electrode's surface during the physisorption process.

Figure 50 shows the amperometric response of Urs/ZnONR/ITO at 300 mV to successive additions of 1 mM urea. It can be seen that the current increases with increase of urea concentration, exhibiting a response time of 3 seconds. The plot between urea concentration and current response shown in inset a) reveals linearity from 1 to 20 mM with a sensitivity of 30 nA mM⁻¹ and detection limit of 0.375 mM, calculated with a blank standard deviation of 3.75×10^{-8} . Inset b) of figure 50 presents the Lineweaver-Burk plot of the current response to urea concentrations. It was used to find the Michaelis-Menten kinetic constant, K_m , yielding 3 mM.

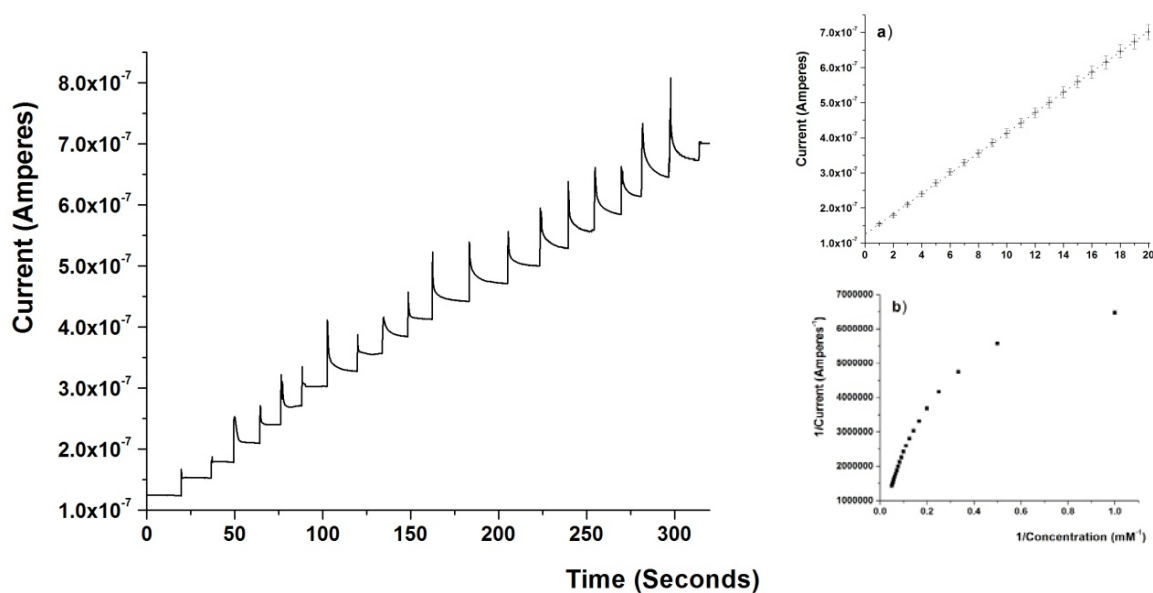


Figure 50 Current response of Urs/ZnONR/ITO bioelectrode to urea concentration in PBS. Inset a) Amperometric response to successive additions of 1mM urea, b) Lineweaver-Burk plot

Figure 51 shows the amperometric response of the Urs/ZnO/NR bioelectrode in the presence of the interferants 1 mM urea, 1mM urea with 0.1 mM ascorbic acid, and 1 mM urea with 5 mM glucose. The inset reveals an increase in current of 1.3 % and 1.2% for urea in presence of glucose and ascorbic acid, respectively.

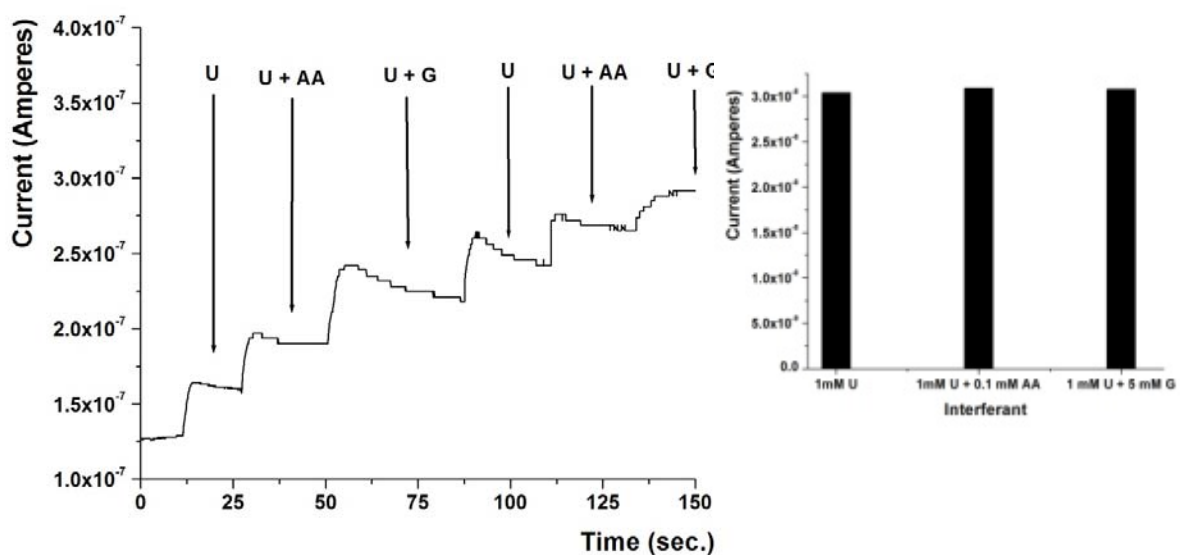


Figure 51 Amperometric response of Urs/ZnONR/ITO bioelectrode for 1 mM urea, 1mM urea + 0.1 mM ascorbic acid, and 1 mM urea + 5 mM glucose solutions in PBS. Inset: Current response to interferants

Table 3 summarizes comparisons of the characteristics of present work along with others urease based amperometric urea biosensors reported in literature [13,60,62-65]. This analysis clearly indicates that the bioelectrode presented here possess efficient activity and sensitivity compared to other fabricated biosensors.

Matrix	Immobilization Method	Km (mM)	Sensitivity (μAmM^{-1})	Linear range (mM)	Detection limit (mM)	Response time (s)	Reference
Hyper-branched Polyester-Au nanoparticles	Covalent	0.96	0.00748	0.01–35	0.01	3	[13]
Polyaniline-Nafion	Cross-linked with Gld	-	0.394	0.0005 -1	0.0005	40	[60]
Poly(pyrrole)/Poly(5-amino-1-naphthol)	Physical	131	0.58	0.22-40	-	-	[62]
	Cross-linked with Gld	4.6	0.80	0.34-100	-	-	
	Covalent	137	3.44	0.58-40	-	-	
Platinum-Graphite Composite	Physical	-	1.95	0.010 - 0.250	0.003	120	[63]
Iron oxide NP - Chitosan	Physical co-immobilization with GD	0.56	12.5	1-17	0.3	10	[64]
ZnO nanoparticles-Chitosan	Physical co-immobilization with GD	0.82	0.13	1-17	0.5	10	[22]
ZnO nanorods	Physical	3	0.03	1-20	0.375	3	This work

Gld = Glutaraldehyde

GD = Glutamate Dehydrogenase

Table 3. Comparison of Urs/ZnONR/ITO bioelectrode with others Urs- based amperometric urea biosensors reported in literature [13,60,62-65].

5 CONCLUSIONS

It has been clearly shown in chapter 3 that ferrocene modified pyrrole can be utilized with unmodified monomer to electrochemically prepare P(Py-FcPy) copolymer films. The presence of ferrocene results in well defined anodic and cathodic peaks and makes the P(Py-FcPy) system quasi-reversible and reusable. The well defined redox peaks further reveal favorable electron transfer and an improved electrochemical signal for electrochemical biosensors. The enzyme glucose oxidase (Gox) is successfully immobilized in a single step during the electrochemical polymerization. The Gox-P(Py-FcPy)/ITO bioelectrode presents enhanced activity and a higher sensitivity ($2.28 \mu\text{A mM}^{-1}$) during glucose detection, as reflected by a small K_m value of 0.96 mM. These results suggest that P(Py-FcPy) copolymer composite films proves to be a promising matrix for enzymes and proteins with enhanced stability and activity for mediator-less biosensor applications. Further studies are suggested to investigate this material in detail, since its interesting electronic properties make this system a potential candidate in polymer electronics and sensor technology.

In chapter 4, urease modified ZnO nanorods (ZnONR) grown onto indium tin oxide (ITO) coated glass surface have been successfully used for amperometric urea biosensor. ZnO nanorods were grown on rf sputtered ZnO seed layer in aqueous solution of zinc nitrate hexahydrate and hexamethylenetetramine. SEM and XRD results confirm the formation of ZnO nanorods in Wurtzite crystalline structure. Cyclic voltammetry studies indicate the quasi-reversible behavior of the fabricated Urs/ZnONR/ITO bioelectrode with optimum activity at pH 7.0 and within 20°C to 30°C temperature range. Amperometric studies reveals a linear behavior in the 1–20 mM urea range with a sensitivity of $0.03 \mu\text{A mM}^{-1}$, a response time of 3 seconds, a detection limit of

0.375 mM and a Michaelis-Menten constant (K_m) of 3 mM. Studies indicate the selectivity of bioelectrode against glucose and ascorbic acid. Future efforts aim to estimate urea in real samples and to use ZnONR/ITO based electrode for binding of other biomolecule for sensitive and selective estimation of other analytes of biological importance. The compatibility of ZnO with existing MEMS technology will lead to the development of miniaturized point of care health monitoring systems.

References

1. M. Singh, N. Verma, A. K. Garg, N. Redhu. Urea biosensors, *Sensor Actuat. B-Chem* 134, 345-351, 2008.
2. G. Dhawan, G. Sumana, B. D. Malhotra. Recent developments in urea biosensors, *Biochem. Eng. J.* 44, 42-52, 2009.
3. D. Aronson, M. A. Mittleman, A. J. Burger. Elevated blood urea nitrogen levels as a predictor of mortality in patients admitted for decompensated heart failure, *Am. J. Med.* 116, 466-473, 2004.
4. S. Wild, G. Roglic, A. Green, R. Sicree, H. King, Global prevalence of diabetes: estimates for the year 2000 and projections for 2030, *Diabetes Care* 27, 1047-1053, 2004.
5. American Diabetes Association. Diagnosis and classification of diabetes mellitus, *Diabetes Care* 33, S62-69, 2010.
6. S. P. O. Jansson, D. K. G. Andersson, K. Svärsudd. Mortality trends in subjects with and without diabetes during a 33 years of follow-up, *Diabetes Care* 33, 551-556, 2010.
7. E-H. Yoo, S-Y. Lee. Glucose biosensors: an overview of use in clinical practice, *Sensors* 10, 4558-4576, 2010.
8. J. Wang, *Analytical electrochemistry*, Wiley VCH, 1994.
9. J. D. Newman, A. P. Turner A.P. *Biosensors: principles and practice*; Portland Press: London, UK, Vol. 27, 147-159, 1992.
10. D. Grieshaber, R. MacKenzie, J. Vörös, E. Reimhult, *Electrochemical biosensors – Sensor principles and architectures*, *Sensors* 8, 1400-1458, 2008.
11. M. Pohanka, P. Skládal. *Electrochemical biosensors – Principles and applications*, *J. Appl. Biomed.* 6, 57-64, 2008.
12. A. P. Turner, B. Chen, S. A. Piletsky. *In vitro diagnostics in diabetes: meeting the challenge*, *Clin. Chem.* 45, 1596-1601, 1999.
13. A. Tiwari, S. Aryal, S. Pilla, S. Gong. An amperometric urea biosensor based on covalently immobilized urease on an electrode made of hyperbranched polyester functionalized gold nanoparticles, *Talanta* 78, 1401-1407, 2009.
14. J. Wang. *Electrochemical glucose biosensors*, *Chem. Rev.* 108, 814-825, 2008.

15. G. G. Guilbault, G. J. Lubrano, An enzyme electrode for the amperometric determination of glucose, *Anal. Chim. Acta.* 64, 439-455, 1973.
16. Musameh, M., Wang, J., Merkoci, A., Lin, Y., Low-potential stable NADH detection at carbon-nanotube-modified glassy carbon electrodes, *Electrochem. Commun.* 4, 743–746, 2002.
17. A. Karaykin, Prussian blue and its analogues: electrochemistry and analytical applications, *Electroanalysis* 13, 813-819, 2001.
18. M. Singh, N. Verma, A. K. Garg, N. Redhu, Urea biosensors, *Sens. Actuat. B* 134, 345-351, 2008.
19. G. Dhawan, G. Sumana, B. D. Malhotra, Recent developments in urea biosensors, *Biochem. Eng. J.* 44, 42-52, 2009.
20. G.G. Guilbault, J. Montalvo, A urea specific enzyme electrode, *J. Am. Chem. Soc.* 91, 2164-2165, 1969.
21. A. Pizzariello, M. Stredanský, S. Stredanská, S. Miertuš, Urea biosensor based on amperometric pH-sensing with hematein as a pH- sensitive redox mediator, *Talanta* 54, 763-772, 2001.
22. P. R. Solanki, A. Kaushik, A. A. Ansari, G. Sumana and B. D. Malhorta, Zinc oxide-chitosan nanobiocomposite for urea sensor, *Appl. Phys. Lett.* 93, 163903(1-3), 2008.
23. T. Osakai, T. Kakutani, M. Senda, A novel amperometric urea sensor, *Anal. Sci.* 4, 529-530, 1988.
24. D. P. Nikolelis, C. G. Siontoru, Bilayer lipid membranes for flow injection monitoring of acetylcholine, urea, and penicillin, *Anal. Chem.* 67, 936-944, 1995.
25. W.-J. Cho, H.-J. Huang, An amperometric urea biosensor based on a polyaniline-perfluorosulfonated ionomer composite electrode, *Anal. Chem.* 70, 3946-3951, 1998.
26. C. Dhand, S. P. Singh, S. K. Arya, M. Datta, B. D. Malhotra, Cholesterol biosensor based on electrophoretically deposited conducting polymer film derived from nano-structured polyaniline colloidal suspension, *Anal Chim Acta* 602, 244–51, 2007.
27. N. Prabhakar, K. Arora, S. P. Singh, M. K. Pandey, H. Singh, B. D. Malhotra, Polypyrrole-polyvinyl sulphonate film based disposable nucleic acid biosensor, *Anal Chim Acta* 589, 6–13, 2007.

28. S.P. Singh, S. K. Arya, P. Pandey, S. Saha, K. Sreenivas, B.D. Malhotra, V. Gupta, Cholesterol biosensor based on rf sputtered zinc oxide nanoporous thin film. *Appl. Phys. Lett.* 91, 1-4, 2007.
29. M. Trojanowicz, T. K. Vel Krawczys, P. W. Alexander, Organic conducting as active materials in electrochemical chemosensors and biosensors, *Anal. Chem.* 42, 199-213, 1997.
30. B. D. Malhotra, A. Chaubey, S. P. Singh, Prospects of conducting polymers in biosensors, *Anal. Chim. Acta* 578, 59-74, 2006.
31. A. Rahman, P. Kumar, D-S. Park, Y-B. Shim, Electrochemical sensors based on organic conjugated polymers, *Sensors* 8, 118-141, 2008.
32. X. Luo, A. Morrin, A. J. Killard, M. R. Smyth, Application of nanoparticles in electrochemical sensors and biosensors, *Electroanalysis* 18, 319-326, 2006.
33. F. López-Gallego, L. Betancor, C. Mateo, A. Hidalgo, N. Alonso-Morales, G. Dellamora-Ortiz, J. M. Guisán, Enzyme stabilization by glutaraldehyde crosslinking of adsorbed proteins on aminated supports, *J. Biotechnol.* 119, 70-75, 2005.
34. P. Pandey, S. P. Singh, S. K. Arya, V. Gupta, M. Datta, S. Singh, B. D. Malhotra, Application of thiolated gold nanoparticles for the enhancement of glucose oxidase activity, *Langmuir* 23, 3333-3337, 2007.
35. W. Jin, F. Bier, Construction and characterization of a multi-layer enzyme electrode: Covalent binding of quinoprotein glucose dehydrogenase onto gold electrodes, *Biosens. Bioelectron.* 10, 823-829, 1995.
36. P. R. Solanki, A. Kaushik, V. V. Agrawal, B. D. Malhotra, Nanostructured metal oxide-based biosensors, *NPG Asia Mater.* 3, 17-24, 2011.
37. Z. Zhao, W. Lei, X. Zhang, B. Wang, H. Jiang, ZnO-Based Amperometric enzyme biosensors, *Sensors* 10, 1216-1231, 2010.
38. Zao Yang, X. Zong, Z. Ye, B. Zhao, Q. Wang, P. Wang, The application of complex multiple forklike ZnO nanostructures to rapid and ultrahigh sensitive hydrogen peroxide biosensors, *Biomaterials* 31, 7534-7541, 2010.
39. F. Xu, Y. Lu, Y. Xie, Y. Liu, Controllable morphology evolution of electrodeposited ZnO nano/micro-scale structures in aqueous solution, *Mat. Des.* 30, 1704-1711, 2009.

40. L.-L. Xing, X.-Y. Xue, Electrochemistry-assisted self-assembly of oriented zinc oxide and long-chain alkyl amine surfactant multilamellar nanostructures, *Solid State Sciences* 12, 1593-1598, 2010.
41. A. Umar, M. M Rahman, A. Al-Hajry, Y.-B. Hahn, Highly-sensitive cholesterol biosensor based on well-crystallized flower-shaped ZnO nanostructures, *Talanta* 78, 284-289, 2009.
42. J. Zhao, J. Zhi, Y. Zhou, W. Yan, A tyrosinase biosensor based on ZnO nanorod clusters/nanocrystalline diamond electrodes for biosensing of phenolic compounds, *Analyt. Sci.* 25, 1083-1087, 2009.
43. S-J. Kim, H-H. Kim, J-B. Kwon, J-G. Lee, B-H. O, S. G. Lee, E-H. Lee, S-G. Park, Novel fabrication of various size ZnO nanorods using hydrothermal method, *Microelectronic Engineering* 87, 1534-1536, 2010.
44. Conducting polymers by Collin Pratt. [delpanantika.com/search/conducting polymers](http://delpanantika.com/search/conducting%20polymers)
45. P. K. Chu, X. Liu, Biomaterials fabrication and processing handbook, John Wiley & Sons, Ltd, West Sussex, 2008.
46. A. Ramanavičius, A. Ramanavičiene, A. Malinauskas, Electrochemical sensors based on conducting polymer-pyrrole, *Electrochem. Acta* 51, 6025-6037, 2006.
47. P. A. Kilmartin, K-C Li, G. A. Bowmaker, N. A. Vigar, R. P. Cooney, J. Travas-Sedjic, Spectroscopic studies of doping reactions in polypyrrole actuators, *Curr. Appl. Phys.* 6, 567-570, 2006.
48. S. Sadki, P. Schottland, N. Brodie, G. Sabouraud, The mechanisms of pyrrole electropolymerization, *Chem. Soc. Rev.* 29, 283-293, 2000.
49. E. Kriván, G. Peintler, C. Visy, Matrix rank analysis of spectral studies on the electropolymerisation and discharge process of conducting polypyrrole/dodecyl sulfate films, *Electrochim. Acta* 50, 1529-1535, 2005.
50. R. J. Geise, J. M. Adams, N. J. Barone, A. M. Yacynych, Electropolymerized films to prevent interferences and electrode fouling in biosensors, *Biosens. Bioelectron.* 6, 151-160, 1991.
51. M. A. Vorotyntsev, S. V. Vasilyeva, Metallocene-containing conjugated polymers, *Adv. Colloid Interface Sci.* 139, 97-149, 2008.

52. F. N. Lloyd, Q. Ah, K. Tamada, M. Hara, Self-assembling properties of 11-ferrocenyl-1-undecanethiol on highly oriented pyrolytic graphite characterized by scanning tunneling microscopy, *e-J. Surf. Sci. Nanotech.* 6, 119–123, 2008.
53. S. A. Merchant, T. O. Tran, M. T. Meredith, T. C. Cline, D. T. Glatzhofer and D. W. Schmidtke, High-sensitivity amperometric biosensors based on ferrocene-modified linear poly(ethylenimine), *Langmuir* 25, 7736-7742, 2009.
54. M. Velázquez-Rosenthal, T. Skotheim, J. Warren, *J. Chem. Soc. Chem. Commun.* Ferrocene –functionalized polypyrrole films, 342-343, 1985.
55. N. C. Foulds, C. R. Lowe, Immobilization of glucose oxidase in ferrocene-modified pyrrole polymers, *Anal. Chem.* 60, 2473-2478, 1988.
56. G. Zotti, S. Zecchin, G. Schiavon, Conductivity in redox modified conducting polymers. 2. Enhanced Redox Conductivity in Ferrocene-Substituted Polypyrroles and Polythiopenes, *Chem. Mater.* 7, 2309-2315, 1995.
57. J. Chen, C. O. Too, G. G. Wallace, Redox-active conducting polymers incorporating ferrocenes. Preparation, characterization and bio-sensing properties of ferrocenylpropyl and –butyl polypyrroles, *Electrochim. Acta.* 47, 4227- 4238, 2002.
58. R. Koncki, Recent developments in potentiometric biosensors for biomedical analysis, *Anal. Chim. Acta* 599, 7-15, 2007.
59. T. Osakai, T. Kakutani, M. Senda, A Novel Amperometric Urea Sensor, *Anal. Sci.* 4, 529-530, 1988.
60. W.-J. Cho, H.-J. Huang, An Amperometric Urea Biosensor Based on a Polyaniline-Perfluorosulfonated Ionomer Composite Electrode, *Anal. Chem.* 70, 3946-3951, 1998.
61. V. S. Tripathi, V. B. Kandimalla, H. Ju, Amperometric biosensor for hydrogen peroxide based on ferrocene-bovine serum albumin and multiwall carbon nanotube modified ormosil composite, *Biosens. Bioelectron.* 21, 1529-1535, 2006.
62. M. P. Massafra, S. I. Córdoba de Torresi, Urea amperometric biosensors based on a multifunctional bi-polymeric layer: Comparing enzyme immobilization methods, *Sens. Actuators B* 137, 476-482, 2009.
63. A. Pizzariello, M. Stredanský, S. Stredanská, S. Miertuš, *Talanta* 54, Urea biosensor based on amperometric pH-sensing with hematein as a pH-sensitive redox mediator 763-772, 2001.

64. A. Kaushik, P. R. Solanki, A. A. Ansari, G. Sumana, S. Ahmad, B. D. Malhotra, Iron oxide-chitosan nanobiocomposite for urea sensor, *Sens. Actuators B* 138, 572-580, 2009.
65. S.G. Ansari, R. Wahab, Z.A. Ansari, Y-S. Kim, G. Khang, A. Al-Hajry, H-S. Shin, Effect of nanostructure on the urea sensing properties of sol-gel synthesized ZnO, *Sens. Actuat. B* 137, 566-573, 2009.
66. G. Fortier, E. Brassard, D. Bélanger, Optimization of a polypyrrole glucose oxidase biosensor, *Biosens. Bioelectron.* 5, 473-490, 1990.
67. H. C. Kim, H. B. Gu, Electrochemical properties of glucose biosensor: polypyrrole/glucose oxidase membrane, *TENCON 99. Proceedings of the IEEE Region 10 Conference*, 2, 1565-1568, 1999.
68. A. Berkkan, A. I. Seckin, K. Pekmez , U. Tamer, Amperometric enzyme electrode for glucose determination based on poly(pyrrole-2-aminobenzoic acid), *J. Solid State Electrochem.* 14, 975-980, 2009.
69. Y. Tsai, S. Li and S. Liao, Electrodeposition of polypyrrole-multiwalled carbon nanotube-glucose oxidase nanobiocomposite film for the detection of glucose, *Biosens. Bioelectron.* 22, 495- 500, 2006.
70. E. M. I. Mala Ekanayake, D. M. G. Prethichandra, K. Kaneto, Polypyrrole nanotube array sensor for enhanced adsorption of glucose oxidase in glucose biosensor, *Biosens. Bioelectron.* 23, 107-113, 2007.
71. F. Tiang, G. Zhu, Bionzymatic amperometric biosensor for glucose based on polypyrrole/ceramic carbon as electrode material, *Anal. Chim. Acta* 451, 251-258, 2002.
72. J. M. Dicks, S. Hattori, I. Karube, A. P. Turner, T. Yokozawa, Ferrocene modified polypyrrole with immobilised glucose oxidase and its application in amperometric glucose microbiosensors, *Ann. Biol. Clin.* 47, 607-619, 1989.
73. P. A. Fiorito and S. I. Córdoba-de-Torresi, *J. Braz. Chem. Soc.*, Glucose amperometric biosensor based on the co-immobilization of glucose oxidase (Gox) and ferrocene in poly(pyrrole) generated from ethanol / water mixtures, 12, 729-733, 2001.
74. C-J. Yu, N-E. Sung, H-K. Lee, H-J. Shin, Y-D. Yun, S-W. Kang, I-J. Lee, Structural properties of low-temperature grown ZnO thin films determined by X-ray diffraction and X-ray absorption spectroscopy, *Thin Solid Films* 519, 4366-4370, 2011.

75. F. Gu, S. Fen Wang, M. K. Lü, G. Jun Zhou, D. Xu, D. R. Yuan, Structure evaluation and highly enhanced luminescence of Dy³⁺-doped ZnO nanocrystals by Li⁺, *Langmuir* 20, 3528-3531, 2004.
76. <http://www.uiowa.edu/~cmrf/methodology/sem/index.html>
77. N. Dharmaraj, P. Prabu, S. Nagarajan, C. H. Kim, J. H. Park, H. Y. Kim, Synthesis of a nickel oxide nanoparticles using nickel acetate and poly(vinyl acetate) precursor, *Mat.Sci. Eng. B* 128, 111-114, 2006.
78. F. Márquez, T. Campo, M. Cotto, R. Polanco, R. Roque, P. Fierro, J. M. Sanz, E. Elizalde, C. Morant, Synthesis and characterization of monodisperse magnetic hollow microspheres, *Soft Nanosci. Lett.* 1, 25-32, 2011.
79. K. Raidongia, M. Eswaramoorthy, Synthesis and characterization of metal oxide nanorod brushes, *Bull. Mater. Sci.* 31, 87-92, 2008.
80. J. R. Ferraro, K. K. Krishnan, *Practical Fourier-transform infrared spectroscopy: Industrial, laboratory and chemical analysis*, Academic Press, 1990, San Diego, CA.
81. W. Kemp, *Organic spectroscopy*, The Macmillan Press Ltd, 1991, Houndmills, Basingstoke, Hampshire.
82. R. S. Macomber, *A complete introduction to modern NMR spectroscopy*, John Wiley & Sons, 1997.
83. <http://teaching.shu.ac.uk/hwb/chemistry/tutorials/molspec/nmr1.htm>
84. J. Koryta, *Ions, electrodes, and membranes*, John Wiley & Sons, 1982.
85. E. Laviron, General expression of the linear potential sweep voltammogram in the case of diffusionless electrochemical systems, *J. Electroanal. Chem.* 101, 19-28, 1979.
86. H. Razmi, A. Taghvimi, Tin hexacyanoferrate nanoparticles based electrochemical sensor for selective and high sensitive determination of H₂O₂ in acidic media, *Int. J. Electrochem. Sci.* 5, 751-762, 2010.
87. D. J. Michael, R. M. Wightman, Electrochemical monitoring of biogenic amine neurotransmission in real time, *J. Pharm. Biomed. Anal.* 19, 33-46, 1999.
88. I. Corb, F. Manea, C. Radovan, A. Pop, G. Burtica, P. Malchev, S. Picken, J. Shcoonman, Carbon-based composite electrodes: preparation, characterization and application in electroanalysis, *Sensors* 7, 2626 – 2635, 2007.

89. G.E. Briggs, J.B.S. Haldane, A note on the kinematics of enzyme action, *Biochem J* 19, 338–339, 1925.
90. D. Pavia, *Introduction to spectroscopy*, 3th edition, Brooks/Cole, 2001.
91. Q. Rui, K. Komori, Y. Tian, H. Liu, Y. Luo, Y. Sakai, Electrochemical biosensor for the detection of H₂O₂ from living cancer cells based on ZnO nanosheets, *Anal. Chem. Acta* 670, 57–62, 2010.
92. N. F. Almeida, E. J. Beckman, M. M. Ataii, Immobilization of glucose oxidase in thin polypyrrole films: influence of polymerization conditions and film thickness on the activity and stability of the immobilized enzyme, *Biotechnol. Bioeng.* 42, 1037-1045, 1993.
93. S. K. Arya, Preparation, characterization, application of some monolayers to cholesterol biosensor, Ph. D thesis, Department of Chemistry, University of Delhi, 2008.
94. Y. Liu, X. Feng, J. Shen, J. J. Zhu, W. Hou, Fabrication of a novel glucose biosensor based on a highly electroactive polystyrene/polyaniline/Au nanocomposite, *J. Phys. Chem. B* 112, 9237- 9242, 2008.
95. J. Njagi, S. Andreescu, Stable enzyme biosensors based on chemically synthesized Au-polypyrrole nanocomposites, *Biosens. Bioelectron.* 23, 168-175, 2007.
96. C. Chen, Y. Jiang, J. Kan, A noninterference polypyrrole glucose biosensor, *Biosens. Bioelectron.* 22, 639-643, 2006.
97. K. M. Manesh, H. T. Kim, P. Santhosh, A. I. Gopalan, K. P. Lee, A novel glucose biosensor based on immobilization of glucose oxidase into multiwall carbon nanotubes-polyelectrolyte-loaded electrospun nanofibrous membrane, *Biosens. Bioelectron.* 23, 771- 779, 2008.
98. J. D. Qiu, M. Q. Deng, R. P. Liang, M. Xiong, Ferrocene-modified multiwalled carbon nanotubes as building block for construction of reagentless enzyme-based biosensor, *Sens. Actuat. B* 135, 181- 187, 2008.
99. J.J. Song, S.W. Lim, Effect of seed layer on the growth of ZnO nanorods, *J. Phys. Chem. C* 111, 596- 600, 2007.
100. S. Saha, S.K. Arya, S.P. Singh, K. Sreenivas, B.D. Malhotra, V. Gupta, Zinc oxide-potassium ferricyanide composite thin film matrix for biosensing applications, *Anal. Chim. Acta* 653, 212- 216, 2009.

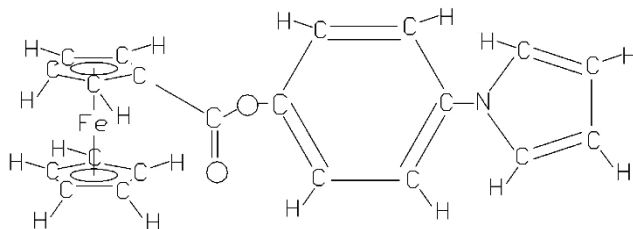
The following references are appended for the completeness of bibliography:

N. Palomera, J. L. Vera, E. Meléndez, J. E. Ramírez-Vick, M. S. Tomar, S. K. Arya, S. P. Singh, Redox active poly(pyrrole-N-ferrocene-pyrrole) copolymer based mediator-less biosensor, *J. Electroanal. Chem.* 658, 33- 37, 2011.

N. Palomera, M. Balaguera, S. K. Arya, S. Hernández, M. S. Tomar, J. E. Ramírez-Vick, S. P. Singh, Zinc oxide nanorods modified indium tin oxide surface for amperometric urea biosensor, *J. Nanosci. Nanotechno.* 11, 1- 7, 2011.

N. Palomera, M. Balaguera, S. K. Arya, S. Hernández, M. S. Tomar, J. E. Ramírez-Vick, S. P. Singh, Zinc oxide nanorods films for electrochemical urea biosensor, Symposium JJ: Biological Hybrid Materials for Life Sciences, 2011 Material Research Society Spring meeting. Manuscript ID: MRSS11-1355-JJ09-16.

Appendix A: Elemental analysis of 4-(1H-Pyrrol-1-yl) phenyl ferrocenecarboxylate.



4-(1H-Pyrrol-1-yl) phenyl ferrocenecarboxylate

Elemental Formula: C₂₁H₁₇O₂NFe

Molecular weight:

C: 12.0107 g/mol H: 1.0079 g/mol O: 15.9994 g/mol N: 14.0067 g/mol Fe: 55.8450

C₂₁H₁₇O₂NFe: 12.0107*21 + 1.0079*17 + 15.9994*2 + 14.0067*1 + 55.8450*1 =

371.2108 g/mol

Weight percent composition of carbon, hydrogen and nitrogen:

$$\text{C: } \frac{12.0107 \times 21}{371.2108} \times 100\% = 67.9465$$

$$\text{H: } \frac{1.0079 \times 17}{371.2108} \times 100\% = 4.6158$$

$$\text{N: } \frac{14.0067 \times 1}{371.2108} \times 100\% = 3.7732$$

ATLANTIC MICROLAB, INC.

Sample No. A01

P.O. Box 2288
Norcross, Georgia 30091
(770) 242-0082

www.atlanticmicrolab.com

PROFESSOR/SUPERVISOR:

P.O. #: To be paid by credit card ID-021709

SUBMITTER

Company / School UPR-Mayaguez

Address PO BOX 9019

Mayaguez P.R. 00681

NAME E. Melendez

DATE 11/18/09

Element	Theory	Found		Single <input type="checkbox"/> Duplicate <input type="checkbox"/>	
				Elements Present:	
C	67.9500	67.67		Analyze for: C H <i>N</i>	
H	4.6200	4.43		Hygroscopic <input type="checkbox"/> Explosive <input type="checkbox"/>	
<i>N</i>	<i>3.77</i>	3.68		M.P. _____ B.P. _____	
				To be dried: Yes <input type="checkbox"/> No <input type="checkbox"/>	
				Temp. _____ Vac. _____ Time _____	
				FAX Service <input checked="" type="checkbox"/> or EMAIL Service <input checked="" type="checkbox"/>	
				FAX# /EMAIL <u>JLVERA@yahoo.com</u> 787-2	
				Rush Service <input type="checkbox"/> (SEE CURRENT PRICE LIST)	
				Phone Service <input type="checkbox"/>	
				Phone No. <u>787-832-4040 X2600</u>	

Date Received **NOV 25 2009**

Date Completed **NOV 25 2009**

Remarks:

Elemental analysis results from Atlantic Lab Inc. for synthesized 4-(1H-Pyrrol-1-yl) phenyl ferrocenecarboxylate.